Marta Raquel da Costa Ribeiro

PhD Thesis

Silk fibroin/nanohydroxyapatite porous scaffolds for bone regeneration

Dissertação submetida à Faculdade de Engenharia da Universidade do Porto para obtenção do grau de Doutor em Engenharia Biomédica

Faculdade de Engenharia

Universidade do Porto

2017

This thesis was supervised by:

Professor Maria Pia Ferraz

UFP – Universidade Fernando Pessoa

Professor Fernando Jorge Monteiro

FEUP – Faculdade de Engenharia, Universidade do Porto

i3S – Instituto de Investigação e Inovação em Saúde, Universidade do Porto

INEB – Instituto de Engenharia Biomédica, Universidade do Porto

This thesis was advised by:

Professor Maria Helena Fernandes

FMDUP – Faculdade de Medicina Dentária, Universidade do Porto, Portugal

The work described in this thesis was conducted at:

FEUP – Faculdade de Engenharia, Universidade do Porto, Portugal

i3S – Instituto de Investigação e Inovação em Saúde, Universidade do Porto, Portugal

INEB – Instituto de Engenharia Biomédica, Universidade do Porto, Portugal

FMDUP - Faculdade de Medicina Dentária, Universidade do Porto, Portugal

UNICAMP – Faculdade de Engenharia Química, Universidade Estadual de Campinas, SP, Brasil

POLYMAT – Universidade do País Basco, San Sebastian, Espanha

The research described in this thesis was financed by:

FEDER funds through the Programa Operacional Factores de Competitividade – COMPETE and by Portuguese funds through FCT – Fundação para a Ciência e a Tecnologia in the framework of the PhD grant (SFRH/BD/90400/2012) and the NaNOBiofilm project (PTDC/SAUBMA/ 111233/2009).

ACKNOWLEDGENTS

First of all I would like to express my sincere gratitude to my supervisors, Professor Maria Pia Ferraz and Professor Fernando Jorge Monteiro, for giving me the opportunity to develop this work, for all their support, advices and encouragement during all these years.

Many thanks to Biocomposites team for the nice moments shared. You have provided such a warm and joyful atmosphere and never-ending encouragement. The friendship outside the work has been invaluable for me.

Many thanks to Professor Marisa Beppu for receiving me so well at University of Campinas, Faculty of Chemical Engineering, in Brazil, and for all work suggestions and advices. Special thanks go to Mariana de Moraes for sharing her broad knowledge about silk fibroin polymer, productive discussions and friendship.

I also would like to thank to Haritz Sardon for his generosity to let me work in POLYMAT, University of Basque Country, in Spain, for his precious help in developing an antibacterial hydrogel, and for introducing me in the polymer chemistry area.

Many thanks to Professor Maria Helena Fernandes for allowing me to perform the cell culture studies, under her supervision at the Laboratory for Bone Metabolism and Regeneration, Faculty of Dental Medicine, University of Porto, and for all working suggestions, fruitful discussions and constructive criticism. She certainly helped me to improve this work.

I also would like to thank all the scientific and technical staff who instructed and helped me to use different techniques and analysis methods. From Portugal, Ricardo Vidal (FTIR and various technical support), Maria Lázaro (confocal microscopy), and Daniela Silva (SEM). From Brazil, Claudenete Leal, Celso Carmago, Adilson Brandão,

Hugo Teixeira, and Rafaela Mendes (SEM, FTIR, XRD, TGA and lyophilization). From Spain, Mariano Meléndez (TEM), and Alba González (TGA).

I also would like to thank to Fluidinova S.A., Portugal, and Bratac, Brazil, for the provision of NanoXIM powder and cocoons of *Bombyx mori* silkworm, respectively.

Naturally, my family as well as my good friends played a central role in making this thesis possible, providing me a lot of nice moments and constant encouragement. They have been excellent counterbalance for the work.

Finally, I would like to acknowledge my FCT Grant (SFRH/BD/90400/2012) as well as the NaNOBiofilm (PTDC/SAUBMA/111233/2009) project for all financial support.

ABSTRACT

Bone tissue engineering has emerged as a promising alternative in cases of injured and diseased bone, which may not be capable of self-repairing. In such clinical circumstances, an appropriate biomaterial should be applied to the defective site to substitute lost bone and to initiate bone regeneration. The regeneration of bone tissue requires a suitable microenvironment that closely mimics the host site for desired cellular responses, which is typically provided by three-dimensional (3D) scaffolds that acts as an architectural template. A 3D scaffold for bone tissue engineering needs to fulfill stringent requirements, such as biocompatibility, appropriate mechanical support, controlled degradation consistent with sufficient structural integrity, containing a porous structure with interconnected pores, and osteoconductive properties. It should also have adequate physicochemical behavior to direct cell-material and cell-cell interactions. Furthermore, the possibility of promoting bone tissue growth while simultaneously preventing biofilm formation, and consequently implant-related infections, by developing antimicrobial surfaces as integral component of 3D hydrogels would be particularly advantageous for orthopedic surgery applications. Recent advances have greatly expanded the processing windows for silk fibroin (SF) porous hydrogels. SF is a natural, biocompatible, and biodegradable polymer having a great potential for the successful regeneration of damaged bone tissue. This polymer can be combined with a bioactive ceramic producing a new material for bone implants. In this context, nanophased hydroxyapatite (nanoHA) has received considerable attention due to its excellent bioactive and osteoconductive properties as it bonds to bone and enhances bone tissue formation, increasing the osteogenic potential of the material. The purpose of the present work was to develop and characterize a novel composite hydrogel of SF and nanoHA for bone regeneration. SF based hydrogels incorporating different percentages of nanoHA, by using a new and innovative method, were developed. These hydrogels of SF with nanoHA were subsequently frozen or non-frozen to evaluate the effect of this on the material properties. The physicochemical properties of the composite material incorporating nanoHA were studied. Biological investigations with human bone marrow stromal cells

(hBMSCs) and antimicrobial studies against orthopedic pathogens related to implanted medical devices were conducted. Results showed an interconnected porous structure combined with micro- and macroporosity, and the frozen hydrogels presented higher pore sizes when compared to the non-frozen materials. The hydrogel with 15 wt% nanoHA, obtained by the freezing method, yielded a composite with improved mechanical properties together with a higher amount of uniformly dispersed nanoHA particles throughout the SF matrix, making the composite hydrogel suitable for bone regeneration. Additionally, preliminary biological data performed with osteoblast-like cells MG63 showed promising results regarding osteoblastic cell response on frozen SF/nanoHA materials. Subsequently, biological investigations of hBMSCs viability, proliferation and differentiation to the osteoblastic phenotype were carried-out to exploit the suitability of the SF/15 wt% nanoHA hydrogel for bone regenerative strategies. The biological results highlighted that the SF/nanoHA hydrogels can act as a matrix for hBMSCs attachment and proliferation, which was significantly improved on frozen composite materials. Furthermore, a test for alkaline phosphatase (ALP) and bone morphogenetic protein 2 (BMP-2) expression suggested improved osteoblast differentiation for frozen SF/nanoHA hydrogels. In addition, an ALP live stain method allowed the observation of cell infiltration, and consequently migration, with active production of ALP by the infiltrated cells, which can ensure bone in-growth and bone tissue regeneration. Equally important, the rapid emergence of resistant bacterial strains to antibiotics prompted us to develop new materials exhibiting antimicrobial properties. SF/nanoHA hydrogels were modified with *in situ* synthetized silver and gold nanoparticles (AgNPs and AuNPs) and the antimicrobial activity toward orthopedic pathogens associated to implant infections was evaluated. It was found that the bacterial inhibition of hydrogels with AuNPs was not so high when compared to materials with AgNPs. Furthermore, the hydrogels containing 0.5% of AgNPs presented strong antibacterial activity, reducing the bacterial attachment and further accumulation, while simultaneously allowing for the adhesion and spreading of osteoblastic cells. These results suggested that these antimicrobial hydrogels may be used to prevent material colonization and, subsequent implant-related infections, without compromising bone tissue regeneration.

RESUMO

A engenharia de tecidos surge como uma alternativa promissora em casos de lesões ósseas em que não há a possibilidade de auto-regeneração. Nestas circunstâncias, a aplicação de um biomaterial apropriado no defeito ósseo é fundamental para iniciar e permitir a regeneração óssea. Para tal, a utilização de uma matriz tridimensional (3D) pode proporcionar o microambiente necessário para obter a resposta celular pretendida. A matriz 3D necessita de possuir determinadas propriedades de forma a preencher os requisitos para este tipo de abordagem regenerativa. O material deve ser biocompatível, com suficiente suporte mecânico, uma degradação controlada consistente com integridade estrutural, possuir uma estrutura porosa com poros interconectados, e propriedades osteocondutoras. Um comportamento físico-químico adequado de forma a direcionar as interações célula-material e célula-célula também é fundamental. Além disso, a possibilidade de ter um material que além de promover o crescimento do tecido ósseo também previna a formação de biofilme, e consequentemente as infeções relacionadas com implantes, é uma mais valia para aplicações cirúrgicas ortopédicas. O desenvolvimento de hidrogéis porosos de fibroína da seda (SF) é uma área em grande expansão. A SF é um polímero natural, biocompatível e biodegradável com grande potencial em estratégias de regeneração do tecido ósseo. A combinação deste polímero com um cerâmico bioativo conduz à produção de um novo material para ser aplicado em implantes ósseos. Neste contexto, a nanohidroxiapatite (nanoHA) atrai enorme atenção devido à sua excelente bioatividade e osteocondutividade, uma vez que se liga ao osso e conduz à formação de novo tecido ósseo, aumentando assim o potencial osteogénico do material. Desta forma, o objetivo deste trabalho foi desenvolver e caraterizar um novo hidrogel composto por SF e nanoHA para a regeneração óssea. Para tal, diferentes percentagens de nanoHA foram incorporadas nos hidrogéis de SF através de um novo método, e alguns dos materiais foram submetidos a congelamento para avaliar diferenças nas propriedades dos materiais congelados e não congelados. As propriedades físico-químicas dos materiais obtidos com nanoHA foram estudadas. Os hidrogéis foram também utilizados para a realização de estudos biológicos com células

do estroma da medula óssea (hBMSCs) e estudos antimicrobianos com microrganismos patogénicos associados a dispositivos médicos. Os resultados mostraram um material com estrutura porosa, com poros interconectados, e com micro e macro porosidade. Além disso, os hidrogéis submetidos a congelamento apresentaram tamanho de poros maior quando comparados com os materiais não congelados. O hidrogel com 15% de nanoHA, obtido pelo método de congelamento, apresentou melhores propriedades mecânicas juntamente com uma maior quantidade de partículas de nanoHA uniformemente dispersas na matriz de SF, tornando este material adequado para a regeneração óssea. Dados biológicos preliminares, obtidos através da utilização de células osteoblásticas MG63, mostraram resultados promissores relativamente à resposta das células osteoblásticas nos hidrogéis de SF com nanoHA. Consequentemente, realizaram-se estudos biológicos de viabilidade, proliferação, e diferenciação osteoblástica com hBMSCs, para explorar o potencial do hidrogel de SF com 15% de nanoHA para a regeneração óssea. Estes resultados mostraram que os hidrogéis de SF com nanoHA podem atuar como uma matriz para a adesão e proliferação das hBMSCs, um comportamento que foi significativamente melhor nos materiais compósitos submetidos a congelamento. Além disso, através da avaliação da expressão da fosfatase alcalina (ALP) e da proteína morfogenética óssea tipo 2 (BMP-2) observou-se uma diferenciação osteoblástica mais evidente nos hidrogéis de SF com nanoHA congelados. Adicionalmente, um método de coloração para a ALP em células vivas permitiu observar infiltração celular, e consequentemente migração celular, com produção ativa de ALP pelas células infiltradas, o que pode assim assegurar o crescimento ósseo e por conseguinte a regeneração do tecido ósseo. Igualmente importante de destacar é o rápido surgimento de estirpes bacterianas resistentes a antibióticos, sendo necessário o desenvolvimento de novos materiais com propriedades antimicrobianas. Neste seguimento, os hidrogéis de SF com nanoHA foram modicados com nanopartículas de prata e ouro (AgNPs e AuNPs), sintetizadas *in situ* no material compósito, e a atividade antimicrobiana destes hidrogéis foi avaliada com espécies relevantes envolvidas em infeções de implantes ósseos. Os resultados mostraram que a inibição bacteriana dos hidrogéis com AuNPs não foi tão elevada quando comparada com os materiais com AgNPs. Além disso, os hidrogéis com 0.5%

de AgNPs apresentaram robusta atividade antimicrobiana, reduzindo a adesão bacteriana e subsequente acumulação, e em simultâneo permitiram a adesão das células osteoblásticas. Assim, estes resultados sugerem que estes hidrogéis antimicrobianos podem ser utilizados para prevenir a colonização do material e, subsequente infeção, sem comprometer a regeneração do tecido ósseo.

PUBLICATIONS

The work performed in this thesis is based on the following international scientific publications:

Ribeiro M, de Moraes MA, Beppu MM, Monteiro FJ, Ferraz MP. The role of dialysis and freezing on structural conformation, thermal properties and morphology of silk fibroin hydrogels. Biomatter, 2014; 4:e28536.

Ribeiro M, de Moraes MA, Beppu MM, Garcia MP, Fernandes MH, Monteiro FJ, Ferraz MP. Development of silk fibroin/nanohydroxyapatite composite hydrogels for bone tissue engineering. European Polymer Journal, 2015; 67:66-77.

Ribeiro M, Fernandes MH, Beppu MM, Monteiro FJ, Ferraz MP. Silk fibroin/nanohydroxyapatite hydrogels for promoted bioactivity and osteoblastic proliferation and differentiation of human bone marrow stromal cells (Submitted).

Ribeiro M, Ferraz MP, Monteiro FJ, Fernandes MH, Beppu MM, Mantione D, Sardon H. Antibacterial silk fibroin/nanohydroxyapatite hydrogels with silver and gold nanoparticles for bone regeneration. Nanomedicine: Nanotechnology, Biology, and Medicine, 2016; 13:231-239.

AIMS OF THE THESIS

There is a high demand by the orthopedic medical community for implant materials that are capable to promote bone tissue growth while preventing bacterial adhesion and, consequently, implant-associated infections. Hence, the aim of this thesis was to develop silk fibroin (SF) porous hydrogels mineralized with nanohydroxyapatite (nanoHA) for bone regeneration. SF is a natural, biocompatible, and biodegradable polymer having a great potential for the regeneration of damaged bone tissue. In the context of creating more effective bioactive hydrogels, this polymer can be combined with a nanoHA ceramic producing a new composite material for bone implants. NanoHA is one of the most widely used calcium phosphate ceramics due to its chemical similarities to the inorganic component of natural bone tissue. Additionally, the excellent bioactive and osteoconductive properties of nanoHA can increase the osteogenic potential of the material, as it bonds to bone and enhances bone tissue formation. Therefore, the present work was focused on the preparation and characterization of new SF/nanoHA porous hydrogels mimicking the physiologic environment present during bone tissue formation. In this context, hydrogels were assayed for bone cell functions and bacterial adhesion. The specific aims proposed in this work are listed below:

- Preparation of SF/nanoHA porous hydrogels by impregnation of nanosized particles of hydroxyapatite into fibroin solution, and subsequent physicochemical characterization.

- *In vitro* biological performance of SF/nanoHA hydrogels using human bone marrow stromal cells, cultured up to 21 days, and evaluated for cell adhesion, morphology, viability, proliferation, and differentiation events.

- Assessment of the antimicrobial effect of SF/nanoHA hydrogels modified with *in situ* synthetized silver and gold nanoparticles against major agents of biomaterial-associated infections in orthopedics.

TABLE OF CONTENTS

CHAPTER I

Introduction

1. Motivation behind bone tissue engineering

Tissue engineering is a multidisciplinary field focused on the development of biological substitutes to repair or regenerate tissue functionality with the aim of helping to restore the functions during regeneration and subsequent integration with the host tissue [1, 2]. The fundamental concept behind tissue engineering it to utilize the body's natural biological response to tissue damage in conjunction with engineering principles. In this regard, significant attention is being given to three-dimensional scaffolds with specific physical, mechanical and biological properties. An ideal scaffold for bone tissue engineering is a matrix that acts as a temporary substrate for cell growth, proliferation and support for new tissue formation, and simultaneously is degraded to provide location for the newly formed tissue [1-3].

Bone is a dynamic and highly vascularized tissue that forms the main elements of the skeleton and continues to remodel throughout the lifetime of an individual. Bones not only provide the mechanical support for locomotion, but also offers protection to vulnerable internal organs. In addition to these structural functions it is considered as the main reservoir of mineral ions such as calcium, phosphate and other inorganic ions intimately involved in homeostasis by regulating the concentration of key electrolytes in the blood [3, 4]. The importance of bone becomes even clearer in the case of diseases such as osteogenesis imperfecta, osteoarthritis, osteomyelitis, and osteoporosis where bone does not perform adequately. These diseases along with traumatic injury, orthopaedic surgeries (i.e., total joint arthroplasty, spine arthrodesis, implant fixation) and primary tumour resection lead to or induce bone defects or voids [3]. Bone is nowadays one of the most transplanted tissues, with an incidence of nearly 15 million fracture cases per year [5]. Traditionally, the treatment of bone defects has relied on autografts, where bone tissue is transplanted from one site to another in the same patient, but the donor site morbidity and pain, limited supply especially in elderly and fragile population, constrained by anatomical limitations are significant problems [6-8]. As an alternative option, allografts, bone tissue transplanted from one individual to another, offer the advantage of allowing the surgeon to place a graft of the same anatomic location, and consequently with very similar mechanical and biochemical properties. However, they also have drawbacks, mainly associated with the risk of

donor to recipient infection, disease transmission and adverse host immune response along with possible graft rejection [6-9]. Considering these severe drawbacks of the current treatment methods, as well as constantly increasing incidence of bone defects as a consequence of the aging population, there is clearly a huge demand on the development of novel and more sophisticated synthetic biomaterials, for which the bone tissue engineering has a potential to answer.

With respect to the biomaterial, a functional scaffold for bone tissue engineering should meet stringent requirements, such as biocompatibility with host tissues without eliciting any immune response, appropriate mechanical support to withstand the mechanical loading *in vivo*, contain a porous architecture with interconnected pores to encourage cell ingrowth and vascularization, and osteoinductive properties to recruit and differentiate osteoprogenitors to the defect region. It must also possess appropriate chemical and topographical properties to positively influence cellular adhesion, proliferation and differentiation, and a controlled degradation consistent with sufficient structural integrity until the newly grown tissue has replaced the scaffold's are properties that should also be addressed. In filling up bone defects, considerations such as the manufacturability and easy clinical handling are also essential [3, 10, 11].

In order to gain insight into choosing the type of materials that can best mimic the physicochemical properties of bone, a clear concept of the bone biology, physiology, and anatomy of bone is essential.

1.1. Bone properties

Bone is a sophisticated composite organized into hierarchical architecture over several length scales, from macroscopic to nanoscale dimensions, where the basic building blocks are the plate-like HAp nanocrystals incorporated into collagen fibers, as shown in Figure 1. Bone is a natural composite material consisting primarily of a type I collagen-containing organic phase as a matrix and a an inorganic phase composed of natural apatite, a non-stoichiometric, partially substituted and partially crystalline variety of hydroxyapatite ($Ca_{10}(PO_4)_6(OH)_2$). Bone matrix is built up of type I collagen

amounting to about 90% of total bone protein and the remaining organic component is composed of a large number non-collagenous proteins like osteocalcin, osteonectin, osteopontin, bone sialoprotein and several proteoglycans. The hardness of bone is attributed to the deposition of complex mineral substances, calcium hydroxyapatite composed of calcium, phosphorus, sodium, magnesium, fluoride and other ions in trace amounts, within the soft organic matrix of collagen, which is responsible for the toughness, flexibility and visco-elasticity [4, 12-14].

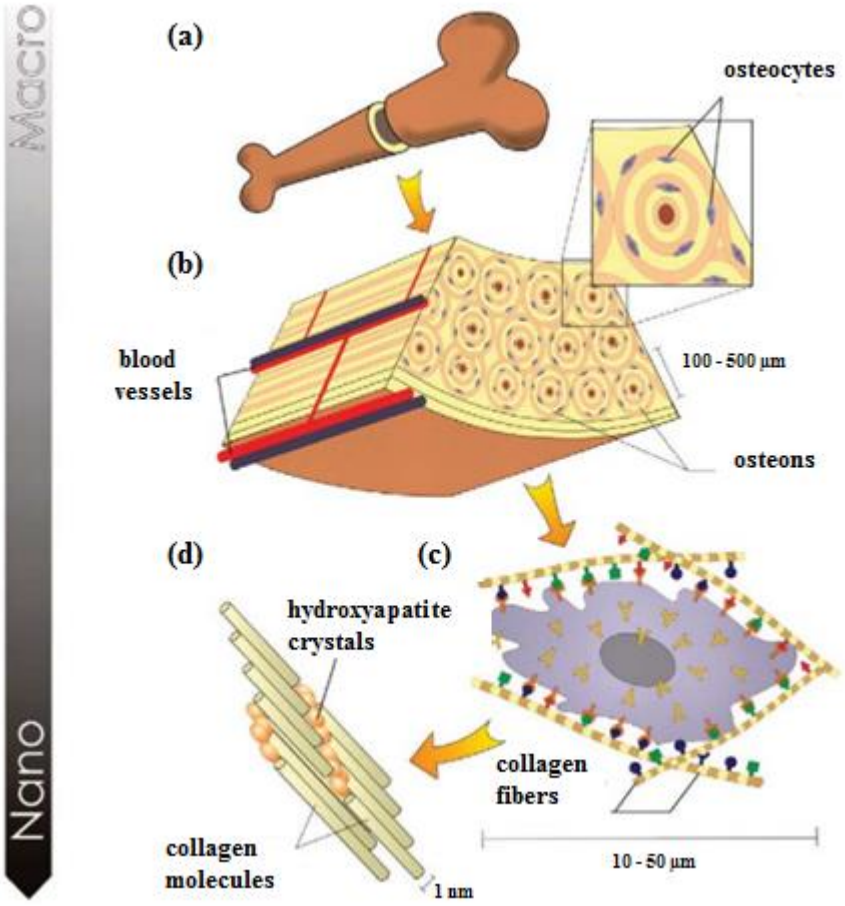

Figure 1 - Bone is a complex, hierarchically structured biological material that comprises macro, micro and nano components. Bone has a strong calcified outer compact layer (a), which comprises many cylindrical Haversian systems, or osteons (b). The resident cells are coated in a forest of cell membrane receptors that respond to specific binding sites (c) and the well-defined nanoarchitecture of the surrounding extracellular matrix (d) [4].

Two different mature bone structures can be identified in different parts of the bone: cortical (compact) and trabecular (cancellous) bone. Trabecular bone constitutes 20%

of the total adult bone tissue and is a spongy structure with 50-90% porosity, filled with bone marrow. Cortical bone is a compact structural tissue, comprising 80% of adult bone tissue, with only 10% porosity [10, 15, 16]. The cortical bone contains osteons (Harversian systems), which are composed of a central canal (Haversian canal) surrounded by lamellae of bone matrix, and within the lamellae there are osteocytes embedded in tiny spaces (lacunae). The Harversian canal encompasses blood vessels and nerve cells throughout the bone and communicates with osteocytes in lacunae through canaliculi, The periosteum consists of an outer fibrous layer and an inner one that has osteogenic potential and enables the bone to enlarge [14, 17].

Bone contains different cell types, namely osteoblasts (bone matrix producing cells), osteocytes (mature osteoblasts that are embedded in the mineralized matrix), osteoclasts (bone matrix degrading cells) and osteoprogenitors (immature cells capable of differentiating into osteoblasts - found in the bone marrow and periosteum) [15]. Undifferentiated mesenchymal stem cells (MSCs) give rise to osteoprogenitor cells which in turn form osteoblasts. Osteoprogenitor cells are also located in periosteum, endosteum, and Haversian canals and placed on standby, ready for a stimulus signal to start proliferating and differentiating into osteoblasts before forming bone. Osteoblasts are responsible for the formation and organization of bone extracellular matrix and its subsequent mineralization. Osteocytes represent terminally differentiated osteoblasts and function within networks to support bone structure and metabolism. These cells communicate with each other and with the surrounding medium through extensions of their plasma membrane. Therefore osteocytes are thought to act as mechanosensors, osteoclasts where and when to resorb bone and osteoblasts where and when to form it. Osteoclasts are derived from mononuclear precursor cells of the monocyte-macrophage lineage. The most functional characteristic feature of osteoclasts is their unique ability to dissolve bone mineral, which is mainly crystalline hydroxyapatite. In order to finalize bone resorption after mineral dissolution they also perform an enzymatic degradation of organic bone matrix [18-23].

Bone is constantly renewed through the balance between bone formation and bone resorption. This restructuring process called bone remodeling maintains the integrity of the skeleton by removing old bone of high mineral density and high prevalence of

fatigue micro-cracks through repetitive cycles of bone resorption performed by osteoclasts and bone formation carried out by osteoblasts [14, 24, 25]. Several regulatory systems, both systemic and local, are required to keep these two processes in balance, and an imbalance between bone resorption and bone formation is often linked to metabolic bone diseases [22, 26]. Cellular communication between bone cells, as osteoblasts, osteocytes and osteoclasts is essential for bone remodeling, comprising a sequence of stages. The activation of resorption is thought to be mediated by the death of osteocytes in the neighborhood of a micro-crack. This leads to osteoclast precursor recruitment, osteoclastogenesis and bone resorption. After the osteoclasts have finished resorbing, they die by apoptosis, and switch between resorption and formation called the reversal phase takes place during which osteoblast precursors are recruited. After this phase, bone formation is carried out by osteoblasts until the resorbed area is rebuilt with new bone, after which the cycle is concluded, a process likely to be controlled by osteocytes [22, 25-28].

Nevertheless, for different reasons such as defects size, infection, and many others, injured and diseased bone may not be capable of self-repairing. In such clinical circumstances, an appropriate biomaterial should be applied to the defective site to substitute lost bone and to initiate bone tissue regeneration. A variety of different metals, ceramics and polymers have been used to repair or replace damaged bone tissue. Inspired by the hierarchical structure of bone, the combination of materials with desirable properties, while at the same time trying to avoid some of their less attractive properties, is gaining increasing interest in biomaterials research. Therefore, a combination of two or more materials for their favorable properties creates a new composite material with a set of unique characteristics that each individual material does not meet. Composite materials have gained popularity for bone tissue engineering applications because bone is, in fact, a composite material presenting a combination of inorganic and organic components. In this sense, composite based on apatite crystals and natural polymers have received increasing attention in bone tissue engineering due to their ability to biomimetically preserve the structural and biological phenotype of the damaged tissues. Remarkably, polymer-ceramic composite scaffolds benefit from the joint presence of both biodegradable polymers and bioactive ceramics [29, 30].

1.2. Biomimetic composites based on polymers and calcium phosphates

The composites involving biodegradable polymeric matrices and bioactive and bioresorbable CaPs ceramics have been considered as strategic for tissue engineering and regeneration, allowing tailoring the desired degradation and resorption kinetics of the matrix. The interest in bioresorbable ceramics, such as calcium phosphates (CaPs) (i.e., β-tricalcium phosphate, and to a lesser extent nanohydroxyapatite), for bone replacement and repair is well-deserved, given that they have required properties and many other attributes that make them excellent candidates for such applications. In fact, CaPs present favorable biocompatibility, a composition and structure similar to the inorganic phase of bone, and bioactivity. These materials possess surface properties that support osteoblast adhesion and proliferation (osteoconduction) and stimulate new bone formation (osteoinduction). Moreover, the CaPs with nanosized features can strongly change the physical properties of the polymer matrix, generating biocomposites with optimized properties when compared to their individual components [31-33].

Biodegradable polymers from natural origin, like polysaccharides (i.e., chitin, cellulose, glycosaminoglycans) and proteins (i.e., elastin, collagen, silk), as their name implies, are derived from natural sources. The use of natural polymers as scaffolds in bone tissue engineering has been gaining widespread attention owing to their significant similarities with the extracellular matrix (ECM), biocompatibility, biodegradability, chemical versatility, low cost and ease of processing. Among naturally derived polymers, silk fibroin provides an important set of material options for biomaterials and scaffolds due to its biocompatibility, controllable degradation rate, high oxygen and water vapor permeability, and the presence of easily accessible chemical groups for functional modifications [31, 34-36].

1.2.1. Silk fibroin

Silks are naturally occurring protein polymers commonly produced by a wide variety of insects and spiders. In nature silks are used as materials for web construction and prey

capture (spider webs), safety line (draglines) and reproduction enclosures (cocoons) [37, 38]. Spider silk is and intriguing material that is lightweight, extremely strong and elastic, and it is spun near ambient temperatures and pressures using water as the solvent, which gives rise to and environmentally safe, biodegradable material. Nevertheless, it is not possible to maintain domesticated spiders to produce massive amounts of silk, thus directing our attention to silk fibroin, a mass-producible natural protein produced by silkworms [39]. The silkworm *Bombyx mori* produces silk to weave its cocoon, which consists primarily of two protein components, fibroin and sericin. Fibroin is the water insoluble structural protein component of silk fibers whereas sericin is the water-soluble glue-like protein that holds SF fibers together (Figure 2) [37, 39-41]. Silk has several advantages over other protein based biomaterials, which are derived from tissues of allogeneic or xenogeneic origins. Also, the processing of such materials is expensive due to the stringent protein isolation and purification procedures. In contrast, silk fiber purification is routinely carried out using a simple alkaline solution based degumming process, which yields the starting material for sericin free silk based biomaterials. The degummed silk fibroin is then dissolved in a ternary solvent, dialyzed and formed in an aqueous SF solution. Moreover, it is economically advantageous to use silk for biomedical applications, because of availability of large scale processing infrastructure for traditional silk textile industries [31, 35, 42, 43].

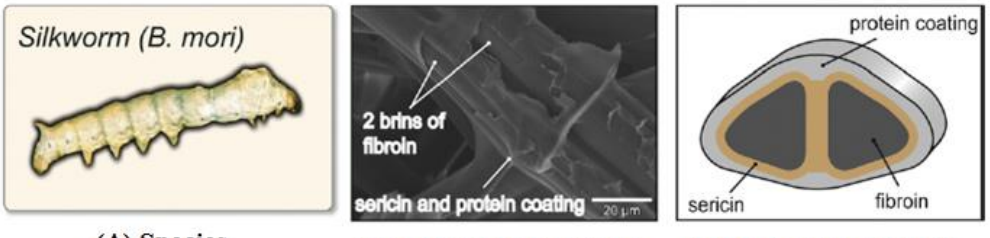

Figure 2 - Photograph of a *Bombyx mori* silkworm (A), electron micrograph of partially degummed *B. mori* silkworm cocoon fibers (B) and schematic illustration of the composite structure of a cocoon fiber (C), in which the two brins of fibroin and the coating of sericins and other proteins postulated to protect the cocoon against microbes and predators are pointed out [44].

Silk fibroin (SF) is the core protein which accounts for 70% of the cocoon, and consists of two proteins, light chain (M_w approximately 26 kDa) and heavy chain M_w approximately 390 kDa), which are present in a 1:1 ration and connected by a disulfide link. SF is characterized as natural amphiphilic block copolymer composed of hydrophobic (ordered, highly conserved) and hydrophilic (less ordered, relatively more complex) blocks. The primary structure of SF consist of a predominance of the amino acids glycine, alanine, serine, valine, and tyrosine with characteristic repetitive sequences of GAGAGS, GAGAGY, and GAGAGVGY, which are responsible for the formation of antiparallel β-sheets in the spun fibers. SF is composed of relatively large hydrophilic chain end blocks (N and C-termini) with smaller hydrophilic internal blocks and large internal hydrophobic blocks where the repeats listed above are encoded (Figure 3). Hydrophilic blocks provide solubility in water and are responsible for SF elasticity and toughness, while hydrophobic blocks form intermolecular β-sheet structures leading to the insolubility and high strength of SF [40, 41, 43, 45-47].

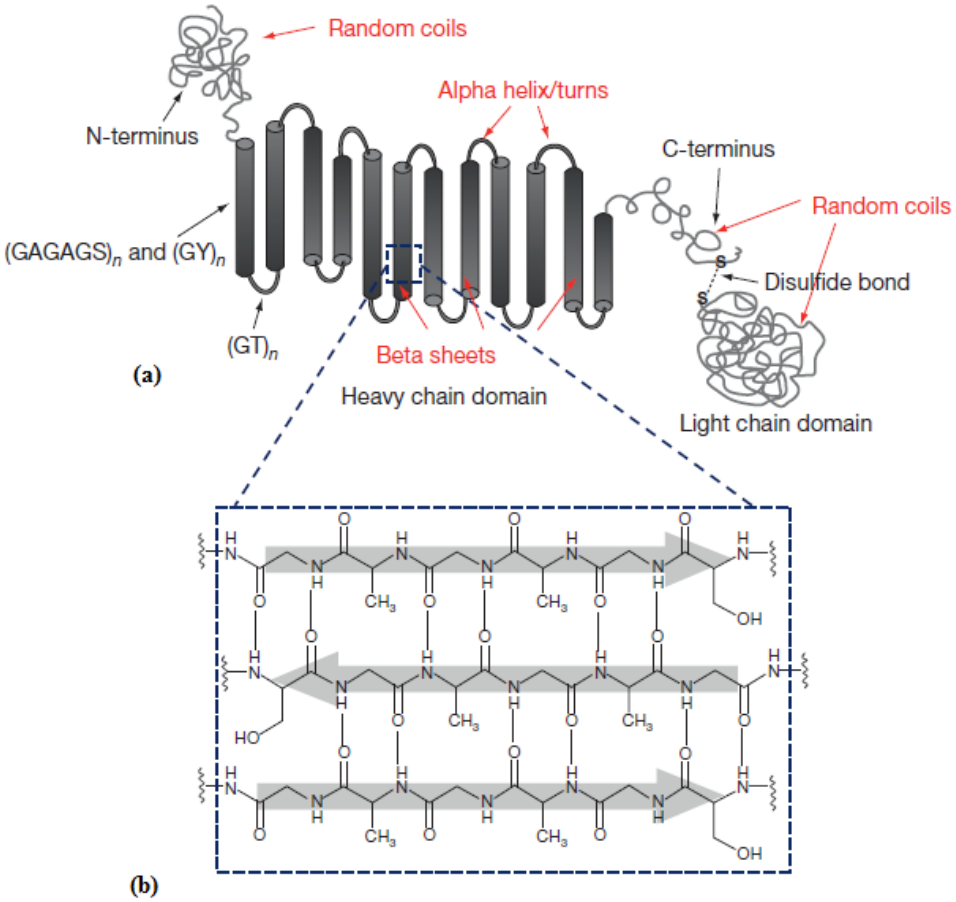

Figure 3 - Secondary structure of one *B. mori* silk fibroin chain (a); (Gly-Ala-Gly-Ala-Gly-Ser)$_n$ amino acid repeat units that self-assemble into antiparallel β-sheets (b) [48].

The molecular conformation of SF is an important parameter that needs to be controlled, since it affects its physical and chemical properties. SF has two types of molecular conformation of the secondary structure, called silk I and silk II. Silk I is a metastable form of SF that is soluble in water and non-crystalline; random coil and α-helix conformations are usually called silk I. On the other hand, silk II is a highly stable and organized structure that is insoluble in water; the β-sheet conformation is called silk II (Figure 3). Generally, both silk I and silk II are present in SF products, but it is their relative proportions that will define the final properties [49-51].

The biocompatibility and long-term stability of silk fibroin scaffolds has been shown [38]. Recently hydrogel-based scaffolds are gaining attention in the field of tissue engineering. Hydrogels have attracted extensive interest because of their advantageous properties similar to those of the native extracellular matrix (ECM), such as biocompatibility and the ability to absorb high amounts of water or biological fluids (up to thousands of times their dry weight) without dissolving in them, thus maintaining their three-dimensional (3D) structure and function. Their high permeability allows the exchange of oxygen, nutrients, and soluble metabolites [52-55].

1.2.1.1. Silk fibroin-based hydrogels

Hydrogels are created by the cross-linking of polymer chains, leading to the formation of a three-dimensional (3D) network, structurally integral, hydrophilic matrix. Hydrogels exhibit solid-like mechanical behavior, with high compliance and elastic strain, while consisting mostly of liquid. Hydrogels formed from synthetic polymers offer the benefit of gelation and gel properties that are controllable and reproducible through the use of specific molecular weights, block structures, and modes of crosslinking. Generally, gelation of naturally derived polymers is reported to be less controllable. However, the hydrogels formed from natural polymers are more compatible for hosting cell and bioactive molecules. Moreover, natural polymers can be processed under mild, ambient conditions. The process of gelation occurs when the

polymer chains crosslink either chemically or physically into networks, triggered by chemical reagents (i.e., cross-linkers) or physical stimulants (i.e., pH, temperature) [48, 56-59].

An important advantage of SF for the preparation of hydrogels, compared to other polymers, is its ability to physically crosslink without any chemical modification. However, to produce SF derived materials, solvents with high ionic strength are used to break down the strong hydrogen bonds within the β-sheet molecular structure of the silk fibers. These solvents usually contain high concentration of salts that are further removed by dialysis. Once the ionic force of the solvent decreases during dialysis, SF solution becomes metastable and may undergo a sol–gel transition. The hydrogel formation occurs because SF chains tend to aggregate, passing from an amorphous conformation (random coil) to a more stable structure (β-sheet). The formation of β-sheets acts as physical cross-linking to stabilize the hydrogel and it is irreversible under physiological conditions unless degraded by enzymatic or oxidative processes. Due to the β-sheet formation, SF exhibit relatively slow degradation *in vitro* and *in vivo* when compared to collagens and many other biopolymers. This feature makes the use of SF, specifically in biomaterial formats for tissue engineering, advantageous when compared with most other natural or synthetic polymers, allowing the maintenance of the mechanical integrity during new tissue formation. Moreover, the degradation products of silk fibroin materials have been shown to be harmless to the human body [40, 47, 51, 60-64].

SF-based composite hydrogels with enhanced physicochemical and biological properties have been developed for tissue engineering applications [57, 65]. This composite biomaterial can be tailored to meet specific mechanical, functional and biological requirements of the host tissues. SF biodegradable polymer can be combined with a bioactive ceramic producing a new material for bone implants. SF acts as the main structural and tissue component of the hydrogel, providing mechanically stable structures that undergo slow biodegradation over extended periods of time, while a bioactive ceramic is able to bind the surrounding osseous tissue and enhance bone tissue formation, increasing the osteogenic potential of the composite hydrogel [34, 66].

1.2.2. Hydroxyapatite

The chemical similarity to the mineral component of mammalian bones and teeth has fueled the use of calcium phosphates as bone substitute materials. In fact, they can be employed with different shapes and functionalities within the clinical area. Ceramics of the calcium phosphate family are the most important class of materials in bone regeneration and because of the apatitic structure of bone tissue synthetic apatites are the most widely studied of all calcium phosphate phases. One of the most widely used synthetic calcium phosphate ceramics is hydroxyapatite (HA) due to its chemical similarities to the inorganic component of natural bone tissue. Synthetic HA with a chemical formula of $Ca_{10}(PO_4)_6(OH)_2$ and a hexagonal crystalline structure, has a theoretical composition of 39.68 wt% Ca, 18.45 wt% P; Ca/P wt ratio of 2.151 and Ca/P molar ratio of 1.667. It has higher stability in aqueous media than other calcium phosphate ceramics within a pH range of 4.2-8.0 [67-71].

HA is a preferred material for bone repair because of its stability under *in vivo* conditions, compositional similarity, biocompatibility, osteoconductivity, bioresorbable properties, and ability to promote osteoblasts functions. As a bioactive ceramic HA exhibits strong affinity to host hard tissues and the chemical bonding with the host tissues offers a greater advantage compared to most other bone substitutes, such as allografts or metallic implants [69, 72-75].

The recent trend in bioceramics research is shifting towards nanotechnology offering a unique approach to overcome shortcomings of many conventional materials and in improving their biological properties. The resorption process of synthetic microsized HA is different from that of bone mineral. Apatite crystals of bone mineral are in nano-size with a very large surface area. These crystals are grown in an organic matrix and have very loose crystal-to-crystal bonds, and therefore, the resorption of bone mineral by the osteoclasts is homogeneous. On the contrary, microsized HA presents a low surface area and have strong crystal-to-crystal bonds, which result in a tow stage resorption process: disintegration of particles and de-suspension of the crystals. Moreover, mineral bone shows higher bioactivity compared to synthetic HA. In this sense, nanophased HA presents outstanding functional properties due to its grain size, large surface area to volume ratio and ultra-fine structure similar to biological apatite.

Consequently, nanosized HA ceramics are expected to have homogeneous resorption and better bioactivity than microsized HA. Additionally, nanoHA powders exhibit improved and enhanced densification due to their greater surface area, which may improve fracture toughness, as well as other mechanical properties [69, 72, 74-76].

Hydrogels produced from a natural or synthetic polymeric hydrogel matrix, incorporating inorganic nanosized HA, can provide not only improved mechanical properties, but also tuning the bioactive characteristics to the matrix. For example, nanosized HA was incorporated into a poly(ethylene glycol) (PEG) hydrogel matrix. The incorporation of nanoHA significantly enhanced the mechanical, physical and chemical properties of the nanocomposite. The presence of nanoHA also improved osteoblast adhesion when compared with PEG hydrogels [77]. In another study, an injectable and thermos-sensitive PEG-poly(ε-caprolactone) (PCL)-PEG copolymer/collagen/nanoHA hydrogel composite for guided bone regeneration was developed and the *in vivo* biocompatibility and biodegradability was investigated by implanting the hydrogel composite in rats. The results showed that the biodegradable hydrogel composite had good biocompatibility and better performance in guided bone regeneration than the self-healing process [78].

2. Implant-associated infections

Implant-associated infections in orthopaedics are serious complications with consequent devastating effects in bone and in surrounding soft tissues. Depending on the nature of the injury or disease, 2-10% of orthopedic hardware facilitates host infection with increasing incidences for open fractures, combat-related injuries, and revision joint replacements. In addition to human pain and suffering, direct medical costs associated with such infections are extremely high and often result in the removal of the orthopedic implants and the need for a follow-up operation. Sources of infectious bacteria include the environment of the operating room, surgical equipment, clothing worn by medical and paramedical staff, resident bacteria on the patient's skin and bacteria already residing in the patient's body. Although sterilization and the use of aseptic techniques greatly reduce the levels of bacteria found in

hospital settings, pathogenic microorganisms are still found at the site of approximately 90% of all implants [79-82].

Implant-associated infections are the result of bacteria adhesion to an implant surface and subsequent biofilm formation at the implantation site. In the last twenty years, infections caused by bacterial biofilms have reemerged as major health threat. Hospital-acquired infections are now responsible for more deaths annually in the United States than emphysema, AIDS, Parkinson's disease, and homicide combined and cost the U.S. health care system over $20 billion annually. It is estimated, according to the National Institutes of Health, that biofilms contribute to more than 80% of bacterial infections in humans leading the Centers for Disease Control to declare biofilms among the most pressing clinical impediments of the century [81, 83, 84].

2.1. Pathogenesis and microbiology

Implant-associated infections occur either by direct inoculation of microorganisms into the surgical wound during surgery or immediately thereafter (perioperative infection); by microbial spread through blood or lymph from a distant focus of infection (hematogenous infection); or by contiguous spread from an adjacent infectious focus (contiguous infection). Early and delayed infections are predominantly acquired during implant surgery and caused by highly or less virulent organisms, respectively, whereas late infections are predominantly acquired by hematogenous seeding from remote infections [85-87].

A very large proportion of all implant-related infections are caused by staphylococci (roughly four out of five), and two single staphylococcal species, respectively *Staphylococcus aureus* and *Staphylococcus epidermidis*, account together for two out of three infection isolates. They represent, in absolute, the main causative agents in orthopedics, while CoNS species other than *S. epidermidis*, and, especially among them, *Staphylococcus hominis* and *Staphylococcus haemolyticus*, contribute to an additional 13% of the infections. In order of relevance in terms of prevalence then there follow *Pseudomonas aeruginosa* and *Enterococcus faecalis* [88-90].

2.2. Processes governing biofilm formation

Biofilm formation is commonly considered to occur in three main stages: attachment to a surface, proliferation and formation of the characteristic, mature biofilm structure, and finally detachment, which is also often called dispersal (Figure 4) [91, 92].

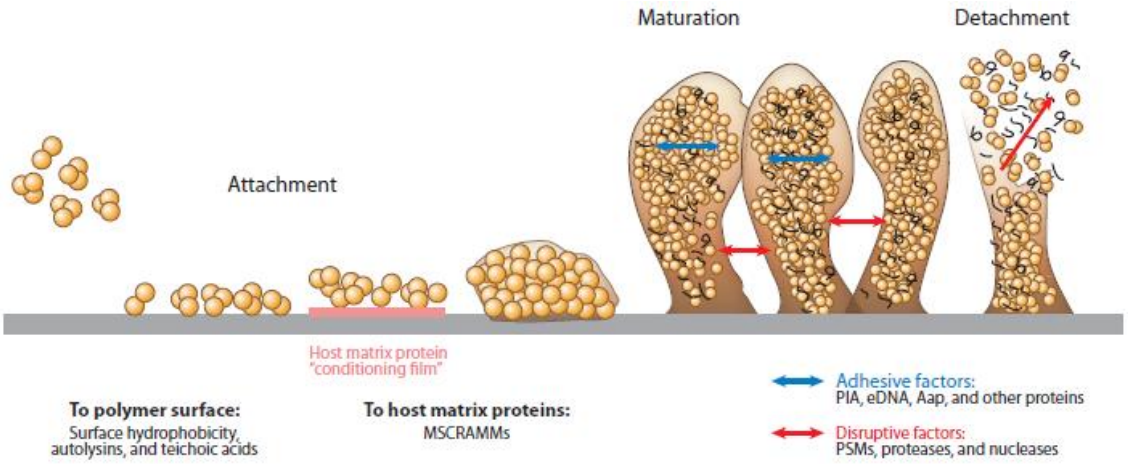

Figure 4 – Phases of biofilm development, which include initial attachment, maturation, and final detachment. Attachment may occur directly to a surface or to a "conditioning film" formed by host proteins. Then, biofilm maturation proceeds via the agglomeration of cells, which is dependent on adhesive molecules. Formation of the characteristic channel-containing biofilm structure is dependent on disruptive factors, which also ultimately facilitate the last phase of biofilm development, detachment [92].

Initial bacterial attachment can occur on abiotic or biotic surfaces. Attachment to an abiotic surface is dependent on the physicochemical characteristics of the material and bacterial surfaces. This type of attachment is thus driven mostly by hydrophobic or electrostatic interactions. However, the involvement of specific bacterial surface molecules in this process, such as the surface protein autolysin or teichoic acids, has been described in staphylococci. Attachment to a biotic surface such as human tissue is governed by entirely different, much more specific interactions. Staphylococci express a large variety of surface-anchored proteins that bind to host matrix proteins,

collectively called MSCRAMMs (microbial surface components recognizing adhesive matrix molecules). These interactions are of vital importance for biofilm-associated infections on biomedical implants, as such implants become covered by a conditioning film consisting of host plasma and connective tissue proteins and glycoproteins (such as fibronectin, vitronectin, fibrinogen, albumin, and immunoglobulins) soon after insertion. Many of these proteins subsequently serve as specific receptors for colonizing microorganisms or incoming mammalian cells [80, 91-94].

Biofilm maturation comprises adhesive processes that link bacteria together during proliferation and disruptive processes that form channels in the biofilm structure. In staphylococci, arguably the most important adhesive biofilm molecule is an exopolysaccharide named polysaccharide intercellular adhesin (PIA). Together with other polymers such as teichoic acids and proteins forms the main part of what has often been called “slime”, the extracellular matrix of biofilm-forming staphylococci. DNA released from lysed bacteria, called extracellular DNA (eDNA), also forms part of that network. As in the case of teichoic acids, the negative charge of DNA may play a crucial role in interacting with other surface structures. The disruptive processes are necessary for nutrients to reach cells in deeper biofilm layers, indicating that biofilm maturation requires cell-cell-disruptive factors. Quorum-sensing (QS), a regulatory mechanism in microorganisms that controls gene expression in a cell-density-dependent manner, has received much attention as a regulator of biofilm formation and maturation. In addition to biofilm structuring, disruptive processes also ultimately cause the detachment of cell clusters from a biofilm, which controls biofilm expansion and has important consequences for *in vivo* biofilm infection, as it may lead to systemic dissemination. Particularly in staphylococci, biofilm maturation was also proposed to occur by enzymatic degradation of biofilm matrix components most notably by proteases and nucleases. Detached biofilm bacteria may establish secondary biofilm infections elsewhere, possibly with increased severity, such as for example endocarditis [79, 91-93].

Free floating planktonic bacteria without a surrounding biofilm are normally accessible to appropriate systemic antibiotics. However, biofilm formation and persistence has profound implications for the patient, because microorganisms growing as biofilms are significantly more resistant to antibiotic treatment (up to 1000-fold) and host

defenses. The most important innate host defense mechanism is the elimination of bacteria by phagocytes. Activation of these immune cells depends on the recognition of pathogen-associated molecular patterns, but these may also be hidden by matrix components that do not themselves trigger phagocyte activation efficiently. Moreover, prolonged use of antibiotics at higher doses to treat such infections may lead to drug resistance systemic and local toxicity, and potentially compromise bone growth, immune system surveillance and implant osseointegration [79, 80, 91, 93, 95-97]. Therefore, the preparation of multifunctional materials with the ability of repairing bone tissue, while preventing bacterial adhesion and subsequent biofilm formation at the implantation site, should be an important breakthrough in bone disease treatments.

2.3. Strategies for fighting bacterial infections

The quest to design and fabricate new antibacterial surfaces as an integral component of advanced biomaterials remains a high research priority. In order to eliminate or substantially reduce the extent of bacterial adhesion and biofilm formation on the surfaces, intensive efforts have been focused on the production of new antimicrobial biomaterials [98].

Antimicrobial surfaces can be distinguish between passive and active depending on whether there are antibacterial agents delivered locally. Passive surfaces do not release bactericidal agents to the surrounding tissues; these surfaces rely on inhibition of bacterial adhesion and/or kill bacteria upon contact. Passive surfaces are preferred as long as their antibacterial ability is strong enough to prevent biofilm formation. However, the effectiveness of such surfaces is limited and varies greatly depending on bacterial species. Also, the physicochemical properties of the surface can be masked by an adsorbed conditioning film of host proteins, thereby diminishing their effectiveness. In contrast, active surfaces are designed to release pre-incorporated bactericidal agents (i.e., antibiotics, silver ions, and peptides) immediately following the implantation to downregulate infection even in the presence of a surface-adsorbed protein layer [99-101].

Biomaterials endowed with anti-infective properties need to be tailored according to the specific application. The following sections describes various strategies developed to generate such biomaterials and the specific stimuli that are used to trigger antibacterial action. Anti-adhesive surfaces, surfaces with anti-infective organic agents, and surfaces with anti-infective inorganic agents are considered.

2.3.1. Anti-adhesive surfaces

The earliest step in the pathogenesis of foreign-body-related infections is bacterial adhesion. There is obviously no possibility for colonization to occur if bacteria cannot adhere to a solid surface. Anti-adhesive surfaces prevent bacteria attachment due to the presence of an unfavourable surface topography and/or chemistry with respect to the microorganisms. Clearly, bacterial adhesion in protein-free solution can be prevented by anti-adhesive surfaces that do not need to take into account protein behaviour and protein surface conditioning. In most cases, however, the devices are in contact with protein-rich solutions varying in composition depending on the anatomic site of application of the medical device. Therefore, the protein film rapidly formed on the biomaterial surface during the initial exposure to physiologic fluids should also be considered, since various host proteins mediate the bacterial adhesion through the interaction with bacterial adhesins [98, 102]. Poly(ethylene glycol) (PEG) functionalized surfaces have been demonstrated to drastically reduce protein adsorption, due to the formation of an interface layer that prevents direct contact between the surface and protein, thereby reducing bacterial colonization of the surface [103, 104]. Therefore, conditioning protein-surfaces and/or protein-bacteria interactions are good strategies to inhibit bacterial adhesion to a specific biomaterial. Low adhesiveness of these surfaces is certainly a great advantage for catheters, but in other internal applications could possibly hinder tissue adhesion and integration of the implant, since many surfaces that inhibit bacterial adhesion also limit mammalian cell adhesion, which is desired for osteogenesis and implant success. Therefore, since both infection prevention and osseointegration are requirements for a successful implant, it is

necessary to focus specifically on strategies able to inhibit bacterial colonization and concomitantly promote cell functions.

2.3.2. Surfaces with anti-infective organic agents

Controlled release of antibiotics are powerful therapeutic tools and effectively eradicate bacterial contamination. A large number of studies have investigated the efficacy of surfaces coated with covalently linked antibiotics [105-107]. However, high local antibiotic concentrations are only achieved over the short term. While controlled release of antibiotics provide an effective treatment of acute infection, at late treatment times surviving bacteria can slowly re-establish a biofilm that may lead to bacterial dissemination. Moreover, high levels of antibiotics may lead to tissue toxicity, compromising bone growth and implant osseointegration. Also, the effectiveness of surfaces with antibiotics is strongly dependent on the spectrum of activity of the chosen drug, and the possibility of development of antimicrobial resistance in a relatively short time period [108, 109].

Antimicrobial peptides (AMPs) are an extremely interesting group of anti-infective agents and currently sought as the next generation of antibiotics. AMPs are an integral part of the innate immune system of all multicellular organisms to protect them against invading microorganisms [110-112]. Most AMPs are small (12-50 amino acids), have a positive charge, and an amphipathic structure enables them to interact with bacterial membranes. AMPs have a broad spectrum of antimicrobial activity (against Gram-positive and negative bacteria, fungi, parasites, enveloped viruses, and even multidrug-resistant microorganisms) and possess low propensity for developing resistance. With their amphipathic nature, they directly act on the membrane of the pathogen. Cationic AMPs interact by electrostatic forces with the negatively charged surface of microbial membranes, namely, lipopolysaccharides in Gram-negative and teichoic acids in Gram-positive bacteria, causing disruption of bacterial membrane integrity [113-119]. AMPs may represent excellent coating agents with broad spectrum antimicrobial activity for preventing implant-associated infections [120-122]. Despite many attractive attributes, potential systemic and local toxicity, sensitization and

allergy after repeated application, susceptibility to proteases and pH changes, high manufacturing costs, constitute the main limitations associated to the use of AMPs [115, 117].

Recently, molecules and compounds that interfere with the expression of various bacterial phenotypes have shown great premise. Bacterial behavior within biofilms is regulated by the phenomenon of QS, where bacteria release chemical signals and express virulence genes in a cell density dependent manner. Different types of QS signals, also known as autoinducers (AIs), are involved in QS such as oligopeptides in Gram-positive bacteria and *N*-acyl-homoserine lactones (AHLs) in Gram-negative bacteria. Since QS is responsible for virulence in the clinically relevant bacteria, inhibition of QS appears to be a promising strategy to control these pathogenic bacteria. The interference with the microbial QS system by quorum quenching (QQ) is a potential approach that may lead to the development of the next generation anti-infective agents based on interfering with bacterial communication to block QS-mediated pathogenic infection. In particular, diverse QQ agents have been identified from various sources and organisms. All of the QQ agents may be classified into two groups according their molecular weight, small molecular and macromolecular QQ agents, which are also referred to as QS inhibitors and QQ enzymes, respectively. This QQ strategy does not aim to kill the pathogen or limit cell growth but to shut down the expression of the pathogenic gene. Thus, since the QQ approach does not affect the survival of the pathogen, it could avoid the appearance of resistances, which has been proposed as one of the main advantages of QQ strategies [123-128]. Nevertheless a recent study has demonstrated that QQ compounds can generate resistance in *P. aeruginosa* [129].

2.3.3. Surfaces with anti-infective inorganic agents

Recently, the confluence of nanotechnology and biology has brought to fore metals in the form of nanoparticles (NPs) as potent antimicrobial agents. Inorganic NPs with antimicrobial activity have been the center of research due to their physicochemical properties that can be exploited to promote remarkable applications in biomedicine.

High surface area to volume ratio of the NPs enhances their interaction with microbes leading to the upsurge in the research on NPs and their potential application as antimicrobials [130, 131]. The exact mechanisms for antibacterial effect of metallic nanoparticles are still being investigated but two more popular proposed possibilities include free metal ion toxicity arising from dissolution of the metals from surface of the NPs (i.e., Ag^+ from AgNPs) and oxidative stress via the generation of reactive oxygen species (ROS) on surfaces of the NPs [132]. Among metallic NPs, silver and gold nanoparticles gained importance as novel antimicrobial agents due to their strong antimicrobial properties against a wide range of microorganisms including multidrug-resistant bacteria.

Silver nanoparticles are the most widely used nanomaterial in healthcare today. AgNPs have been shown to be effective against a wide array of pathogens, such as fungi, viruses, and many bacterial species [133-135]. It has also been showed that AgNPs are potential antimicrobial agents against drug-resistant bacteria [136]. These superior antimicrobial, antifungal, and antiviral properties of AgNPs mean that are frequently present in coatings for bone implants, medical devices, catheters, and dental composites [137, 138]. The mechanisms underlying AgNPs microbial toxicity remain the subject of intense debate. Both contact killing and/or ion mediated killing have been proposed as the action mechanism of antimicrobial activity of AgNPs. The mechanism of silver ions release was showed by Xiu Z *et al*. where the toxicity of the AgNPs was explained by the presence of released Ag^+ [139]. The action mechanism of silver ions is still not completely understood, but there are some hypothesized mechanisms, mainly regarding direct Ag^+-induced membrane damage, Ag^+-related ROS production, and cellular uptake of Ag^+ ions, with consequent disruption of ATP production and hindering of DNA replication activities [140]. Nevertheless, the antimicrobial activity of AgNPs cannot be attributed solely to the released Ag^+ ions but also to the nanoparticle itself [141, 142]. The AgNPs have the ability to attach to the bacterial cell membrane, and also penetrate inside the bacteria causing damage by interacting with phosphorous- and sulfur-containing compounds like DNA. The NPs preferably attack the respiratory chain and cell division that finally lead to cell death [138].

Gold nanoparticles also have recently attracted a lot of attention because of their biocompatibility [143]. Additionally, the antimicrobial activity of AuNPs has been recently reported [144-146]. The exact mechanism of bacterial growth inhibition has not been elucidated yet, however some reports present the bacterial wall damage as the cause of the bacterial cell death. The AuNPs can interact with the functional groups on the bacterial cell surface to inactive bacteria and destroy them [147, 148].

Inorganic metal oxide nanoparticles, such as zinc oxide (ZnO) and titanium dioxide (TiO_2), are also being explored and extensively investigated as potential antimicrobials [131, 149]. The antimicrobial properties of zinc oxide-containing nanoparticles are mediated by the strong adherence of ZnO NPs to bacterial cell membranes and destruction of lipids and proteins of the membrane, resulting in a leakage of intracellular contents and eventually the bacterial cell death. In addition, generation of hydrogen peroxide and Zn^{+2} ions, which damage the bacterial cell, were suggested to be key antibacterial mechanisms of ZnO NPs [133, 150, 151]. Titanium dioxide-containing nanoparticles are the most studied for photocatalytic antimicrobial activity among various NPs. In a process called photocatalysis, TiO_2 NPs generates reactive oxygen species (ROS), including hydrogen peroxide and hydroxyl radicals, upon exposure to ultraviolet (UV) light. Then ROS damage bacterial cell membranes, thereby compromising membrane semipermeability, interfering with oxidative phosphorylation, and sometimes causing cell death [133, 152].

References

[1] Armentano I, Dottori M, Fortunati E, Mattioli S, Kenny JM. Biodegradable polymer matrix nanocomposites for tissue engineering: A review. Polymer Degradation and Stability 2010;95:2126-46.

[2] Thein-Han WW, Misra RDK. Biomimetic chitosan–nanohydroxyapatite composite scaffolds for bone tissue engineering. Acta Biomaterialia 2009;5:1182-97.

[3] Porter JR, Ruckh TT, Popat KC. Bone tissue engineering: a review in bone biomimetics and drug delivery strategies. Biotechnol Prog 2009;25:1539-60.

[4] Stevens MM. Biomaterials for bone tissue engineering. Mater Today 2008;11:18-25.

[5] Gómez S, Vlad MD, López J, Fernández E. Design and properties of 3D scaffolds for bone tissue engineering. Acta Biomaterialia 2016;42:341-50.

[6] Swetha M, Sahithi K, Moorthi A, Srinivasan N, Ramasamy K, Selvamurugan N. Biocomposites containing natural polymers and hydroxyapatite for bone tissue engineering. Int J Biol Macromol 2010;47:1-4.

[7] Fu Q, Saiz E, Rahaman MN, Tomsia AP. Bioactive glass scaffolds for bone tissue engineering: state of the art and future perspectives. Mat Sci Eng C-Mater 2011;31:1245-56.

[8] O'Brien FJ. Biomaterials & scaffolds for tissue engineering. Materials Today 2011;14:88-95.

[9] Lavernia CJ, Malinin TI, Temple HT, Moreyra CE. Bone and tissue allograft use by orthopaedic surgeons. The Journal of arthroplasty 2004;19:430-5.

[10] Costa-Pinto AR, Reis RL, Neves NM. Scaffolds based bone tissue engineering: the role of chitosan. Tissue Eng Part B Rev 2011;17:331-47.

[11] Liu Y, Lim J, Teoh SH. Review: development of clinically relevant scaffolds for vascularised bone tissue engineering. Biotechnol Adv 2013;31:688-705.

[12] Zhang Y, Venugopal JR, El-Turki A, Ramakrishna S, Su B, Lim CT. Electrospun biomimetic nanocomposite nanofibers of hydroxyapatite/chitosan for bone tissue engineering. Biomaterials 2008;29:4314-22.

[13] Hutmacher DW, Schantz JT, Lam CX, Tan KC, Lim TC. State of the art and future directions of scaffold-based bone engineering from a biomaterials perspective. J Tissue Eng Regen Med 2007;1:245-60.

[14] Proff P, Romer P. The molecular mechanism behind bone remodelling: a review. Clin Oral Investig 2009;13:355-62.

[15] Cartmell S. Controlled release scaffolds for bone tissue engineering. Journal of pharmaceutical sciences 2009;98:430-41.

[16] Hadjidakis DJ, Androulakis, II. Bone remodeling. Annals of the New York Academy of Sciences 2006;1092:385-96.

[17] Wu S, Liu X, Yeung KWK, Liu C, Yang X. Biomimetic porous scaffolds for bone tissue engineering. Materials Science and Engineering: R: Reports 2014;80:1-36.

[18] Jang J-H, Castano O, Kim H-W. Electrospun materials as potential platforms for bone tissue engineering. Advanced drug delivery reviews 2009;61:1065-83.

[19] Jayakumar P, Di Silvio L. Osteoblasts in bone tissue engineering. Proc Inst Mech Eng H 2010;224:1415-40.

[20] Clarke B. Normal bone anatomy and physiology. Clin J Am Soc Nephrol 2008;3 Suppl 3:S131-9.

[21] Vaananen HK, Laitala-Leinonen T. Osteoclast lineage and function. Arch Biochem Biophys 2008;473:132-8.

[22] Feng X, McDonald JM. Disorders of bone remodeling. Annu Rev Pathol 2011;6:121-45.

[23] Melke J, Midha S, Ghosh S, Ito K, Hofmann S. Silk fibroin as biomaterial for bone tissue engineering. Acta Biomaterialia 2016;31:1-16.

[24] Kassem M, Abdallah BM, Saeed H. Osteoblastic cells: Differentiation and trans-differentiation. Archives of Biochemistry and Biophysics 2008;473:183-7.

[25] Nakashima T. [Stress and cell communication between bone cells]. Clin Calcium 2013;23:1595-603.

[26] Henriksen K, Neutzsky-Wulff AV, Bonewald LF, Karsdal MA. Local communication on and within bone controls bone remodeling. Bone 2009;44:1026-33.

[27] Nakahama K. Cellular communications in bone homeostasis and repair. Cell Mol Life Sci 2010;67:4001-9.

[28] Gallagher JC, Sai AJ. Molecular biology of bone remodeling: implications for new therapeutic targets for osteoporosis. Maturitas 2010;65:301-7.

[29] Amini AR, Laurencin CT, Nukavarapu SP. Bone tissue engineering: recent advances and challenges. Critical reviews in biomedical engineering 2012;40:363-408.

[30] Gentile P, Mattioli-Belmonte M, Chiono V, Ferretti C, Baino F, Tonda-Turo C, et al. Bioactive glass/polymer composite scaffolds mimicking bone tissue. J Biomed Mater Res A 2012;100:2654-67.

[31] Pina S, Oliveira JM, Reis RL. Natural-based nanocomposites for bone tissue engineering and regenerative medicine: a review. Adv Mater 2015;27:1143-69.

[32] Wagoner Johnson AJ, Herschler BA. A review of the mechanical behavior of CaP and CaP/polymer composites for applications in bone replacement and repair. Acta Biomater 2011;7:16-30.

[33] Samavedi S, Whittington AR, Goldstein AS. Calcium phosphate ceramics in bone tissue engineering: a review of properties and their influence on cell behavior. Acta Biomater 2013;9:8037-45.

[34] Puppi D, Chiellini F, Piras AM, Chiellini E. Polymeric materials for bone and cartilage repair. Progress in Polymer Science 2010;35:403-40.

[35] Kundu B, Rajkhowa R, Kundu SC, Wang X. Silk fibroin biomaterials for tissue regenerations. Advanced drug delivery reviews 2013;65:457-70.

[36] Vepari C, Kaplan DL. Silk as a biomaterial. Progress in Polymer Science 2007;32:991-1007.

[37] Wang Y, Kim HJ, Vunjak-Novakovic G, Kaplan DL. Stem cell-based tissue engineering with silk biomaterials. Biomaterials 2006;27:6064-82.

[38] Wang Y, Rudym DD, Walsh A, Abrahamsen L, Kim HJ, Kim HS, et al. In vivo degradation of three-dimensional silk fibroin scaffolds. Biomaterials 2008;29:3415-28.

[39] Malafaya PB, Silva GA, Reis RL. Natural–origin polymers as carriers and scaffolds for biomolecules and cell delivery in tissue engineering applications. Advanced drug delivery reviews 2007;59:207-33.

[40] Kim U-J, Park J, Joo Kim H, Wada M, Kaplan DL. Three-dimensional aqueous-derived biomaterial scaffolds from silk fibroin. Biomaterials 2005;26:2775-85.

[41] Bhardwaj N, Chakraborty S, Kundu SC. Freeze-gelled silk fibroin protein scaffolds for potential applications in soft tissue engineering. International Journal of Biological Macromolecules 2011;49:260-7.

[42] Qiang Z, Shuqin Y, Mingzhong L. Silk Fibroin Based Porous Materials. Materials (1996-1944) 2009;2:2276-95.

[43] Rockwood DN, Preda RC, Yucel T, Wang X, Lovett ML, Kaplan DL. Materials fabrication from Bombyx mori silk fibroin. Nat Protoc 2011;6:1612-31.

[44] Hardy JG, Scheibel TR. Composite materials based on silk proteins. Progress in Polymer Science 2010;35:1093-115.

[45] Kasoju N, Bora U. Silk fibroin in tissue engineering. Advanced healthcare materials 2012;1:393-412.

[46] Ak F, Oztoprak Z, Karakutuk I, Okay O. Macroporous silk fibroin cryogels. Biomacromolecules 2013;14:719-27.

[47] Matsumoto A, Chen J, Collette AL, Kim UJ, Altman GH, Cebe P, et al. Mechanisms of silk fibroin sol-gel transitions. The journal of physical chemistry B 2006;110:21630-8.

[48] Ribeiro M, de Moraes MA, Beppu MM, Monteiro FJ, Ferraz MP. The role of dialysis and freezing on structural conformation, thermal properties and morphology of silk fibroin hydrogels. Biomatter 2014;4:e28536.

[49] Sashina ES, Bochek AM, Novoselov NP, Kirichenko DA. Structure and solubility of natural silk fibroin. Russian Journal of Applied Chemistry 2006;79:869-76.

[50] Vasconcelos A, Freddi G, Cavaco-Paulo A. Biodegradable Materials Based on Silk Fibroin and Keratin. Biomacromolecules 2008;9:1299-305.

[51] Cao Y, Wang B. Biodegradation of silk biomaterials. Int J Mol Sci 2009;10:1514-24.

[52] Pasqui D, Torricelli P, De Cagna M, Fini M, Barbucci R. Carboxymethyl cellulose-hydroxyapatite hybrid hydrogel as a composite material for bone tissue engineering applications. J Biomed Mater Res A 2014;102:1568-79.

[53] Geckil H, Xu F, Zhang X, Moon S, Demirci U. Engineering hydrogels as extracellular matrix mimics. Nanomedicine (London, England) 2010;5:469-84.

[54] Peppas NA, Hilt JZ, Khademhosseini A, Langer R. Hydrogels in Biology and Medicine: From Molecular Principles to Bionanotechnology. Advanced Materials 2006;18:1345-60.

[55] Gkioni K, Leeuwenburgh SC, Douglas TE, Mikos AG, Jansen JA. Mineralization of hydrogels for bone regeneration. Tissue Eng Part B Rev 2010;16:577-85.

[56] Wang X, Kluge JA, Leisk GG, Kaplan DL. Sonication-induced gelation of silk fibroin for cell encapsulation. Biomaterials 2008;29:1054-64.

[57] Lv Q, Hu K, Feng Q, Cui F. Fibroin/collagen hybrid hydrogels with crosslinking method: preparation, properties, and cytocompatibility. J Biomed Mater Res A 2008;84:198-207.

[58] Guziewicz N, Best A, Perez-Ramirez B, Kaplan DL. Lyophilized silk fibroin hydrogels for the sustained local delivery of therapeutic monoclonal antibodies. Biomaterials 2011;32:2642-50.

[59] Lammel AS, Hu X, Park SH, Kaplan DL, Scheibel TR. Controlling silk fibroin particle features for drug delivery. Biomaterials 2010;31:4583-91.

[60] Xiao W, He J, Nichol JW, Wang L, Hutson CB, Wang B, et al. Synthesis and characterization of photocrosslinkable gelatin and silk fibroin interpenetrating polymer network hydrogels. Acta Biomater 2011;7:2384-93.

[61] Nagarkar S, Patil A, Lele A, Bhat S, Bellare J, Mashelkar RA. Some Mechanistic Insights into the Gelation of Regenerated Silk Fibroin Sol. Industrial & Engineering Chemistry Research 2009;48:8014-23.

[62] Nogueira GM, de Moraes MA, Rodas ACD, Higa OZ, Beppu MM. Hydrogels from silk fibroin metastable solution: Formation and characterization from a biomaterial perspective. Materials Science and Engineering: C 2011;31:997-1001.

[63] Altman GH, Diaz F, Jakuba C, Calabro T, Horan RL, Chen J, et al. Silk-based biomaterials. Biomaterials 2003;24:401-16.

[64] Horan RL, Antle K, Collette AL, Wang Y, Huang J, Moreau JE, et al. In vitro degradation of silk fibroin. Biomaterials 2005;26:3385-93.

[65] Hu X, Lu Q, Sun L, Cebe P, Wang X, Zhang X, et al. Biomaterials from Ultrasonication-Induced Silk Fibroin−Hyaluronic Acid Hydrogels. Biomacromolecules 2010;11:3178-88.

[66] Poursamar SA, Azami M, Mozafari M. Controllable synthesis and characterization of porous polyvinyl alcohol/hydroxyapatite nanocomposite scaffolds via an in situ colloidal technique. Colloids and surfaces B, Biointerfaces 2011;84:310-6.

[67] Best SM, Porter AE, Thian ES, Huang J. Bioceramics: Past, present and for the future. Journal of the European Ceramic Society 2008;28:1319-27.

[68] Vallet-Regí M, González-Calbet JM. Calcium phosphates as substitution of bone tissues. Progress in Solid State Chemistry 2004;32:1-31.

[69] Kalita SJ, Bhardwaj A, Bhatt HA. Nanocrystalline calcium phosphate ceramics in biomedical engineering. Materials Science and Engineering: C 2007;27:441-9.

[70] Alves Cardoso D, Jansen JA, Leeuwenburgh SC. Synthesis and application of nanostructured calcium phosphate ceramics for bone regeneration. J Biomed Mater Res B Appl Biomater 2012;100:2316-26.

[71] Vallet-Regi M, Ruiz-Hernandez E. Bioceramics: from bone regeneration to cancer nanomedicine. Adv Mater 2011;23:5177-218.

[72] Fathi MH, Hanifi A, Mortazavi V. Preparation and bioactivity evaluation of bone-like hydroxyapatite nanopowder. Journal of Materials Processing Technology 2008;202:536-42.

[73] Tripathi G, Basu B. A porous hydroxyapatite scaffold for bone tissue engineering: Physico-mechanical and biological evaluations. Ceramics International 2012;38:341-9.

[74] Kalita SJ, Verma S. Nanocrystalline hydroxyapatite bioceramic using microwave radiation: Synthesis and characterization. Materials Science and Engineering: C 2010;30:295-303.

[75] Zhou H, Lee J. Nanoscale hydroxyapatite particles for bone tissue engineering. Acta Biomater 2011;7:2769-81.

[76] Raksujarit A, Pengpat K, Rujijanagul G, Tunkasiri T. Processing and properties of nanoporous hydroxyapatite ceramics. Materials & Design 2010;31:1658-60.

[77] Gaharwar AK, Dammu SA, Canter JM, Wu CJ, Schmidt G. Highly extensible, tough, and elastomeric nanocomposite hydrogels from poly(ethylene glycol) and hydroxyapatite nanoparticles. Biomacromolecules 2011;12:1641-50.

[78] Fu S, Ni P, Wang B, Chu B, Zheng L, Luo F, et al. Injectable and thermo-sensitive PEG-PCL-PEG copolymer/collagen/n-HA hydrogel composite for guided bone regeneration. Biomaterials 2012;33:4801-9.

[79] Arciola CR, Campoccia D, Speziale P, Montanaro L, Costerton JW. Biofilm formation in Staphylococcus implant infections. A review of molecular mechanisms and implications for biofilm-resistant materials. Biomaterials 2012;33:5967-82.

[80] Schaer TP, Stewart S, Hsu BB, Klibanov AM. Hydrophobic polycationic coatings that inhibit biofilms and support bone healing during infection. Biomaterials 2012;33:1245-54.

[81] Zilberman M, Elsner JJ. Antibiotic-eluting medical devices for various applications. J Control Release 2008;130:202-15.

[82] Nablo BJ, Rothrock AR, Schoenfisch MH. Nitric oxide-releasing sol-gels as antibacterial coatings for orthopedic implants. Biomaterials 2005;26:917-24.

[83] Blackledge MS, Worthington RJ, Melander C. Biologically inspired strategies for combating bacterial biofilms. Current opinion in pharmacology 2013;13:699-706.

[84] Rhoads DD, Wolcott RD, Percival SL. Biofilms in wounds: management strategies. Journal of wound care 2008;17:502-8.

[85] Trampuz A, Zimmerli W. Diagnosis and treatment of implant-associated septic arthritis and osteomyelitis. Current infectious disease reports 2008;10:394-403.

[86] Esposito S, Leone S. Prosthetic joint infections: microbiology, diagnosis, management and prevention. International journal of antimicrobial agents 2008;32:287-93.

[87] Trampuz A, Zimmerli W. Prosthetic joint infections: update in diagnosis and treatment. Swiss medical weekly 2005;135:243-51.

[88] Campoccia D, Montanaro L, Arciola CR. The significance of infection related to orthopedic devices and issues of antibiotic resistance. Biomaterials 2006;27:2331-9.

[89] Teterycz D, Ferry T, Lew D, Stern R, Assal M, Hoffmeyer P, et al. Outcome of orthopedic implant infections due to different staphylococci. International journal of infectious diseases : IJID : official publication of the International Society for Infectious Diseases 2010;14:e913-8.

[90] Dwivedi P, Narvi SS, Tewari RP. Application of polymer nanocomposites in the nanomedicine landscape: envisaging strategies to combat implant associated infections. Journal of applied biomaterials & functional materials 2013;11:e129-42.

[91] Joo HS, Otto M. Molecular basis of in vivo biofilm formation by bacterial pathogens. Chemistry & biology 2012;19:1503-13.

[92] Otto M. Staphylococcal infections: mechanisms of biofilm maturation and detachment as critical determinants of pathogenicity. Annual review of medicine 2013;64:175-88.

[93] Otto M. Staphylococcal biofilms. Curr Top Microbiol Immunol 2008;322:207-28.

[94] Bryers JD. Medical biofilms. Biotechnol Bioeng 2008;100:1-18.

[95] Zimmerli W, Moser C. Pathogenesis and treatment concepts of orthopaedic biofilm infections. FEMS immunology and medical microbiology 2012;65:158-68.

[96] Zimmerli W, Sendi P. Pathogenesis of implant-associated infection: the role of the host. Seminars in immunopathology 2011;33:295-306.

[97] Glinel K, Thebault P, Humblot V, Pradier CM, Jouenne T. Antibacterial surfaces developed from bio-inspired approaches. Acta Biomater 2012;8:1670-84.

[98] Hasan J, Crawford RJ, Ivanova EP. Antibacterial surfaces: the quest for a new generation of biomaterials. Trends in Biotechnology 2013;31:295-304.

[99] Sileika TS, Kim HD, Maniak P, Messersmith PB. Antibacterial performance of polydopamine-modified polymer surfaces containing passive and active components. ACS applied materials & interfaces 2011;3:4602-10.

[100] Hetrick EM, Schoenfisch MH. Reducing implant-related infections: active release strategies. Chemical Society reviews 2006;35:780-9.

[101] Charville GW, Hetrick EM, Geer CB, Schoenfisch MH. Reduced bacterial adhesion to fibrinogen-coated substrates via nitric oxide release. Biomaterials 2008;29:4039-44.

[102] Beloin C, Renard S, Ghigo JM, Lebeaux D. Novel approaches to combat bacterial biofilms. Current opinion in pharmacology 2014;18:61-8.

[103] Harris LG, Tosatti S, Wieland M, Textor M, Richards RG. Staphylococcus aureus adhesion to titanium oxide surfaces coated with non-functionalized and peptide-functionalized poly(l-lysine)-grafted-poly(ethylene glycol) copolymers. Biomaterials 2004;25:4135-48.

[104] Yu Q, Zhang Y, Wang H, Brash J, Chen H. Anti-fouling bioactive surfaces. Acta Biomater 2011;7:1550-7.

[105] Alt V, Bitschnau A, Osterling J, Sewing A, Meyer C, Kraus R, et al. The effects of combined gentamicin-hydroxyapatite coating for cementless joint prostheses on the reduction of infection rates in a rabbit infection prophylaxis model. Biomaterials 2006;27:4627-34.

[106] Antoci V, Jr., King SB, Jose B, Parvizi J, Zeiger AR, Wickstrom E, et al. Vancomycin covalently bonded to titanium alloy prevents bacterial colonization. J Orthop Res 2007;25:858-66.

[107] Neut D, Dijkstra RJ, Thompson JI, van der Mei HC, Busscher HJ. A gentamicin-releasing coating for cementless hip prostheses-Longitudinal evaluation of efficacy using in vitro bio-optical imaging and its wide-spectrum antibacterial efficacy. J Biomed Mater Res A 2012;100:3220-6.

[108] Hickok NJ, Shapiro IM. Immobilized antibiotics to prevent orthopaedic implant infections. Advanced drug delivery reviews 2012;64:1165-76.

[109] Palumbi SR. Humans as the world's greatest evolutionary force. Science 2001;293:1786-90.

[110] Yount NY, Yeaman MR. Emerging themes and therapeutic prospects for anti-infective peptides. Annual review of pharmacology and toxicology 2012;52:337-60.

[111] Salwiczek M, Qu Y, Gardiner J, Strugnell RA, Lithgow T, McLean KM, et al. Emerging rules for effective antimicrobial coatings. Trends Biotechnol 2014;32:82-90.

[112] Scott RW, DeGrado WF, Tew GN. De novo designed synthetic mimics of antimicrobial peptides. Curr Opin Biotechnol 2008;19:620-7.

[113] Matsuzaki K. Control of cell selectivity of antimicrobial peptides. Biochim Biophys Acta 2009;1788:1687-92.

[114] Giuliani A, Pirri G, Nicoletto SF. Antimicrobial peptides: an overview of a promising class of therapeutics. Central European Journal of Biology 2007;2:1-33.

[115] Gordon YJ, Romanowski EG, McDermott AM. A review of antimicrobial peptides and their therapeutic potential as anti-infective drugs. Current eye research 2005;30:505-15.

[116] Auvynet C, Rosenstein Y. Multifunctional host defense peptides: antimicrobial peptides, the small yet big players in innate and adaptive immunity. The FEBS journal 2009;276:6497-508.

[117] Seo MD, Won HS, Kim JH, Mishig-Ochir T, Lee BJ. Antimicrobial peptides for therapeutic applications: a review. Molecules (Basel, Switzerland) 2012;17:12276-86.

[118] Guani-Guerra E, Santos-Mendoza T, Lugo-Reyes SO, Teran LM. Antimicrobial peptides: general overview and clinical implications in human health and disease. Clinical immunology (Orlando, Fla) 2010;135:1-11.

[119] Muszanska AK, Rochford ET, Gruszka A, Bastian AA, Busscher HJ, Norde W, et al. Antiadhesive polymer brush coating functionalized with antimicrobial and RGD

peptides to reduce biofilm formation and enhance tissue integration. Biomacromolecules 2014;15:2019-26.

[120] Kazemzadeh-Narbat M, Kindrachuk J, Duan K, Jenssen H, Hancock RE, Wang R. Antimicrobial peptides on calcium phosphate-coated titanium for the prevention of implant-associated infections. Biomaterials 2010;31:9519-26.

[121] Chen R, Cole N, Willcox MD, Park J, Rasul R, Carter E, et al. Synthesis, characterization and in vitro activity of a surface-attached antimicrobial cationic peptide. Biofouling 2009;25:517-24.

[122] Kazemzadeh-Narbat M, Lai BF, Ding C, Kizhakkedathu JN, Hancock RE, Wang R. Multilayered coating on titanium for controlled release of antimicrobial peptides for the prevention of implant-associated infections. Biomaterials 2013;34:5969-77.

[123] Rasmussen TB, Givskov M. Quorum-sensing inhibitors as anti-pathogenic drugs. International journal of medical microbiology : IJMM 2006;296:149-61.

[124] Chen F, Gao Y, Chen X, Yu Z, Li X. Quorum Quenching Enzymes and Their Application in Degrading Signal Molecules to Block Quorum Sensing-Dependent Infection. International Journal of Molecular Sciences 2013;14:17477.

[125] Kalia VC. Quorum sensing inhibitors: an overview. Biotechnol Adv 2013;31:224-45.

[126] Tang K, Zhang XH. Quorum quenching agents: resources for antivirulence therapy. Marine drugs 2014;12:3245-82.

[127] Romero M, Acuna L, Otero A. Patents on quorum quenching: interfering with bacterial communication as a strategy to fight infections. Recent patents on biotechnology 2012;6:2-12.

[128] Gomes J, Grunau A, Lawrence AK, Eberl L, Gademann K. Bioinspired, releasable quorum sensing modulators. Chem Commun (Camb) 2013;49:155-7.

[129] Maeda T, Garcia-Contreras R, Pu M, Sheng L, Garcia LR, Tomas M, et al. Quorum quenching quandary: resistance to antivirulence compounds. The ISME journal 2012;6:493-501.

[130] Seil JT, Webster TJ. Antimicrobial applications of nanotechnology: methods and literature. Int J Nanomedicine 2012;7:2767-81.

[131] Azam A, Ahmed AS, Oves M, Khan MS, Habib SS, Memic A. Antimicrobial activity of metal oxide nanoparticles against Gram-positive and Gram-negative bacteria: a comparative study. Int J Nanomedicine 2012;7:6003-9.

[132] Besinis A, De Peralta T, Handy RD. The antibacterial effects of silver, titanium dioxide and silica dioxide nanoparticles compared to the dental disinfectant chlorhexidine on Streptococcus mutans using a suite of bioassays. Nanotoxicology 2014;8:1-16.

[133] Blecher K, Nasir A, Friedman A. The growing role of nanotechnology in combating infectious disease. Virulence 2011;2:395-401.

[134] Hindi KM, Ditto AJ, Panzner MJ, Medvetz DA, Han DS, Hovis CE, et al. The antimicrobial efficacy of sustained release silver-carbene complex-loaded L-tyrosine polyphosphate nanoparticles: characterization, in vitro and in vivo studies. Biomaterials 2009;30:3771-9.

[135] Knetsch MLW, Koole LH. New Strategies in the Development of Antimicrobial Coatings: The Example of Increasing Usage of Silver and Silver Nanoparticles. Polymers 2011;3:340.

[136] Lara HH, Ayala-Núñez NV, Ixtepan Turrent LdC, Rodríguez Padilla C. Bactericidal effect of silver nanoparticles against multidrug-resistant bacteria. World Journal of Microbiology and Biotechnology 2010;26:615-21.

[137] Chaloupka K, Malam Y, Seifalian AM. Nanosilver as a new generation of nanoproduct in biomedical applications. Trends in Biotechnology;28:580-8.

[138] Rai M, Yadav A, Gade A. Silver nanoparticles as a new generation of antimicrobials. Biotechnol Adv 2009;27:76-83.

[139] Xiu ZM, Zhang QB, Puppala HL, Colvin VL, Alvarez PJ. Negligible particle-specific antibacterial activity of silver nanoparticles. Nano Lett 2012;12:4271-5.

[140] Rizzello L, Pompa PP. Nanosilver-based antibacterial drugs and devices: mechanisms, methodological drawbacks, and guidelines. Chemical Society reviews 2014;43:1501-18.

[141] Lubick N. Nanosilver toxicity: ions, nanoparticles—or both? Environmental Science & Technology 2008;42:8617-.

[142] Fabrega J, Fawcett SR, Renshaw JC, Lead JR. Silver Nanoparticle Impact on Bacterial Growth: Effect of pH, Concentration, and Organic Matter. Environmental Science & Technology 2009;43:7285-90.

[143] Bhattacharya R, Mukherjee P. Biological properties of "naked" metal nanoparticles. Advanced drug delivery reviews 2008;60:1289-306.

[144] Zhang Y, Peng H, Huang W, Zhou Y, Yan D. Facile preparation and characterization of highly antimicrobial colloid Ag or Au nanoparticles. Journal of Colloid and Interface Science 2008;325:371-6.

[145] Badwaik VD, Vangala LM, Pender DS, Willis CB, Aguilar ZP, Gonzalez MS, et al. Size-dependent antimicrobial properties of sugar-encapsulated gold nanoparticles synthesized by a green method. Nanoscale research letters 2012;7:623.

[146] Li X, Robinson SM, Gupta A, Saha K, Jiang Z, Moyano DF, et al. Functional Gold Nanoparticles as Potent Antimicrobial Agents against Multi-Drug-Resistant Bacteria. ACS Nano 2014;8:10682-6.

[147] Regiel-Futyra A, Kus-Liśkiewicz M, Sebastian V, Irusta S, Arruebo M, Stochel G, et al. Development of Noncytotoxic Chitosan–Gold Nanocomposites as Efficient Antibacterial Materials. ACS applied materials & interfaces 2015;7:1087-99.

[148] Wani IA, Ahmad T, Manzoor N. Size and shape dependant antifungal activity of gold nanoparticles: a case study of Candida. Colloids and surfaces B, Biointerfaces 2013;101:162-70.

[149] Reddy KM, Feris K, Bell J, Wingett DG, Hanley C, Punnoose A. Selective toxicity of zinc oxide nanoparticles to prokaryotic and eukaryotic systems. Applied physics letters 2007;90:2139021-3.

[150] Huang Z, Zheng X, Yan D, Yin G, Liao X, Kang Y, et al. Toxicological Effect of ZnO Nanoparticles Based on Bacteria. Langmuir : the ACS journal of surfaces and colloids 2008;24:4140-4.

[151] Zhang L, Ding Y, Povey M, York D. ZnO nanofluids – A potential antibacterial agent. Progress in Natural Science 2008;18:939-44.

[152] Carre G, Hamon E, Ennahar S, Estner M, Lett MC, Horvatovich P, et al. TiO2 photocatalysis damages lipids and proteins in Escherichia coli. Appl Environ Microbiol 2014;80:2573-81.

NOTE: In the following Chapters whenever the text reproduces a manuscript from the author of this thesis, published in a scientific journal or under submission, the respective numbers of figures, tables and references are attributed specifically in accordance with that article, exactly as they appear in the original text.

CHAPTER II

The role of dialysis and freezing on structural conformation, thermal properties and morphology of silk fibroin hydrogels

Marta Ribeiro[1,2,*], Mariana A de Moraes[3], Marisa M Beppu[3], Fernando J Monteiro[1,2], Maria P Ferraz[1,4]

[1] Instituto de Engenharia Biomédica; Universidade do Porto; Porto, Portugal.

[2] Departamento de Engenharia Metalúrgica e Materiais; Universidade do Porto, Porto, Portugal.

[3] Faculdade de Engenharia Química; Universidade Estadual de Campinas; Campinas, Brasil.

[4] Centro de Estudos em Biomedicina; Universidade Fernando Pessoa; Porto, Portugal.

Biomatter, 2014; 4:e28536.

Abstract

Silk fibroin has been widely explored for many biomedical applications, due to its biocompatibility and biodegradability. The aim of this work was to study the role of dialysis and freezing on structural conformation, thermal properties and morphology of silk fibroin hydrogels. Hydrogels were prepared after 3 and 7 days of dialysis and the effect of freezing was analyzed. For that purpose, a part of the fibroin hydrogels underwent freezing at -20 °C for 24 hours, followed by lyophilization and the rest of the hydrogels were kept at 8 °C for 24 hours, with further lyophilization. The fibroin hydrogels were characterized by X-ray diffraction (XRD), Fourier transformed infrared spectroscopy (FTIR), thermogravimetric analysis (TGA) and scanning electron microscopy (SEM). Measurements by XRD and FTIR indicated that silk I and silk II structures were present in the fibroin hydrogels and that the secondary structure of fibroin is transformed mostly to β-sheet during the gelation process. Thermal analysis indicated that fibroin hydrogels are thermally stable with the degradation peak at around 330-340 °C. SEM micrographs showed porous structures and the fibroin hydrogels subjected to freezing presented a much larger pore size. Results indicate that the dialysis time and freezing did not alter the material crystallinity, conformation or thermal behavior; however, hydrogel microstructure was strongly affected by dialysis time and freezing, showing controlled pores size. This study provides fundamental knowledge on silk fibroin hydrogels preparation and properties and the studied hydrogels are promising to be used in the biomaterial field.

Keywords: Biomaterials; Biopolymer; Silk fibroin; Gelation; Scaffold

Introduction

Replacement of functional tissues requires the development of three-dimensional (3D) scaffolds that can provide an optimum microenvironment for tissue growth and regeneration [1, 2]. Pore architecture in 3D polymeric scaffolds is known to play a critical role in tissue engineering as it provides the growth, adhesion, migration and proliferation of cells. Therefore, the scaffolds should have suitable properties such as interconnecting network of pores for the effective migration, growth and attachment of cells, sufficient porosity for the effective transport of nutrients and waste, biocompatibility, and biodegradation properties, for being exploited in tissue engineering applications [3].

Silk fibroin (SF) derived from *Bombyx mori* silkworm is a structural protein which possesses many important properties for tissue engineering and regenerative medicine, such as versatile processing, slow biodegradation, good biocompatibility, low immunogenicity, low inflammatory response, adjustable mechanical properties, high permeability to oxygen and water vapor and resistance to enzymatic degradation [4-6].

The cocoon of the silkworm is mainly composed of two protein components, fibroin and sericin. Fibroin is the water insoluble structural protein component of silk fibers whereas sericin is the water-soluble glue-like protein that holds SF fibers together [4]. Since the sericin contamination was identified to be the main source of problems, such as unwanted immunological reactions *in vivo* [7, 8], purified SF has become a novel, promising biomaterial and has found increasing numbers of applications in clinical devices including in tissue engineering of cartilage, bone, muscle, ligament and tendon tissues [9-13]. Fibroin is the core protein which accounts for 70% of the cocoon and is a hydrophobic glycoprotein [4]. SF consists mainly of the amino acids glycine, alanine and serine which form antiparallel β-sheets in the spun fibers and provide stability and interesting mechanical properties to the fibers [4, 14]. SF can assume distinct conformations; α-helix and random-coil conformations (also called silk I) and the β-sheet conformation (silk II). Silk I is a metastable form that is soluble in water and silk II is insoluble in water and is the most stable structure, where SF chains are connected by hydrogen bonds between the adjacent segments of polypeptide chains [5, 15-17].

SF fibers, extracted from *B. mori* cocoons, are insoluble in water and in the majority of organic solvents. SF dissolves in concentrated acid solutions and in concentrated aqueous, organic and aqueous-organic salts solutions [18]. These solutions contain highly concentrated salts that need to be removed by dialysis in order to prepare SF-based materials, such as hydrogels [19], films [17] and nanoparticles [20]. SF solution after dialysis is metastable (predominance of silk I) and it can easily convert to a more stable form, by a conformational transition to silk II, forming stable hydrogels. SF gelation from aqueous solution is a kinetic process and depends on factors such as SF concentration, temperature, pH [21] and presence of other materials, such as poly(*N*-isopropylacrylamide) [22] and poly(ethylene oxide) polymers [23]. SF gelation process is also influenced by dialysis parameters, since the rate of salt removal will directly influence the conformational transition of SF. The rate of salt removal can influence SF conformational transition, since the salt is responsible for SF solvation and stabilization in solution. When salt is removed, a metastable solution is obtained and at this point gelation is just a kinetic process. If the necessary amount of salt is not removed during dialysis, SF-based materials cannot be prepared due to the strong salt solvation. On the contrary, the more salt is removed, the more rapid is the gelation process [19]. Thus, dialysis is a key parameter on SF gelation and the study of dialysis time is important to define SF hydrogels properties.

Cryogenic processes, based on freezing of hydrogels, and subsequent lyophilization, are widely used for scaffold preparation because of the biocompatibility of both the template and the process for template removal [24-26]. During the freezing step, solvent crystals grow at a controllable rate and solute molecules are excluded from the frozen solvent until the sample is completely frozen. The freezing step is very important in order to produce desirable porous structures, with control over the pores size and quantity, depending on parameters such as freezing temperature and rate [27].

The purpose of the present study was to study the role of dialysis and freezing on structural conformation, thermal properties and morphology of silk fibroin hydrogels. Hydrogels were prepared after 3 and 7 d of dialysis and the effect of freezing was analyzed. The structure and properties of SF hydrogels were determined by X-ray

diffraction (XRD), Fourier transformed infrared spectroscopy (FTIR), thermogravimetric analysis (TGA) and scanning electron microscopy (SEM).

Results

Crystallinity

Figure 1 shows the X-ray diffractograms of SF hydrogels prepared from SF solution subjected to different dialysis time and freezing. The halos at 2θ = 20.4°, 2θ = 20.2°, 2θ = 20.7° and 2θ = 20.6° appearing in the XRD spectra of SF hydrogels formed at 37 °C after 3 d of dialysis subjected to freezing (Fig. 1A), SF hydrogels formed at 37 °C after 3 d of dialysis kept at 8 °C (Fig. 1B), SF hydrogels formed at 37 °C after 7 d of dialysis subjected to freezing (Fig. 1C) and SF hydrogels formed at 37 °C after 7 d of dialysis kept at 8 °C (Fig. 1D), respectively, are attributed to the silk II (β-sheet) conformation [14, 20, 28-30].

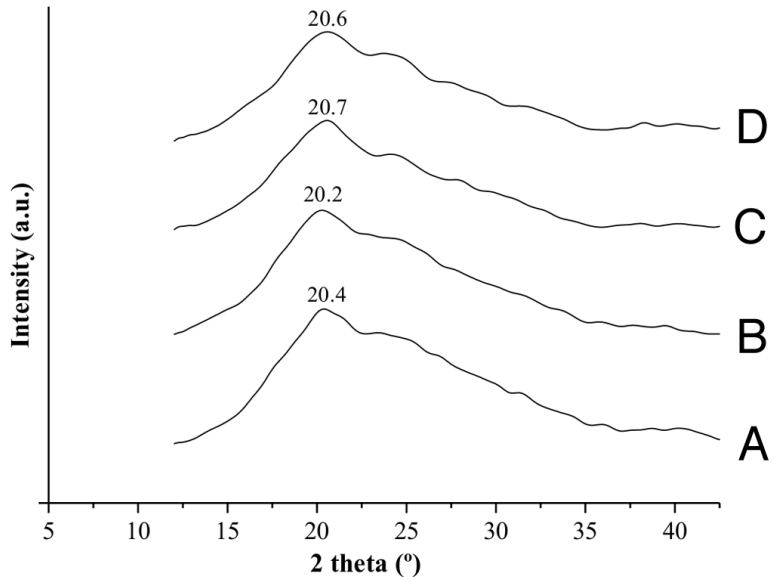

Figure 1. X-ray diffractograms of SF hydrogels formed at 37 °C after 3 d of dialysis subjected to freezing (A) or kept at 8 °C (B) and SF hydrogels formed after 7 d of dialysis subjected to freezing (C) or kept at 8 °C (D).

Structural conformation

By analyzing the infrared spectrum, the structural conformation of SF can be determined, depending on the wavenumber location of the absorption bands of amides I, II and III. Amide I, II, and III bands are attributed to C = O stretching, N-H deformation, and O-C-N bending, respectively [31].

The infrared spectra of the SF hydrogels are shown in Figure 2. The SF hydrogel formed at 37 °C after 3 d of dialysis and subjected to freezing (Fig. 2A) presented absorption bands at 1625 cm^{-1} (amide I) and 1525 cm^{-1} (amide II), corresponding to the silk II structural conformation [32-34]. Other adsorption band was observed at 1234 cm cm^{-1} (amide III), which is characteristic of the silk I conformation [35].

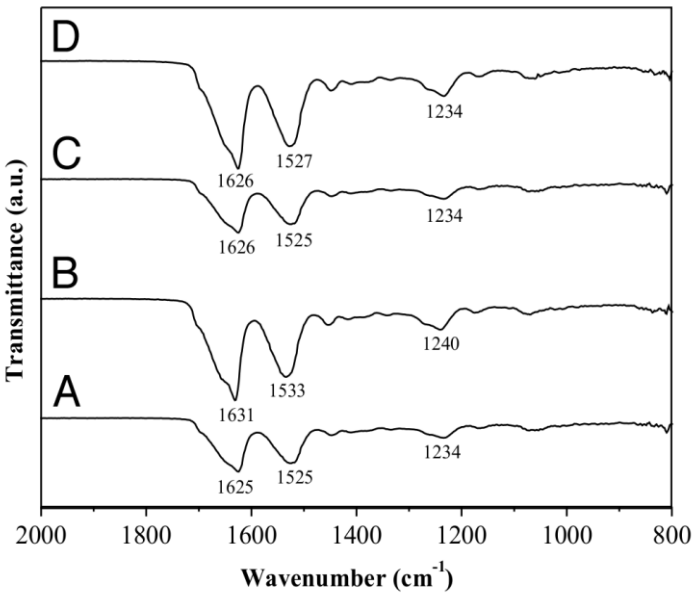

Figure 2. FTIR-ATR spectra of SF hydrogels formed at 37 °C after 3 d of dialysis subjected to freezing (A) or kept at 8 °C (B) and SF hydrogels formed after 7 d of dialysis subjected to freezing (C) or kept at 8 °C (D).

The SF hydrogel formed at 37 °C after 3 d of dialysis and kept at 8 °C (Fig. 2B) showed adsorption bands at 1631 cm^{-1} (amide I) and 1533 cm cm^{-1} (amide II), indicating the existence of the silk II structural conformation [32-34]. The adsorption band at 1240 cm^{-1} (amide III) is characteristic of the silk I conformation [36].

The SF hydrogels formed after 7 d of dialysis subjected to freezing or not (Fig. 2C and D, respectively) presented similar spectra, with adsorption band at 1635 cm^{-1} (amide I)

corresponding to the SF silk II structural conformation [32-34]. The adsorption bands at 1525 and 1527 cm^{-1} (amide II), for SF hydrogels formed after 7 d of dialysis subjected to freezing or not (Fig. 2C and D, respectively), is also attributed to the SF silk II structural conformation [32, 34]. The adsorption band at 1234 cm^{-1} (amide III), for both SF hydrogels formed after 7 d of dialysis is ascribed as silk I structural conformation [35].

In all the analyzed hydrogels the co-existence of silk I and silk II conformations was observed, which is typical of SF hydrogels.

Thermal analysis

Thermogravimetric curves of SF hydrogels are shown in Figure 3. The thermograms of all samples showed similar trend. The initial weight loss of SF hydrogels at around 100 °C is due to loss of water. The second weight loss took place within the temperature range between 270 and 380 °C and is associated with the breakdown of side chain groups of amino acid residues as well as the cleavage of peptide bonds [37, 38].

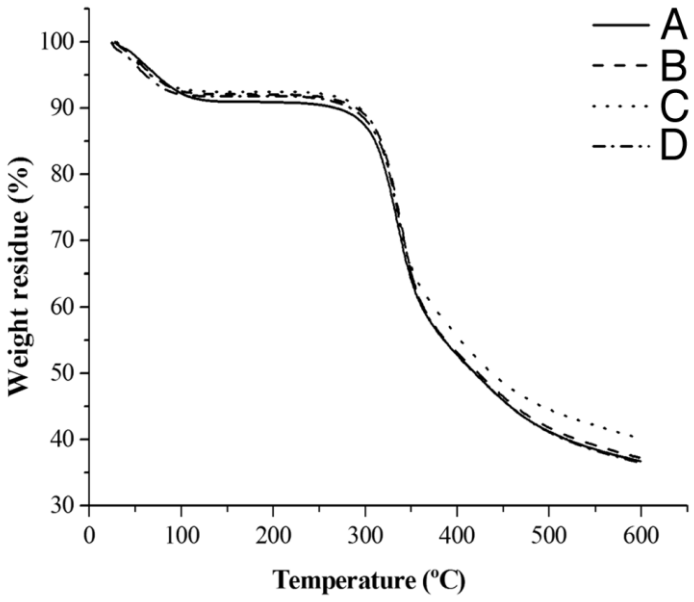

Figure 3. TGA curves of SF hydrogels formed at 37 °C after 3 d of dialysis subjected to freezing (A) or kept at 8 °C (B) and SF hydrogels formed after 7 d of dialysis subjected to freezing (C) or kept at 8 °C (D).

For observation of SF hydrogels degradation peaks, derivate of the thermogravimetric curves were analyzed, as shown in Figure 4. It is possible to observe that all samples presented similar behavior, with a peak at around 330–340 °C, which is attributed to the thermal degradation of SF hydrogels.

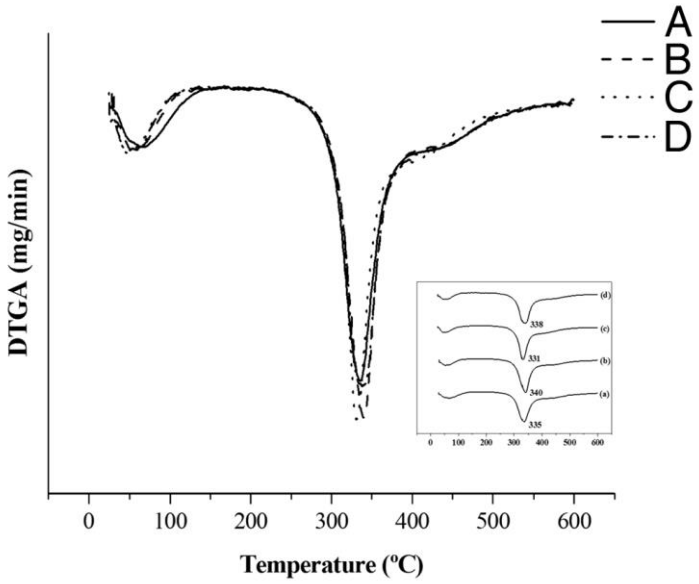

Figure 4. DTGA wide scan curves of SF hydrogels and detected degradation peaks (inset) in all hydrogels. SF hydrogels formed at 37 °C after 3 d of dialysis subjected to freezing (A) or kept at 8 °C (B) and SF hydrogels formed after 7 d of dialysis subjected to freezing (C) or kept at 8 °C (D).

Morphology

Figure 5 shows the micrographs of the SF hydrogels porous structure obtained by SEM. These revealed that all samples had 3D morphologies with uniform porous structures and they showed the effect of freezing on SF hydrogels formed at 37 °C after 3 d of dialysis (Fig. 5A) and SF hydrogels formed after 7 d of dialysis (Fig. 5C), which were frozen at -20 °C for 24 h, compared with the SF hydrogels kept at 8 °C (Fig. 5B and D). The SF hydrogels subjected to freezing presented a pore size much larger than the hydrogels kept at 8 °C. Moreover, it is possible to see that the SF hydrogels formed after 7 d of dialysis kept at 8 °C showed a thicker fibroin network with smaller pores (Fig. 5D) than SF hydrogels formed after 3 d of dialysis (Fig. 5B).

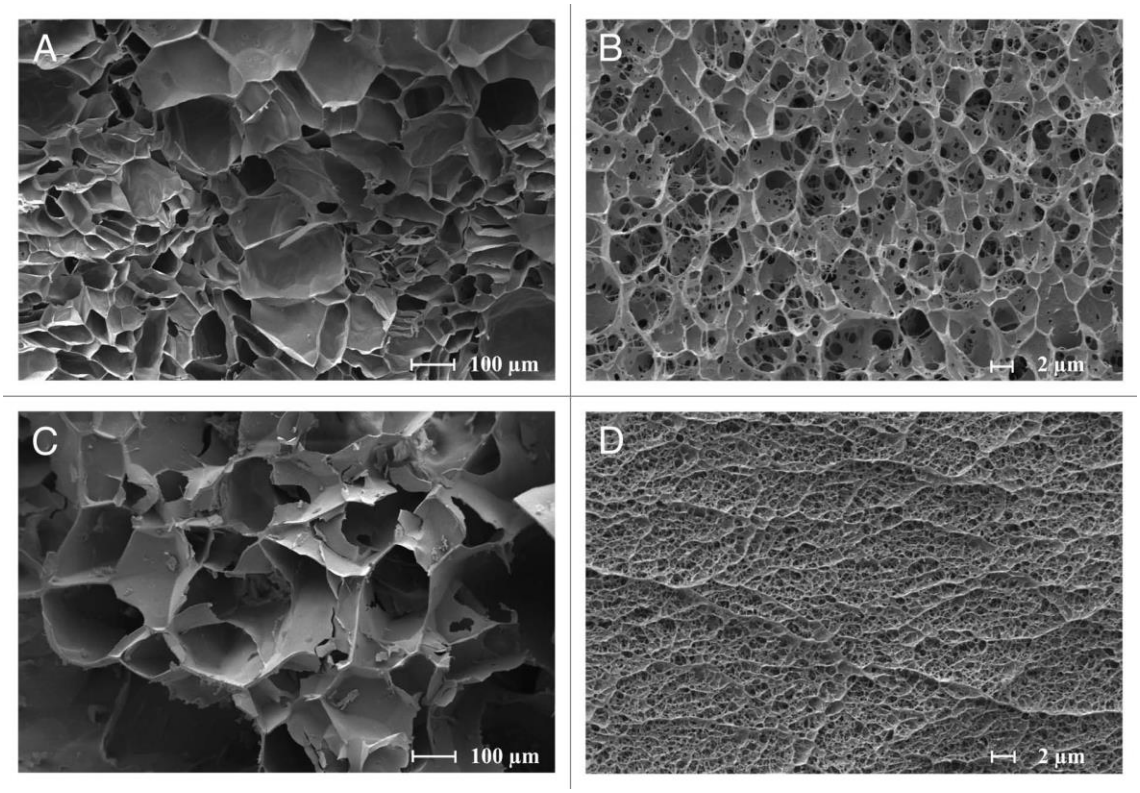

Figure 5. SEM micrographs of the porous structure SF hydrogels formed at 37 °C after 3 d of dialysis subjected to freezing (A) or kept at 8 °C (B) and SF hydrogels formed after 7 d of dialysis subjected to freezing (C) or kept at 8 °C (D).

Discussion

Significant work has been performed over the last decade to develop natural polymers for biomedical applications, particularly for biocompatible implantable materials [39]. Among natural polymers, silk is an interesting candidate component for tissue engineering. The goal of this research was to study the role of dialysis and freezing on structural conformation, thermal properties and morphology of silk fibroin hydrogels.

The SF solution, before dialysis, is supersaturated and can be stored without undergoing gelation for several months. This happens due to the high ionic strength that promotes SF fibers solvation. During the dialysis, the salt ions diffuse from SF solution into the dialysis water and the ionic force decreases. This allows more interaction between SF molecules and the solution may undergo a sol-gel transition [19].

Through X-ray diffraction measurement, some information about SF crystalline structure and its conformations of silk I and silk II can be obtained from its crystal structure transition. The distinct halos found in the X-ray diffractograms at 2θ = 20.4°, 2θ = 20.2°, 2θ = 20.7° and 2θ = 20.6° for SF hydrogels presented typical patterns of β-sheet structure (silk II). Previous studies by Kim *et al*. presented that all hydrogels prepared in your work showed a distinct halo at 2θ = 20.6°, which is attributed to β-sheet crystalline structure of SF [14]. Kundu *et al*. observed a halo at 2θ = 20.2° denoting the silk II structure appeared in the XRD pattern of the SF nanoparticles made from *B. mori* protein [20]. Kim *et al*. observed a halo at 2θ = 20.4° for SF scaffolds indicating that is a β-sheet crystalline structure (silk II) [28]. Lv *et al*. showed the presence of the diffraction halo at 2θ = 20.7° in silk fibroin films, corresponding to β-sheet structure [30]. This β-sheet conformation is formed during SF solution gelation, as a result of SF molecular chain dehydration and their intra and intermolecular hydrogen bond formations. In solution, SF molecules are predominantly organized into the α-helix and random coil structure. However, this structure tends to convert to the β-sheet upon hydrogel formation, which is thermodynamically more stable [40]. No remarkable differences were observed in the XRD spectra of the SF hydrogels formed under different conditions within this study.

FTIR spectroscopy is very sensitive to conformational modifications of silk fibroin. Each SF crystalline form shows a specific absorption band in distinct vibrational regions associated with the amide groups in proteins. The more interesting infrared bands to analyze proteins are the amide bands: amide I, amide II and amide III [31]. Results of FTIR investigation showed that there were slight shifts of the adsorption bands of amides but without conformational changes. This indicates that SF presented in the hydrogel is highly stable and does not change its conformation due to changes in external factors.

Thermal decomposition of SF is mainly influenced by the intrinsic morphological and physical properties of the protein [41, 42]. The results obtained by TGA suggest that SF hydrogels thermal degradation occurs at 330–340 °C, which according to the literature is related to SF materials with crystalline β-sheet (silk II) conformation [42, 43]. This result is in agreement with the XRD result, which determined that the secondary structure of SF hydrogels is predominantly β-sheet (silk II). By FTIR analysis was

possible to verify the presence of silk I conformation on the amide III absorption band, indicating that this structure may occur in the fibroin hydrogels, but in a lower proportion when compared with the silk II.

Morphology of SF hydrogels, reveled by SEM micrographs, indicates the presence of a porous structure with three-dimensional interconnectivity [14, 43-47]. The SF hydrogels subjected to freezing (-20 °C) showed larger pore size when compared with SF hydrogels kept at 8 °C. The SF hydrogels kept at 8 °C were frozen with liquid nitrogen before the lyophilization. In the lyophilization procedure, pore size of the material is controlled by the size of the ice crystals formed during freezing. The freezing process with liquid nitrogen is particularly rapid and, ideally, the water presented within the pores of the hydrogel turns into ice crystals that sublimate during lyophilization, maintaining the same shape and size of the pores of the hydrogel. However, when the freezing process is performed at a higher temperature, such as freezing at -20 °C, ice nucleation is slow and the nuclei tend to grow into larger ice crystals, which leads to the generation of materials with large and random pores [48]. The porous features resulting from freezing are in good agreement with precise results. Guan *et al*. showed that when polyurethane scaffolds were frozen in liquid nitrogen small pores were observed and most of the pores were less than 10 µm in size [49]. Chun *et al*. observed that the pore size of porous poly(D,L-lactic-co-glycolic acid) scaffolds frozen at liquid nitrogen temperature was smaller than 5 µm, but the pore size was enlarged up to 30–50 µm when frozen at -20 °C for 24 h [50]. Similarly, Ma *et al*. observed that when the temperature was decreased from -20 °C to -196 °C (liquid nitrogen) the pore size of poly(L -lactic acid) scaffolds was greatly decreased from 115–140 µm to 20–40 µm [51]. Chung *et al*. also showed that the pores of alginate/galactosylated chitosan scaffolds formed after liquid nitrogen treatment were small than the pores formed after freezing at -20 °C and -70 °C [52].

Other processes for the preparation of porous materials include: solvent casting/particulate leaching [38], emulsion templating [39] and phase separation [40]. In general, these methods require the use of large amounts of organic solvents and a lengthy washing or etching procedure [38, 42, 43]. A freezing process can provide certain advantages over the traditionally used techniques cited above [44]. Water is an environment-friendly solvent and the use of ice crystals as porogens is green and

sustainable. This is particularly beneficial for biological applications. When removing the solvent, the freezing process does not bring impurities into the samples and a further purifying process is therefore not necessary.

Materials and Methods

Preparation of silk fibroin solution

Cocoons of *Bombyx mori* silkworm were supplied by Bratac. To obtain pure SF fibers from silkworm cocoons it was necessary to perform a degumming process of silk cocoons to remove the sericin coating. This process was achieved by initially washing the cocoons with distilled water to remove any impurity, followed by the immersion of cocoons in 1 g/L of Na_2CO_3 solution at 85 °C for 1 h and 30 min, with solution change every 30 min. A final wash in distilled water was done to remove Na_2CO_3 residues. The SF fibers were dried and dissolved in a ternary solvent of $CaCl_2$:CH_3CH_2OH:H_2O, in a molar ratio of 1:2:8, at 85 °C until total dissolution, to a SF salt solution of 10% (w/v) [17].

Preparation of fibroin hydrogels

We studied two different methods for the preparation of fibroin hydrogels. In the first method, SF solution at a concentration of 10% (w/v) was dialyzed (cellulose membrane, Viscofan 22 EU – 20 USA) against distilled water for 3 d, at 8 °C, with water change every 24 h. After dialysis, the solution was filtered by gauze to remove small amounts of aggregates. The final concentration of the silk fibroin aqueous solution was 4% (w/v), which was determined by weighing the remaining solid after drying. The dialyzed solution was placed on specific molds (diameter: 25 mm) in a thermostatic bath at 37 °C until the formation of gels (3 d). Hydrogel formation was observed when the sample presented an opaque white color and did not fall when the mold was inverted for 30 s [14, 53]. Cylinder-shaped samples sized 25 mm in diameter and 10 mm in thickness were used. The SF hydrogels were then subjected to a freezing at -20 °C for 24 h. To analyze the effect of freezing, control samples of SF hydrogels were kept at 8 °C for 24 h.

In the second method, SF salt solution in a concentration of 10% (w/v) was dialyzed (cellulose membrane, Viscofan 22 EU – 20 USA) against distilled water at 8 °C, with water change every 24 h, until the formation of hydrogels inside the dialysis tube (7 d). The influence of freezing on this hydrogels was also analyzed by freezing SF hydrogels at -20 °C for 24 h, while the control samples (non-frozen hydrogels) were kept at 8 °C for 24 h.

Four different types of samples were prepared: 1) dialysis for 3 d followed by hydrogel formation at 37 °C and freezing by 24 h at -20 °C; 2) dialysis for 3 d followed by hydrogel formation at 37 °C and kept at 8 °C for 24 h; 3) dialysis for 7 d until hydrogel formation inside the tube and freezing by 24 h at -20 °C and 4) dialysis for 7 d until hydrogel formation inside the tube and kept at 8 °C for 24 h.

All hydrogels were characterized after freezing by liquid nitrogen and lyophilization (Liobras, L101, Brazil) within the first 24 h to prevent structural changes.

Characterization

X-ray Diffraction

Changes in the crystallinity of hydrogels were followed with X-ray diffraction (XRD), performed by a X'Pert-MPD diffractometer (Philips Analytical X Ray) with Cu-Kα radiation, with a wavelength of 1.54 Å. The X-ray source was operated at 40 kV and 40 pA. The scanning speed was 0.06°/s, step size of 0.02°, and the measurement range was 2θ = 10–40°. Three samples were used for each type of material.

Fourier Transformed Infrared Spectroscopy

The structural changes of silk fibroin hydrogels were analyzed in the range of 675–4000 cm^{-1}, with a resolution of 4 cm^{-1}, using Fourier transformed infrared spectroscopy with attenuated total reflection apparatus (FTIR-ATR) (Nicolet 6700, Thermo Scientific). FTIR was used to identify the secondary structure of the protein samples through the location of the peaks of amide I, II and III. Three samples were used for each type of material.

Thermogravimetric Analysis

Thermogravimetric analysis (TGA) measurements were performed on the hydrogels using a thermogravimetric analyzer (TGA-50, Shimadzu) in the temperature range of 30–600 °C with a slope of 10 °C/min and a N_2 flow of 50 mL/min, in order to analyze the influence of dialysis and freezing on the weight loss of the samples with respect to the temperature. Three samples were used per each type of material.

Scanning Electron Microscopy

The cross-section morphology of fibroin hydrogels was observed by scanning electron microscopy (SEM). The analysis was performed on the lyophized samples coated with a gold layer and then examined with an EVO MA15 scanning electron microscope (Zeiss), at 200× and 5000× magnification, with an accelerating voltage of 10 kV.

Conclusions

The present work describes the formation and characterization of silk fibroin hydrogels. Three-dimensional silk fibroin hydrogels were successfully prepared with an interconnected porous structure. From the results of X-ray diffraction and FTIR-ATR analysis, it is concluded that SF transforms into β-sheet after gelation, and both silk I and silk II structures exist simultaneously in all hydrogels. Thermal analysis showed the degradation peak for all SF hydrogels at around 330–340 °C, indicating high thermal resistance for these hydrogels. Longer dialysis time (7 d) resulted in a thicker fibroin network after lyophilization, showing that the dialysis time has an effect on the material porous structure and morphology. The effect of freezing was also visible on the porous structure of SF hydrogels, considerably increasing pore sizes. These scaffolds may hold promise in bone tissue engineering, and the degradation rate of the SF porous structures and *in vitro* citocompatibility tests are subject of future work.

Acknowledgments

This work was financed by FEDER funds through the Programa Operacional Factores de Competitividade – COMPETE and by Portuguese funds through FCT – Fundação para a Ciência e a Tecnologia in the framework of the NaNOBiofilm project (PTDC/SAUBMA/111233/2009) and PhD grant (SFRH/BD/90400/2012), whose support is acknowledged. The support of Project 346/13 CAPES (Brazil)-FCT (Portugal) Call 21/2012, and CNPq (Brazil) is acknowledged.

References

[1] Deville S, Saiz E, Tomsia AP. Freeze casting of hydroxyapatite scaffolds for bone tissue engineering. Biomaterials 2006; 27:5480-9; PMID:16857254; http://dx.doi.org/10.1016/j.biomaterials.2006.06.028

[2] Turco G, Marsich E, Bellomo F, Semeraro S, Donati I, Brun F, Grandolfo M, Accardo A, Paoletti S. Alginate/Hydroxyapatite biocomposite for bone ingrowth: a trabecular structure with high and isotropic connectivity. Biomacromolecules 2009; 10:1575-83; PMID:19348419; http://dx.doi.org/10.1021/bm900154b

[3] Liu C, Xia Z, Czernuszka JT. Design and development of three-dimensional scaffolds for tissue engineering. Chem Eng Res Des 2007; 85:1051-64; http://dx.doi.org/10.1205/cherd06196

[4] Altman GH, Diaz F, Jakuba C, Calabro T, Horan RL, Chen J, Lu H, Richmond J, Kaplan DL. Silk-based biomaterials. Biomaterials 2003; 24:401-16; PMID:12423595; http://dx.doi.org/10.1016/S0142-9612(02)00353-8

[5] Vepari C, Kaplan DL. Silk as a Biomaterial. Prog Polym Sci 2007; 32:991-1007; PMID:19543442; http://dx.doi.org/10.1016/j.progpolymsci.2007.05.013

[6] Wang Y, Kim HJ, Vunjak-Novakovic G, Kaplan DL. Stem cell-based tissue engineering with silk biomaterials. Biomaterials 2006; 27:6064-82; PMID:16890988; http://dx.doi.org/10.1016/j.biomaterials.2006.07.008

[7] Kurioka A, Yamazaki M, Hirano H. Primary structure and possible functions of a trypsin inhibitor of Bombyx mori. Eur J Biochem 1999; 259:120-6; PMID:9914483; http://dx.doi.org/10.1046/j.1432-1327.1999.00030.x

[8] Takahashi M, Tsujimoto K, Yamada H, Takagi H, Nakamori S. The silk protein, sericin, protects against cell death caused by acute serum deprivation in insect cell culture. Biotechnol Lett 2003; 25:1805-9; PMID:14677702; http://dx.doi.org/10.1023/A:1026284620236

[9] Altman GH, Horan RL, Lu HH, Moreau J, Martin I, Richmond JC, Kaplan DL. Silk matrix for tissue engineered anterior cruciate ligaments. Biomaterials 2002; 23:4131-41; PMID:12182315; http://dx.doi.org/10.1016/S0142-9612(02)00156-4

[10] Bayraktar O, Malay O, Özgarip Y, Batigün A. Silk fibroin as a novel coating material for controlled release of theophylline. Eur J Pharm Biopharm 2005; 60:373-81; PMID:15996578; http://dx.doi.org/10.1016/j.ejpb.2005.02.002

[11] Gobin AS, Butler CE, Mathur AB. Repair and regeneration of the abdominal wall musculofascial defect using silk fibroin-chitosan blend. Tissue Eng 2006; 12:3383-94; PMID:17518675; http://dx.doi.org/10.1089/ten.2006.12.3383

[12] Wang Y, Kim HJ, Vunjak-Novakovic G, Kaplan DL. Stem cell-based tissue engineering with silk biomaterials. Biomaterials 2006; 27:6064-82; PMID:16890988; http://dx.doi.org/10.1016/j.biomaterials.2006.07.008

[13] Li C, Vepari C, Jin HJ, Kim HJ, Kaplan DL. Electrospun silk-BMP-2 scaffolds for bone tissue engineering. Biomaterials 2006; 27:3115-24; PMID:16458961; http://dx.doi.org/10.1016/j.biomaterials.2006.01.022

[14] Kim UJ, Park J, Li C, Jin HJ, Valluzzi R, Kaplan DL. Structure and properties of silk hydrogels. Biomacromolecules 2004; 5:786-92; PMID:15132662; http://dx.doi.org/10.1021/bm0345460

[15] Asakura T, Yao J, Yamane T, Umemura K, Ulrich AS. Heterogeneous structure of silk fibers from Bombyx mori resolved by 13C solid-state NMR spectroscopy. J Am Chem Soc 2002; 124:8794-5; PMID:12137522; http://dx.doi.org/10.1021/ja020244e

[16] Kawahara Y, Furukawa K, Yamamoto T. Self-expansion behavior of silk fibroin film. Macromol Mater Eng 2006; 291:458-62; http://dx.doi.org/10.1002/mame.200500350

[17] de Moraes MA, Nogueira GM, Weska RF, Beppu MM. Preparation and Characterization of Insoluble Silk Fibroin/Chitosan Blend Films. Polymers 2010; 2:719-27; http://dx.doi.org/10.3390/polym2040719

[18] Sashina ES, Bochek AM, Novoselov NP, Kirichenko DA. Structure and solubility of natural silk fibroin. Russ J Appl Chem 2006; 79:869-76; http://dx.doi.org/10.1134/S1070427206060012

[19] Nogueira GM, de Moraes MA, Rodas ACD, Higa OZ, Beppu MM. Hydrogels from silk fibroin metastable solution: Formation and characterization from a biomaterial perspective. Mat Sci Eng C-Mater 2011; 31:997-1001; http://dx.doi.org/10.1016/j.msec.2011.02.019

[20] Kundu J, Chung YI, Kim YH, Tae G, Kundu SC. Silk fibroin nanoparticles for cellular uptake and control release. Int J Pharm 2010; 388:242-50; PMID:20060449; http://dx.doi.org/10.1016/j.ijpharm.2009.12.052

[21] Wang X, Kluge JA, Leisk GG, Kaplan DL. Sonication-induced gelation of silk fibroin for cell encapsulation. Biomaterials 2008; 29:1054-64; PMID:18031805; http://dx.doi.org/10.1016/j.biomaterials.2007.11.003

[22] Wang T, Zhang LL, He XJ. Preparation and Characterization of a Novel Hybrid Hydrogel Composed of Bombyx mori Fibroin and Poly (N-isopropylacrylamide). J Nanomater 2013;2013; http://dx.doi.org/10.1155/2013/832710

[23] Hardy JG, Scheibel TR. Composite materials based on silk proteins. Prog Polym Sci 2010; 35:1093-115; http://dx.doi.org/10.1016/j.progpolymsci.2010.04.005

[24] Mandal BB, Kundu SC. Non-bioengineered silk fibroin protein 3D scaffolds for potential biotechnological and tissue engineering applications. Macromol Biosci 2008; 8:807-18; PMID:18702171; http://dx.doi.org/10.1002/mabi.200800113

[25] Ren L, Tsuru K, Hayakawa S, Osaka A. Novel approach to fabricate porous gelatin-siloxane hybrids for bone tissue engineering. Biomaterials 2002; 23:4765-73; PMID:12361615; http://dx.doi.org/10.1016/S0142-9612(02)00226-0

[26] Fukasawa T, Deng ZY, Ando M, Ohji T, Goto Y. Pore structure of porous ceramics synthesized from water-based slurry by freeze-dry process. J Mater Sci 2001; 36:2523-7; http://dx.doi.org/10.1023/A:1017946518955

[27] Zhang H, Cooper AI. Aligned porous structures by directional freezing. Adv Mater 2007; 19:1529-33; http://dx.doi.org/10.1002/adma.200700154

[28] Kim UJ, Park J, Kim HJ, Wada M, Kaplan DL. Three-dimensional aqueous-derived biomaterial scaffolds from silk fibroin. Biomaterials 2005; 26:2775-85; PMID:15585282; http://dx.doi.org/10.1016/j.biomaterials.2004.07.044

[29] Wang H, Zhang Y, Shao H, Hu X. A study on the flow stability of regenerated silk fibroin aqueous solution. Int J Biol Macromol 2005; 36:66-70; PMID:15916801; http://dx.doi.org/10.1016/j.ijbiomac.2005.03.011

[30] Lv Q, Cao C, Zhu H. Clotting times and tensile properties of insoluble silk fibroin films containing heparin. Polym Int 2005; 54:1076-81; http://dx.doi.org/10.1002/pi.1814

[31] Rusa CC, Bridges C, Ha SW, Tonelli AE. Conformational changes induced in Bombyx mori silk fibroin by cyclodextrin inclusion complexation. Macromolecules 2005; 38:5640-6; http://dx.doi.org/10.1021/ma050340a

[32] Hu X, Shmelev K, Sun L, Gil ES, Park SH, Cebe P, Kaplan DL. Regulation of silk material structure by temperature-controlled water vapor annealing. Biomacromolecules 2011; 12:1686-96; PMID:21425769; http://dx.doi.org/10.1021/bm200062a

[33] Hu X, Kaplan D, Cebe P. Determining Beta-Sheet Crystallinity in Fibrous Proteins by Thermal Analysis and Infrared Spectroscopy. Macromolecules 2006; 39:6161-70; http://dx.doi.org/10.1021/ma0610109

[34] Lu Q, Hu X, Wang X, Kluge JA, Lu S, Cebe P, Kaplan DL. Water-insoluble silk films with silk I structure. Acta Biomater 2010; 6:1380-7; PMID:19874919; http://dx.doi.org/10.1016/j.actbio.2009.10.041

[35] Srisa-Ard M, Baimark Y. Controlling Conformational Transition of Silk Fibroin Microspheres by Water Vapor for Controlled Release Drug Delivery. Particul Sci Technol 2013; 31:379-84; http://dx.doi.org/10.1080/02726351.2013.766289

[36] Kweon HY, Park SH, Ye JH, Lee YW, Cho CS. Preparation of semi-interpenetrating polymer networks composed of silk fibroin and poly(ethylene glycol) macromer. J Appl Polym Sci 2001; 80:1848-53; http://dx.doi.org/10.1002/app.1281

[37] Um IC, Kweon HY, Park YH, Hudson S. Structural characteristics and properties of the regenerated silk fibroin prepared from formic acid. Int J Biol Macromol 2001; 29:91-7; PMID:11518580; http://dx.doi.org/10.1016/S0141-8130(01)00159-3

[38] Nogueira GM, Weska RF, Vieira WC, Polakiewicz B, Rodas ACD, Higa OZ, et al. A New Method to Prepare Porous Silk Fibroin Membranes Suitable for Tissue Scaffolding Applications. J Appl Polym Sci 2009; 114:617-23; http://dx.doi.org/10.1002/app.30627

[39] Malafaya PB, Silva GA, Reis RL. Natural-origin polymers as carriers and scaffolds for biomolecules and cell delivery in tissue engineering applications. Adv Drug Deliv Rev 2007; 59:207-33; PMID:17482309; http://dx.doi.org/10.1016/j.addr.2007.03.012

[40] Matsumoto A, Chen J, Collette AL, Kim UJ, Altman GH, Cebe P, Kaplan DL. Mechanisms of silk fibroin sol-gel transitions. J Phys Chem B 2006; 110:21630-8; PMID:17064118; http://dx.doi.org/10.1021/jp056350v

[41] Tsukada M, Obo M, Kato H, Freddi G, Zanetti F. Structure and dyeability of Bombyx mori silk fibers with different filament sizes. J Appl Polym Sci 1996; 60:1619-27; http://dx.doi.org/10.1002/(SICI)1097-4628(19960606)60:10<1619::AID-APP14>3.0.CO;2-#

[42] Freddi G, Pessina G, Tsukada M. Swelling and dissolution of silk fibroin (Bombyx mori) in N-methyl morpholine N-oxide. Int J Biol Macromol 1999; 24:251-63; PMID:10342772; http://dx.doi.org/10.1016/S0141-8130(98)00087-7

[43] Fang JY, Chen JP, Leu YL, Wang HY. Characterization and evaluation of silk protein hydrogels for drug delivery. Chem Pharm Bull (Tokyo) 2006; 54:156-62; PMID:16462057; http://dx.doi.org/10.1248/cpb.54.156

[44] Nazarov R, Jin HJ, Kaplan DL. Porous 3-D scaffolds from regenerated silk fibroin. Biomacromolecules 2004; 5:718-26; PMID:15132652; http://dx.doi.org/10.1021/bm034327e

[45] Zhu Y, Wan Y, Zhang J, Yin D, Cheng W. Manufacture of layered collagen/chitosan-polycaprolactone scaffolds with biomimetic microarchitecture. Colloids Surf B Biointerfaces 2014; 113:352-60; PMID:24121078; http://dx.doi.org/10.1016/j.colsurfb.2013.09.028

[46] Han J, Zhou Z, Yin R, Yang D, Nie J. Alginate-chitosan/hydroxyapatite polyelectrolyte complex porous scaffolds: preparation and characterization. Int J Biol Macromol 2010; 46:199-205; PMID:19941890; http://dx.doi.org/10.1016/j.ijbiomac.2009.11.004

[47] Sarem M, Moztarzadeh F, Mozafari M, Shastri VP. Optimization strategies on the structural modeling of gelatin/chitosan scaffolds to mimic human meniscus tissue. Mater Sci Eng C Mater Biol Appl 2013; 33:4777-85; PMID:24094187; http://dx.doi.org/10.1016/j.msec.2013.07.036

[48] Qian L, Zhang HF. Controlled freezing and freeze drying: a versatile route for porous and micro-/nano-structured materials. J Chem Technol Biotechnol 2011; 86:172-84; http://dx.doi.org/10.1002/jctb.2495

[49] Guan J, Fujimoto KL, Sacks MS, Wagner WR. Preparation and characterization of highly porous, biodegradable polyurethane scaffolds for soft tissue applications. Biomaterials 2005; 26:3961-71; PMID:15626443; http://dx.doi.org/10.1016/j.biomaterials.2004.10.018

[50] Chun KW, Cho KC, Kim SH, Jeong JH, Park TG. Controlled release of plasmid DNA from biodegradable scaffolds fabricated using a thermally-induced phase-separation method. J Biomater Sci Polym Ed 2004; 15:1341-53; PMID:15648567; http://dx.doi.org/10.1163/1568562042368103

[51] Ma H, Hu J, Ma PX. Polymer scaffolds for small-diameter vascular tissue engineering. Adv Funct Mater 2010; 20:2833-41; PMID:24501590; http://dx.doi.org/10.1002/adfm.201000922

[52] Chung TW, Yang J, Akaike T, Cho KY, Nah JW, Kim SI, Cho CS. Preparation of alginate/galactosylated chitosan scaffold for hepatocyte attachment. Biomaterials 2002; 23:2827-34; PMID:12069321; http://dx.doi.org/10.1016/S0142-9612(01)00399-4

[53] Liu Y, Cheng YD, Xiong SY, Li PJ, Wei YQ, Li MZ. The Effect of Shearing Force on the Gel Formation and Structural Transitions of Regenerated Silk Fibroin. Text Bioeng Inform S 2010:309-15.

CHAPTER III

Development of silk fibroin/nanohydroxyapatite composite hydrogels for bone tissue engineering

Marta Ribeiro [a,b,*], Mariana A. de Moraes [c,d], Marisa M. Beppu [c], Mónica P. Garcia [e], Maria H. Fernandes [e], Fernando J. Monteiro [a,b], Maria P. Ferraz [a,f]

[a] INEB - Instituto de Engenharia Biomédica, Universidade do Porto, Porto, 4150-180, Portugal.

[b] Departamento de Engenharia Metalúrgica e Materiais, Faculdade de Engenharia, Universidade do Porto, Porto, 4200-465, Portugal.

[c] Faculdade de Engenharia Química, Universidade Estadual de Campinas, Campinas, SP, 13083-852, Brazil.

[d] Department of Exact and Earth Sciences, Federal University of São Paulo, UNIFESP, Diadema – SP, Brazil

[e] Laboratory for Bone Metabolism and Regeneration, Faculdade de Medicina Dentária, Universidade do Porto, Porto, 4200-393, Portugal

[f] Centro de Estudos em Biomedicina, Universidade Fernando Pessoa, Porto, 4249-004, Portugal.

European Polymer Journal, 2015; 67:66-77.

Abstract

This work presents a novel composite hydrogel consisting of silk fibroin (SF) and nanohydroxyapatite (nanoHA) prepared by a new and innovative method using ethanol as gelling agent capable of forming hydrogels in few minutes. The properties of the composite material, such as the microstructure as well as the chemical and physical properties were studied. Moreover *in vitro* studies of osteoblastic citocompatibility were performed. The microporosity and macroporosity obtained combined with interconnected porous structure and a uniform dispersion of nanoHA particles throughout the fibroin matrix makes composite hydrogel suitable for bone regeneration. The compression modulus of composite hydrogels was increased as the nanoHA concentration increased from 10 to 15 wt% and the water uptake ability of these materials decreased with the incorporation of nanoHA. The metabolic and alkaline phosphatase activities of osteoblastic cells were improved with the incorporation of nanoHA in the SF matrix providing a more promising material for bone tissue engineering.

Keywords: bone tissue engineering; hydrogel; silk fibroin; nanohydroxyapatite; biocomposite

1. Introduction

Bone tissue engineering has emerged as a promising alternative in cases of bone loss, overcoming problems of rejection and donor scarcity associated to the clinical used bone grafts [1, 2]. By combining three-dimensional structures (3D) - scaffolds, cells and growth factors, bone tissue engineering seeks to achieve a long lasting and fully functional regeneration of bone [3]. Materials with high hydrophilic properties appear suitable for mimicking the aqueous *in vivo* environment. For this reason, hydrogels have been used extensively as 3D matrices [4]. They represent promising systems for the healing and regeneration of damaged tissues since they are highly permeable and facilitate the transport of nutrients and metabolites [4]. Their ability to mimic body tissues and respond to external stimuli has made them important and promising forms of biomaterials for various applications including tissue engineering, controlled drug release devices, etc. [5]. Current research on biodegradable polymers is emerging, combining these structures with osteogenic cells, as an alternative to autologous bone grafts. Different types of biodegradable materials have been proposed to be used as 3D porous scaffolds for bone tissue engineering. Among them, natural polymers are one of the most attractive options, mainly due to their similarities with extracellular matrix (ECM), chemical versatility, good biological performance and inherent cellular interactions [6]. The unique properties of silk fibroin (SF), a protein polymer isolated from the cocoons of the domestic silkworm *Bombyx mori*, such as slow biodegradation, adjustable mechanical properties, low inflammatory response, high permeability to oxygen and water vapor, resistance to enzymatic degradation, favorable processability in combination with biocompatibility, have driven wide interest in this material for a variety of applications, ranging from textiles to biomedical use [7-10]. Based on these features, interest has arisen in the use of *Bombyx mori* SF as starting material for biomaterials and scaffolds for bone tissue engineering. The cocoon of the silkworm is mainly composed of sericin and fibroin. Sericin is a glue-like protein that holds SF fibers together in the cocoon case. SF is composed of a repetitive sequence of amino acids: glycine, alanine and serine, and is not soluble in water due to its high concentration of hydrophobic amino acids [7]. SF

has two types of molecular conformation of the secondary structure, called silk I and silk II. Silk I is a metastable form of SF that is soluble in water and non-crystalline; random coil and α-helix conformations are usually called silk I. On the other hand, silk II is a highly stable and organized structure that is insoluble in water; the β-sheet conformation is called silk II. Generally, both silk I and silk II are present in SF products, but it is their relative proportions that will define the final properties [11-13]. Due to the β-sheet formation, SF exhibits relatively slow degradation *in vitro* and *in vivo* when compared to collagens and many other biopolymers [7, 14]. The biodegradability, mechanical integrity and low inflammatory response of SF [15] ensure its role as one of the promising porous materials for osteogenic applications. In addition, studies demonstrate that SF scaffolds are able to induce calcium phosphate deposition in *in vitro* calcification experiments, demonstrating that SF is a promising scaffold for bone regeneration [16, 17]. We hypothesize that the incorporation of nanosized HA particles (nanoHA) into biodegradable SF hydrogels should improve osteogenic outcomes. Hydroxyapatite [HA, $Ca_{10}(PO_4)_6(OH)_2$] is one of the most widely used synthetic calcium phosphate ceramics due to its chemical similarities to the inorganic component of hard tissues and it possesses exceptional biocompatibility, bioactivity and osteoconductivity [18-22]. Some studies have indicated that nanostructured materials may promote increased specific protein interactions to more efficiently stimulate new bone growth compared to conventional materials [23, 24]. NanoHA shows increased potential to bind to bone, to adsorb macromolecules that may act in the preliminary events leading to bone bonding and tissue regeneration [25, 26]. The aim of this work was to develop a novel composite hydrogel for bone tissue engineering of silk fibroin and nanoHA, an approach that has been poorly explored. The hydrogels were prepared by a new and innovative method, which can be used to form hydrogels in few minutes, using ethanol as gelling agent. The focus of the present study was to accelerate the formation of hydrogels without occurrence of nanoHA aggregation or sedimentation. The attributes of SF in combination with the features of nanoHA will form a material with interesting properties, combining the mechanical integrity and slow degradation of SF with the bioactivity and osteoconductivity of the nanoHA.

2. Materials and Methods

2.1. Preparation of silk fibroin solution

Cocoons of *Bombyx mori* silkworm were supplied by Bratac (São Paulo, Brazil). The cocoons were degummed three times by soaking in 1 g/L of Na_2CO_3 solution at 85 °C for 30 min to remove the sericin of the cocoons, and then rinsing in distilled water to remove Na_2CO_3 residues. The SF fibers were dried and dissolved in a ternary solvent of $CaCl_2$:CH_3CH_2OH:H_2O, in a molar ratio of 1:2:8, at 85 °C until total dissolution, to a SF salt solution of 10% (w/v). The SF salt solution was then dialyzed (cellulose membrane, Viscofan 22 EU – 20 USA) against distilled water for 3 days, at 8 °C, with water changes every 24 hours [27]. The final concentration of the SF aqueous solution was 4% (w/v), which was determined by weighing the remaining solid after drying.

2.2. Preparation of silk fibroin/nanoHA composite hydrogels

For preparing the SF/nanoHA hydrogels, a total of 3.5 mL of SF aqueous solution was placed in specific molds (diameter: 25 mm). The dry powder of nanoHA aggregates (Fluidinova S.A., Maia, Portugal) was first mixed with 1.5 mL of 70% ethanol and then slowly mixed with the SF aqueous solution using a pipet to avoid protein precipitation. The weight percent (wt%) of nanoHA in the hydrogels was 0, 10, 15, 20 and 30. The hydrogels were named according to their nanoHA content. SF/nanoHA hydrogels were prepared at two temperatures. The molds were sealed and kept at a controlled temperature in a thermostatic bath at 37 or 50 °C until hydrogel formation. Gelation time was determined when the sample showed an opaque white color and did not flow when the mold was inverted for 30 s [28, 29]. Part of these hydrogels was frozen at -20 °C for 24 h to evaluate differences in the properties of non-frozen and frozen hydrogels. These hydrogels were identified with the letter F. Moreover, since fibroin is a natural polymer, the gelation time was evaluated from SF solutions prepared in different days to evaluate the reproducibility of the materials and to find a highly reproducible method for the formation of hydrogels. The data reported for gelation time represent the average of ten replicates for each temperature.

2.3. Characterization

2.3.1. *Morphology*

Morphology of non-frozen and frozen hydrogels was characterized by scanning electron microscopy (SEM). The analysis was performed on samples that were frozen with liquid nitrogen, lyophilized, coated with a gold layer and then examined with an EVO MA15 scanning electron microscope (Zeiss, England), with an accelerating voltage of 10 kV. The average pore size of the materials was determined from SEM images using ImageJ software by selecting ten arbitrary areas by measuring approximately 200 pores for each material.

2.3.2. *Mechanical analysis*

The mechanical properties of hydrogels were measured by confined compression test using a SMS (Stable Micro Systems, Surrey UK) TA-xT2 texturometer equipped with a 1 kg load cell at room temperature. The compression limit was 500 g to protect the load cell and the speed test was 0.2 mm/s. Cylinder-shaped samples sized 25 mm in diameter and 10 mm in thickness were used. To minimize the effect of water evaporation, hydrogel samples were kept in sealed packs before measurement. The compressive stress and strain were graphed and the average compression modulus and standard deviation were determined. The compression modulus was calculated by determining the slope of the linear region in the 7.5%-15% of strain in the stress–strain curve. The data reported were the mean of five samples.

2.3.3. *Crystallinity*

The crystallinity of hydrogels was followed with X-ray diffraction, performed by a X'Pert-MPD diffractometer (Philips Analytical X Ray, Netherlands) with Cu-Kα radiation, with a wavelength of 1.54 Å. The X-ray source was operated at 40 kV and 40 pA. The scanning speed was 0.06°/s, step size of 0.02° and the measurement range was 2θ=10-60°.

2.3.4. *Molecular conformation*

The secondary structure of hydrogels was investigated by Fourier transformed infrared spectroscopy (FTIR) with a Perkin-Elmer 2000 FT-IR spectrometer. Measurements were performed with pressed discs made using potassium bromide (KBr) powder. The FTIR spectra were collected between the wavenumber of 4000–400 cm^{-1}, with a resolution of 4 cm^{-1} and with one hundred scans accumulated per sample.

2.3.5. Thermal Properties

The thermal properties of SF/nanoHA hydrogels were examined using a thermogravimetric analyzer (TGA-50, Shimadzu, Japan) in the temperature range of 30-600 °C with a ramp rate of 10 °C/min and a N_2 flow of 50 mL/min.

2.3.6. Swelling Properties

The swelling capacity studies were performed at room temperature by immersing the dried hydrogels in distilled water for 1 h. Different time intervals were selected to measure the weight of the hydrated hydrogels after swelling. During weight measurements, the samples were first removed from the aqueous solution and gently dried with a filter paper to remove the excess solvent. At least five samples with similar weight (ca. 10 mg) were used for each type of hydrogel. The swelling degree of the hydrogels was determined by using the following equation:

$$SD\ (\%) = [(Ws-Wd)/Wd]\times 100$$

where *Ws* and *Wd* were the weights of the swollen and the dry sample, respectively.

2.4. *In vitro* biological studies

2.4.1. Cell culture

Hydrogel sections with 7 mm diameter and 5 mm thickness were sterilized in ethanol solution at 70% (v/v). Osteoblast-like cells (MG63 cell line) were cultured in minimum essential medium (MEM) Eagle, alpha modification (α-MEM) containing 10% fetal

bovine serum, 100 IU/mL penicillin,/2.5 µg/mL streptomycin, (Gibco, UK) and 2.5 µg/mL amphotericin B (Gibco, UK), and 50 µg/mL ascorbic acid (Sigma, USA). The cultures were incubated in a humidified atmosphere of 95% air and 5% carbon dioxide (CO_2) at 37 °C. At 70 – 80% confluence, the adherent cells were washed with PBS and detached with trypsin solution (0.04%, Gibco, UK) at 37 °C for 10 min and counted using a hemocytometer. Previous to the cell seeding, the samples were incubated with complete culture medium for 30 min at 37 °C in a humidified atmosphere of 95% air and 5% CO_2. Then, the culture medium was completely removed from the hydrogels. Afterward, cells were seeded at a density of 1×10^5 cells/scaffold on the top of the hydrogels, and tissue culture polystyrene (TCPS) plates were used as control. Moreover, the SF hydrogels were used as controls of the SF/nanoHA hydrogels. All samples were cultured for 3 different time points (1, 4 and 7 days).

2.4.2. Resazurin assay

At each time point, the metabolic activity was evaluated by the resazurin assay. The same sample was followed throughout the culture time, i.e. it was assessed at all time-points. The resazurin is a simple and non-reactive assay, where a non-fluorescent blue component is reduced by the living cells to a pink fluorescent component. Fresh medium with 10% (v/v) of resazurin was added to the cells, which were incubated at 37 °C in a humidified atmosphere of 95% air and 5% CO_2 for 3 h. Then, 100 µL were transferred to a 96-well plate and the fluorescence intensity was measured in a microplate reader (Synergy HT, BioTek, USA) at 535 nm excitation wavelength and 590 nm emission wavelength. The data reported were the average of three samples.

2.4.3. Confocal laser scanning microscopy

Cells were fixed with 3.7% formaldehyde (Sigma-Aldrich) for 15 min and then washed twice in PBS. Then, the materials were incubated for 30 min with 0.1% (v/v) Triton X-100 solution (Sigma-Aldrich) and 30 min with 1% bovine serum albumin solution in PBS (BSA, Sigma-Aldrich). Osteoblast-like cells were stained for F-actin cytoskeleton with alexafluor phalloidin 594 (Invitrogen) in 1% BSA solution for 30 min at room temperature. Samples were washed twice with PBS and nuclei were stained with DAPI

(40-6-diamidine-2-phenylindole, Invitrogen) for 10 min. Finally, the materials were washed twice with PBS and the morphology was evaluated with a Spectral Confocal Microscope Leica TCS-SP5 AOBS (Leica).

2.4.4. Alkaline phosphatase activity and protein content

At each time point, colonized hydrogels were washed twice in PBS and they were placed at 37 °C and 5% CO_2 for 1 h with 0.5 mL of ultrapure water. Subsequently, they were placed in a freezer at -80 °C and then thawed at room temperature to lyse the cell membranes. Alkaline phosphatase (ALP) activity was assayed by the hydrolysis of p-nitrophenol phosphate (Sigma), in alkaline buffer solution, 2-amino-2-methyl-1-propanol (Sigma), at pH 10.5. After 1 h of incubation at 37 °C, the reaction was stopped by adding NaOH (5M, Sigma), and the hydrolysis product (*p*-nitrophenol) was measured at 405 nm, using a plate reader (BioTek). ALP activity was normalized to total protein content and was expressed as nanomoles of *p*-nitrophenol produced per minute per microgram of total protein (nmol min^{-1}/μg protein). Total protein content was measured by Lowry's method with bovine serum albumin used as a standard.

2.5. Statistical analysis

The results were expressed as the average ± standard deviation (SD). The statistical analysis of the results was carried out using the one-way analysis of variance (ANOVA) followed by *post hoc* Tukey HSD multiple comparison test. Levels of $p < 0.05$ were considered to be statistically significant.

3. Results

3.1. Preparation of SF/nanoHA composite hydrogels

Initial experiments showed that the hydrogel of pure SF takes 67 h and 48 h to complete the gelation process under 37 °C and 50 °C, respectively. This long time to complete the gelation process prompt us to develop a new method to accelerate the formation of SF/nanoHA hydrogels without nanoHA aggregation and/or

sedimentation. For that, ethanol was used as gelling agent for SF as well as a dispersion agent for nanoHA. Ethanol concentrations of 30, 50, 70, 80, 90 and 100% were tested. Interestingly, for ethanol concentrations in the SF solution higher than 70%, large amounts of fibroin precipitated. For concentrations lower than 70%, deposition of nanoHA was observed. This occurred because, at this condition, SF solution took more than 15 minutes to gelify and it was found that the maximum time for the formation of hydrogels without nanoHA deposition was 15 minutes. The dry powders of nanoHA aggregates were mixed with the ethanol solution in a particular ratio. However, when the nanoHA content was higher than 15 wt%, nanoHA aggregation occurred. The SF/nanoHA ratios chosen for this work were 90:10 and 85:15 wt%. SF hydrogels without nanoHA were used as controls.

Table 1 shows the gelation time of SF/nanoHA hydrogels, in the presence of 70% ethanol, with respect to temperature and concentration of nanoHA. The use of 70% ethanol allowed the formation of hydrogels within 15 minutes without nanoHA deposition or SF precipitation. The gelation time of SF/nanoHA hydrogels was similar for both temperatures.

Table 1. Gelation time of SF/nanoHA hydrogels, in the presence of 70% ethanol, with respect to temperature and concentration of nanoHA. Values are average ± SD.

Temperature (°C)	nanoHA wt%	Gelation Time (min)
37	0	7.6 ± 1.2
	10	6.0 ± 0.8
	15	7.3 ± 1.0
50	0	6.9 ± 1.0
	10	6.3 ± 1.2
	15	6.5 ± 1.1

3.2. Characterization of silk fibroin/nanoHA hydrogels

3.2.1. Morphology and porosity

Morphology and porosity of hydrogels were analyzed by SEM. Pores between 1.0 and 264.2 µm were measured by the Image J software (Fig. 1).

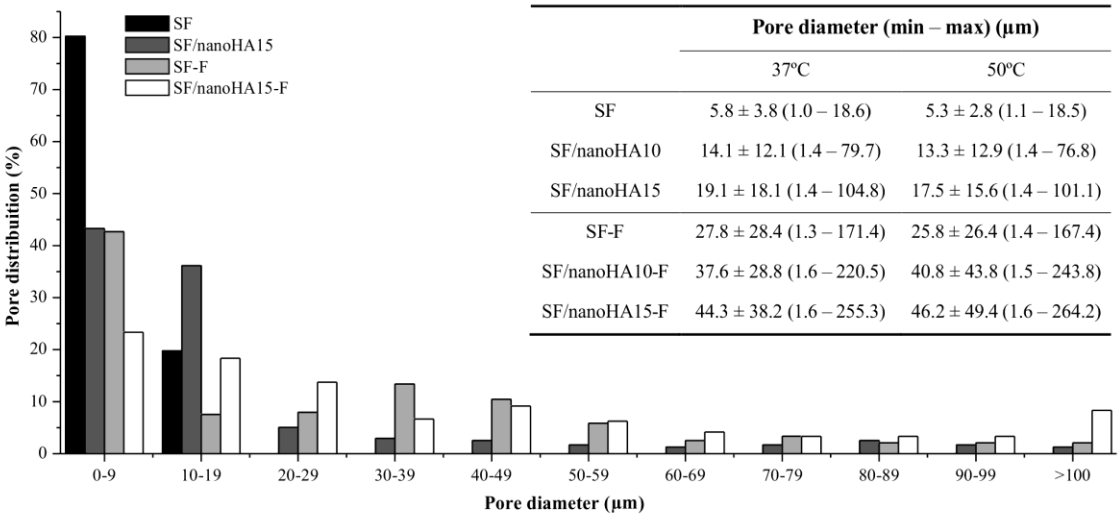

	Pore diameter (min – max) (µm)	
	37ºC	50ºC
SF	5.8 ± 3.8 (1.0 – 18.6)	5.3 ± 2.8 (1.1 – 18.5)
SF/nanoHA10	14.1 ± 12.1 (1.4 – 79.7)	13.3 ± 12.9 (1.4 – 76.8)
SF/nanoHA15	19.1 ± 18.1 (1.4 – 104.8)	17.5 ± 15.6 (1.4 – 101.1)
SF-F	27.8 ± 28.4 (1.3 – 171.4)	25.8 ± 26.4 (1.4 – 167.4)
SF/nanoHA10-F	37.6 ± 28.8 (1.6 – 220.5)	40.8 ± 43.8 (1.5 – 243.8)
SF/nanoHA15-F	44.3 ± 38.2 (1.6 – 255.3)	46.2 ± 49.4 (1.6 – 264.2)

Fig. 1. Pore diameter and pore size distribution of non-frozen and frozen SF and SF/nanoHA composite hydrogels. Pore dimensions were grouped, from 0 to over 100 µm. Pore diameter values are average ± SD.

The pore sizes of hydrogels prepared at 37 °C and 50 °C were similar and therefore only SEM images concerning to materials prepared at 37 °C are shown. The incorporation of nanoHA into SF solution at 37 °C and 50 °C increased the average pore sizes. The frozen hydrogels showed higher pore sizes when compared to the non-frozen hydrogels. Pore size distribution in all the hydrogels is also shown in Fig. 1. The SF hydrogels only presented pores between 0 and 20 µm. All the others hydrogels showed a heterogeneous pores distribution.

Figs. 2 and 3 show the SEM images of non-frozen and frozen SF and SF/nanoHA hydrogels, respectively. SEM observations revealed a uniform porous structure within SF hydrogels (Fig. 2(a) and (b)). The SF/nanoHA composite hydrogels exhibited an

irregular porous structure (Fig. 2(c) and (d)), which indicate that nanoHA addition influenced the hydrogels porous structure.

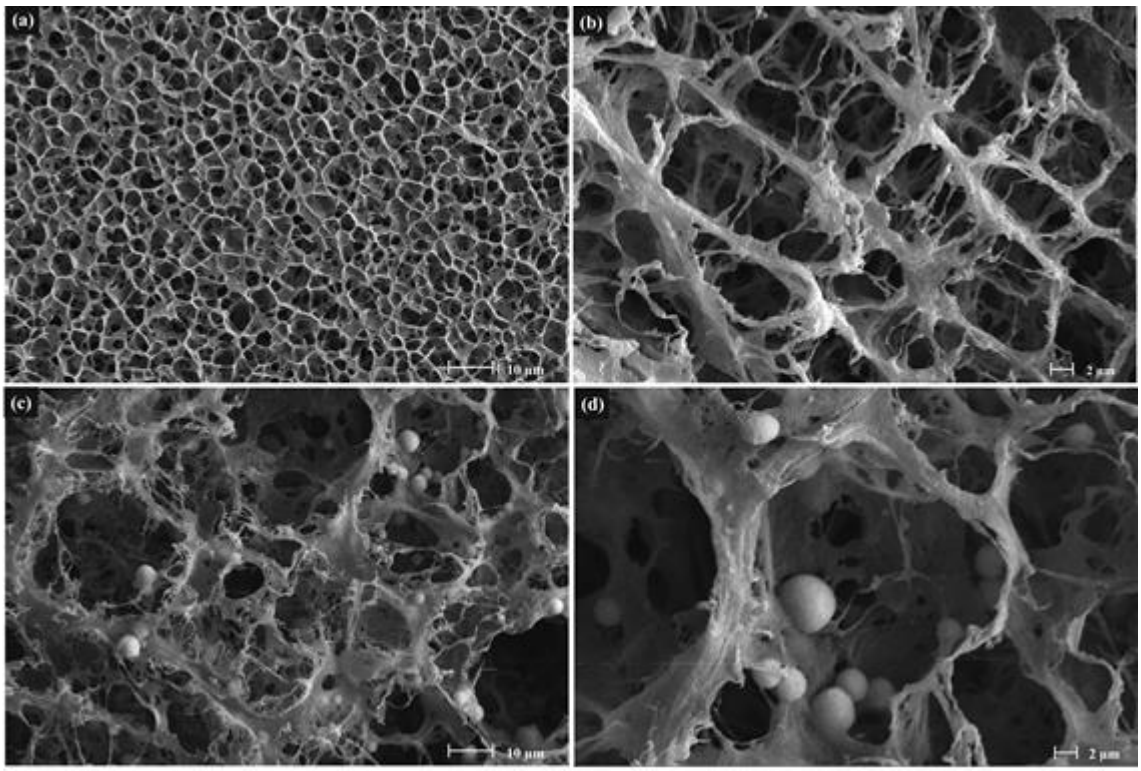

Fig. 2. SEM images of non-frozen SF hydrogels (a and b) and SF/nanoHA15 composite hydrogels (c and d).

The frozen SF hydrogels also presented an irregular porous structure indicating the influence of freezing on the porous structure (Fig. 3(a) and (b)). The frozen SF/nanoHA hydrogels also revealed an irregular porous structure (Fig. 3(c) and (d)). Similar porous structure was observed for SF/nanoHA nanocomposite hydrogels containing 10 and 15 wt% of nanoHA, implying that this variation in nanoHA content did not alter the microstructure of the material. Therefore, only SEM images of SF/nanoHA composite with 15 wt% of nanoHA are shown. The high magnification SEM micrographs showed an interconnected 3D structure (Figs. 2(b), (d) and 3(b), (d)) and non-agglomerated distribution of nanoHA aggregates within the SF matrices (Fig. 2(d) and 3(d)).

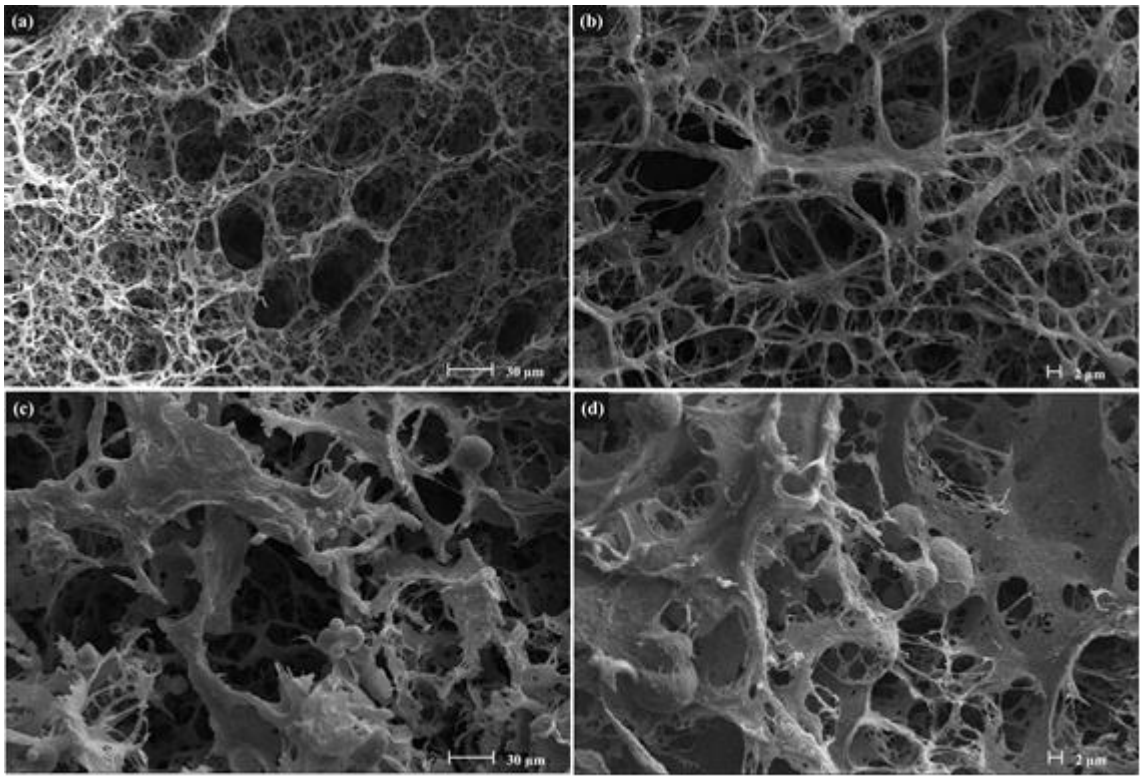

Fig. 3. SEM images of frozen SF hydrogels (a and b) and frozen SF/nanoHA15 composite hydrogels (c and d).

3.2.2. Mechanical properties

The effect of the nanoHA particles incorporation on the compression modulus of the composite hydrogels prepared at 37 °C is presented in Fig. 4A. The addition of 10 wt% of nanoHA caused a decrease of compression modulus in composite hydrogels compared to the SF hydrogels. However, the compression modulus of hydrogels increased from 92.2 kPa to 109.8 kPa as the nanoHA concentration increased from 10 to 15 wt%. The frozen SF hydrogels presented lower compression modulus than non-frozen SF hydrogels. Nevertheless, the compression modulus of frozen composite hydrogels showed increasing values with the increase in nanoHA content, namely 65.4 kPa, 92.4 kPa and 111.6 kPa when the nanoHA concentration was 0, 10 and 15 wt%, respectively. Additionally, the materials presented similar mechanical properties for both temperatures (Fig. 4(B)).

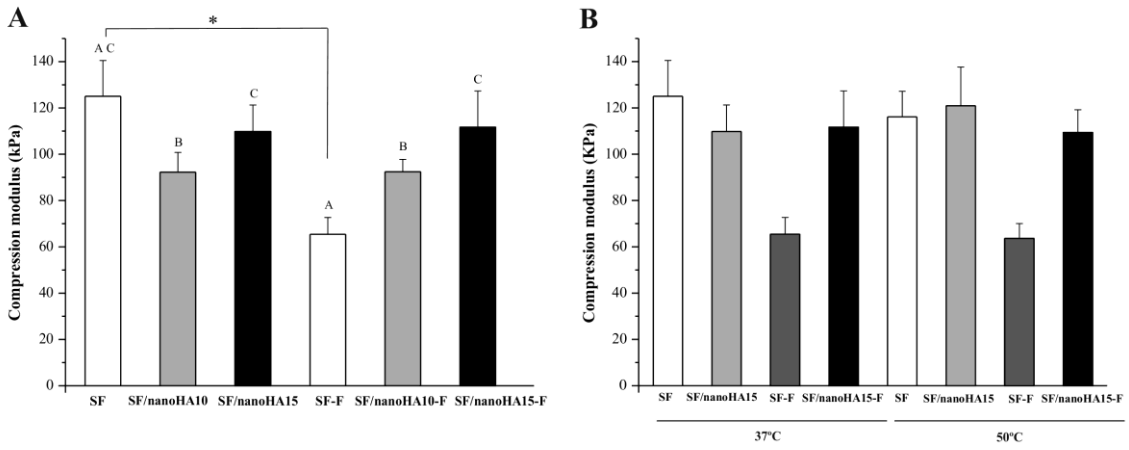

Fig. 4. Compression modulus of (A) non-frozen and frozen SF and SF/nanoHA composite hydrogels prepared at 37 °C; and (B) non-frozen and frozen SF hydrogels and SF/nanoHA15 composite hydrogels prepared at 37 °C and 50 °C. Different uppercase letters indicate intragroup significant differences ($p<0.05$) according to Tukey HSD. * Intergroup significant differences ($p<0.05$) according to Tukey HSD. Values are average ± SD.

Therefore, the hydrogels prepared at 37 °C were chosen for the following characterizations, since they were prepared in a mild temperature (requiring lower energy) and had similar gelation time (Table 1), pore size (Fig. 1) and mechanical resistance to compression (Fig. 4(B)) when compared to the hydrogel prepared at 50 °C. Also, we choose to continue the experiments with the SF/nanoHA hydrogels with 15 wt% of nanoHA because of the improved mechanical properties and higher amount of bioactive agent, in combination with adequate pore sizes for bone tissue engineering.

3.2.3. Structural analysis

The obtained XRD patterns of hydrogels are shown in Fig. 5A. The distinct halo at 2θ=20.4° for pure SF material (Fig. 5A(a)) was attributed to the silk II form, indicating that the secondary structure conformation is β-sheet [30]. The SF hydrogels prepared with ethanol (Fig. 5A(b)) presented the same halo that the pure SF material at 2θ=20.4°, showing that the ethanol did not affect the crystallinity of the material. The

frozen SF hydrogels (Fig. 5A(c)) also showed the same halo that the pure SF material at 2θ=20.4°, showing that the freezing process did not affect the crystallinity of the material. The existence of 2θ halos, for nanoHA aggregates (Fig. 5A(f)), at 25.9°, 31.9°, 34°, 39.8°, 46.7°, 49.5° and 53.2° correspond to the diffraction planes (002), (211), (202), (310), (222), (213) and (004) of the HA crystallites, respectively [31, 32]. The XRD patterns of the non-frozen and frozen composite hydrogels simultaneously exhibited characteristic halos from silk II structure and nanoHA aggregates (Fig. 5A(d) and (e)). No halo shifts was observed when the nanoHA was added to the SF, indicating that the incorporation of nanoHA did not change the crystallinity of SF in the hydrogel. Three clear diffraction halos corresponding to the (002), (211) and (310) planes of nanoHA crystals were detected in the SF/nanoHA materials. Moreover, these three halos became slightly broader and weaker when compared with pure nanoHA aggregates.

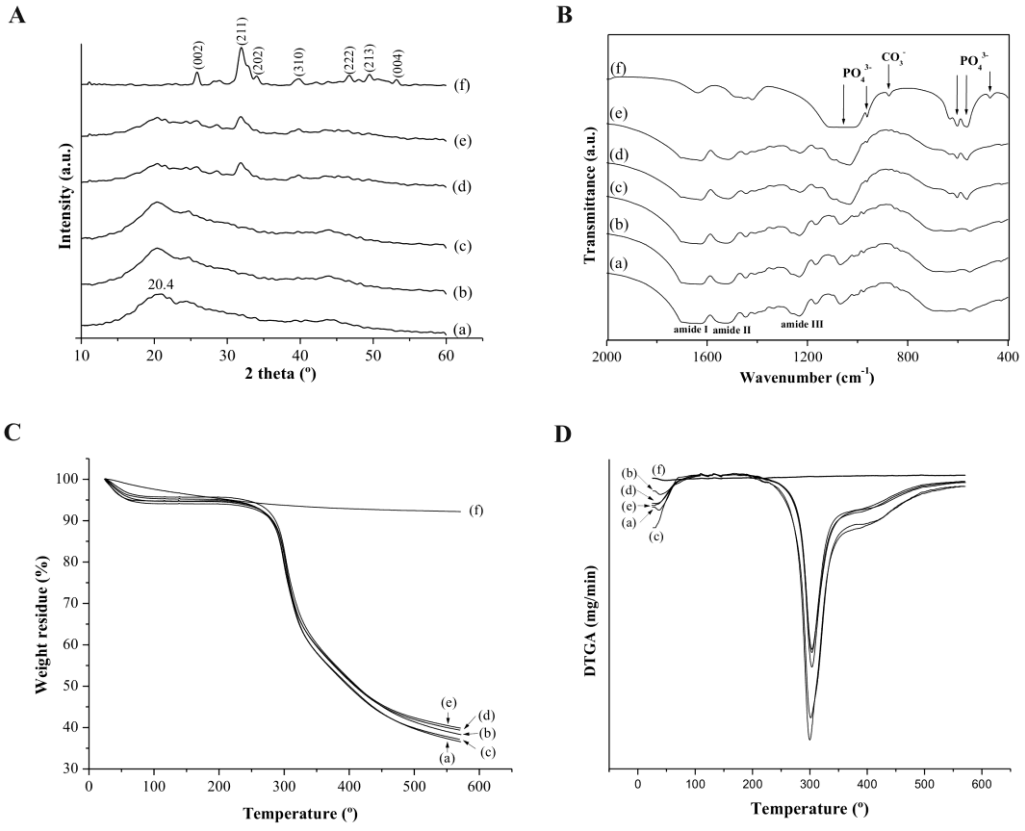

Fig. 5. X-ray diffraction patterns (A), FTIR spectra (B), thermogravimetric curves (C) and differential thermogravimetric curves (D) of pure SF hydrogels (a), SF hydrogels (b), frozen SF hydrogels (c), SF/nanoHA15 hydrogels (d), frozen SF/nanoHA15 hydrogels (e) and pure nanoHA (f).

The FTIR spectrum of pure SF material (Fig.5B(a)) presented typical amide bands of fibroin, that is, 1627 cm^{-1} was ascribed to amide I (C=O stretching) and 1525 cm^{-1} to amide II (N-H deformation), indicating the existence of the SF silk II structural conformation [33-35]. The band at 1233 cm^{-1} was ascribed to amide III (O-C-N bending), which is characteristic of the silk I conformation [36]. This indicates that silk I and silk II structures are presented simultaneously in pure SF hydrogels. The absorption bands of amide I, amide II and amide III of SF hydrogel prepared in the presence of ethanol were also centered at 1627 cm^{-1}, 1525 cm^{-1} and 1233 cm^{-1}, respectively, showing that the ethanol did not affect the structural conformation of SF (Fig. 5B(b)). The frozen SF hydrogel also presented the same absorption bands, showing that the freezing process did not affect the structural conformation of SF (Fig. 5B(c)). The spectrum of pure nanoHA aggregates (Fig. 5B(f)) presented typical absorption bands of HAs. The presence of phosphate (PO_4^{3-}), hydroxyl (OH^-) and H_2O groups was confirmed by the FTIR spectrum in nanoHA aggregates. The bands centered at 1028 cm^{-1}, 962 cm^{-1}, 602 cm^{-1}, 564 cm^{-1} and 472 cm^{-1} were due to the molecular vibrations of phosphate group. The band at 1028 cm^{-1} corresponded to v3 mode vibration of PO_4^{3-} and the band at 962 cm^{-1} corresponded to v1 mode vibration of PO_4^{3-}, whereas bands at 604 and 565 cm^{-1} were due to v4 mode vibration of PO_4^{3-} and the band at 472 cm^{-1} was due to v2 mode vibration of PO_4^{3-}. The band of hydroxyl group appeared at 631 cm^{-1}. The band at 875 cm^{-1} (v2 vibration) is due to carbonate group [19, 37, 38]. A broadband was observed at 3200–3600 cm^{-1}, which indicated adsorbed water on the materials. The spectra of non-frozen and frozen SF/nanoHA hydrogels (Fig. 5B(d) and (e)) showed all major bands of SF and nanoHA.

3.2.4. Thermal properties

Themogravimetric analysis (TGA) and differential thermogravimetric (DTGA) curves of nanoHA, SF hydrogels, and SF/nanoHA hydrogels are shown in Fig. 5C and D. The non-frozen and frozen SF hydrogels and composite hydrogels presented an initial weight loss below 100 °C and, as a temperature is increased, the second weight loss started to decrease sharply at above 200 °C (Fig. 5C(a)-(c)). In addition, the thermal behavior of the composite hydrogels was similar to SF probably due to its higher content in the

composites (Fig. 5C(d) and (e)). There was no significant weight loss of pure nanoHA when the temperature raised from 30 °C to 600 °C (Fig. 5C(f)). Fig. 5D presents the differential thermogravimetric curves for the hydrogels. The non-frozen and frozen SF and SF/nanoHA composite hydrogels presented similar behavior, with peaks of thermal degradation around 300 °C.

3.2.5. Swelling behavior

The most important property of a hydrogel is its ability to absorb and hold an amount of solvent in its network structure. It was observed that water swelling of hydrogels occurred rapidly (Fig. 6), reaching equilibrium of water uptake in approximately 10 min. The addition of nanoHA in the polymeric matrix decreased the swelling degree of SF/nanoHA hydrogels. Moreover, the frozen hydrogels presented higher swelling capacity.

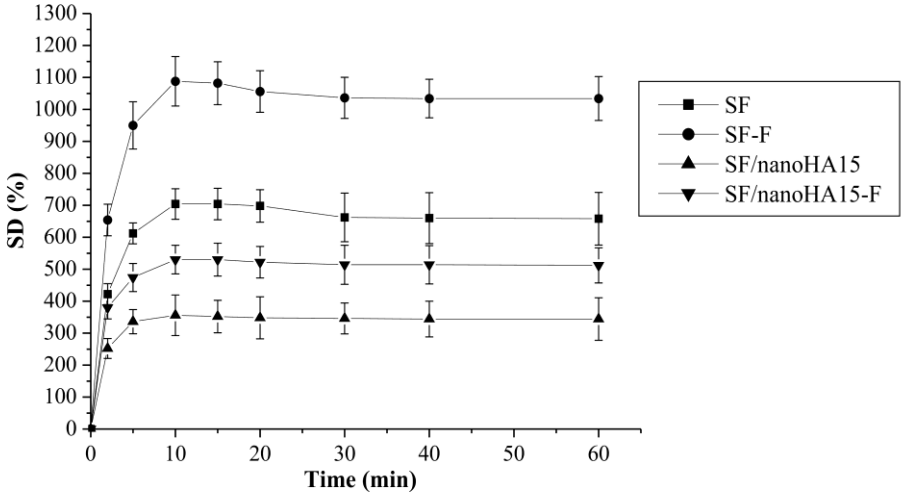

Fig. 6. Swelling degree for non-frozen and frozen SF hydrogels and SF/nanoHA composite hydrogels. Values are average ± SD.

3.3. Citocompatibility and ALP activity of SF/nanoHA composite hydrogels

The metabolic activity of the osteoblast-like cells MG63 in the hydrogels was evaluated by the resazurin assay. SF hydrogels without nanoHA were used as controls. Resazurin assay was performed on days 1, 4, and 7 of cell seeding to monitor the metabolic activity, and the data are shown in Fig. 7.

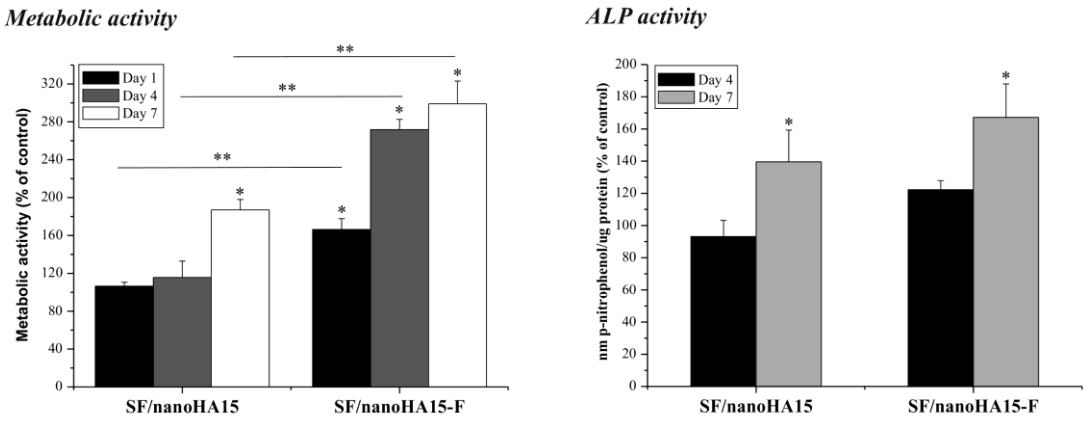

Fig. 7. Metabolic and ALP activities of MG63 osteoblast-like cells cultured on non-frozen and frozen SF/nanoHA15 hydrogels, using non-frozen and frozen SF hydrogels as control, respectively. * Significant differences ($p<0.05$) from the respective control at the same culture time. ** Significant differences ($p<0.05$) between non-frozen and frozen hydrogels. Data are presented as the average ± SD.

The metabolic activity of MG63 cells with frozen SF/nanoHA hydrogels was significant increased at all time-points when compared with to the respective control. However, for the non-frozen hydrogels a significant increase in metabolic activity was only observed at day 7. Moreover, the frozen hydrogels exhibited significantly higher metabolic activity than non-frozen hydrogels at all time-points. SF and SF/nanoHA composite hydrogels were observed by CLSM at day 7 (Fig. 8). Both types of hydrogels allowed the attachment and spreading of the cells, which showed an elongated morphology with well-defined nuclei and cell-to-cell contacts. In addition, cell distribution within the porous hydrogels was evident. Results presented in Figs. 7 and 8 support the compatibility of these 3D hydrogels.

The functional activity of the MG63 osteoblast-like cells on hydrogels was assessed by ALP activity. Fig. 7 showed that ALP activity increased with culture time on non-frozen and frozen SF/nanoHA hydrogels. These results also revealed an enhanced osteogenic response, as measured by ALP expression, for composite hydrogels at day 7.

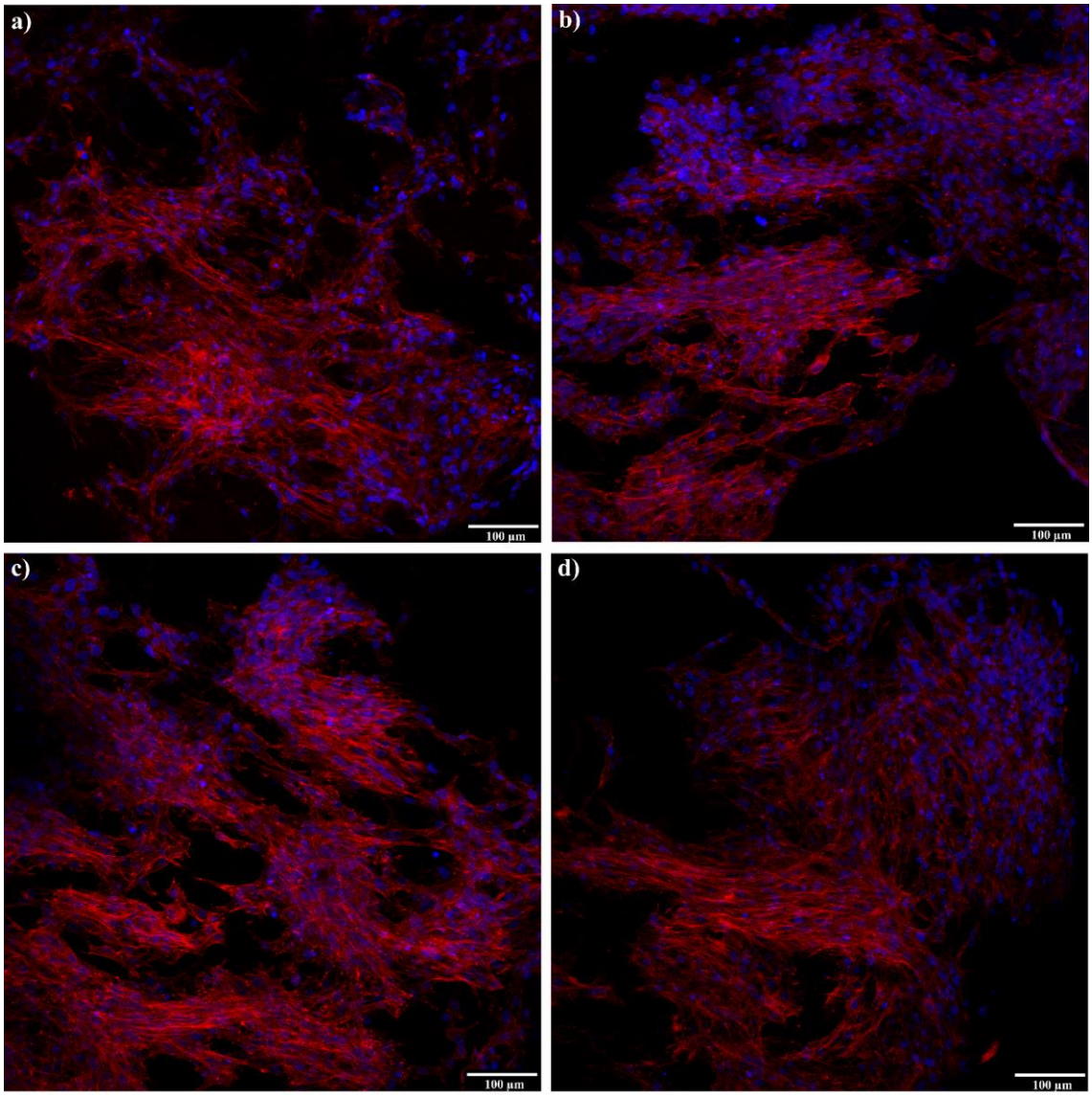

Fig. 8. CLSM images of osteoblastic cells at day 7 on SF hydrogels (a), frozen SF hydrogels (b), SF/nanoHA15 composite hydrogels (c) and frozen SF/nanoHA15 composite hydrogels (d). MG63 cells were stained for F-actin cytoskeleton with phalloidin (red) and nuclei with DAPI (blue).

4. Discussion

This study reports the development of a SF/nanoHA composite hydrogel by a new and innovative approach using ethanol as gelling agent, a method able of forming hydrogels in few minutes. This occurs because the conformational change of SF from

random coil to β-sheet structure was accelerated by the ethanol due to the dehydration of SF chains, allowing more interactions among SF molecules.

The SF/nanoHA hydrogels and frozen SF and SF/nanoHA hydrogels exhibited both microporosity and macroporosity structure with interconnected pores. These features are important for cell attachment and proliferation, cell-matrix interactions, vascularization, diffusion of nutrients and metabolites and *in vivo* bone ingrowth [39-41]. Studies in the literature report that pore sizes >50 μm have been shown to be favorable to new bone formation, whereas the minimum pore sizes for osteoconduction is thought to be 80-100 μm [42-44]. According to Sopyan *et al* [45] and Chang *et al* [46] biomaterials with pore sizes between 50 and 150 μm improve vascularization and cellular viability as well as formation of new bone tissue. Moreover, the distribution of nanoHA particles in the network of SF/nanoHA composite hydrogels is very important and will determine the properties of materials. The SEM images of hydrogels showed that nanoHA particles were homogenously dispersed and embedded throughout the SF structure without aggregation, indicating a good interaction between SF and nanoHA.

Pore size is also an important factor governing mechanical properties. The decrease observed in compression modulus for composite hydrogels with 10 wt% of nanoHA and frozen SF hydrogels, compared to SF hydrogels, could be attributed to the increase in pore sizes as well as the formation of an irregular porous structure. In scaffolds with small pore sizes the load gets distributed evenly throughout the surface to resist compression. Well-connected small pores form a barrier and do not allow the crack to propagate easily [47]. Moreover, other researchers reported that more uniform pore structure in scaffolds improved mechanical properties of the polymer matrices [48, 49]. The compression modulus of non-frozen and frozen composite hydrogels increased with the nanoHA concentration, from 10 to 15 wt%. Considering that the pore structure in the SF/nanoHA hydrogels is not uniform, the increase of mechanical properties of the composite hydrogels should be attributed to the higher nanoHA content. On the other hand, it should be emphasized that the compression modulus of the composite hydrogels was higher than that reported earlier for fibroin based hydrogels [50, 51].

By correlating the XRD and FTIR results, it is possible to state that the prepared non-frozen and frozen SF/nanoHA composite hydrogels possess a structure predominant of silk II and both analyses confirm the existence of nanoHA particles in the composite. Moreover, by XRD analysis it was observed that these composite hydrogels presented broader halos with lower intensity than pure nanoHA aggregates, suggesting that nanoHA particles modulated by the polymer have small crystallite sizes and low crystallinity, similar to natural bone minerals [52, 53]. The thermal degradation behavior of the non-frozen and frozen composite hydrogels was divided into two stages. The first one, below 100 °C, is related to the water evaporation, while the second stage, above 200 °C, is associated with the breakdown of side chain groups of amino acid residues as well as the cleavage of peptide bonds of SF (Fig. 5C(a)-(c)) [17, 54]. These materials were thermally stable with thermal degradation around 300 °C.

All the hydrogels showed high water uptake ability starting the swelling rapidly in the first 10 min and this behavior is a characteristic response that has been observed with porous and hydrophilic materials. The incorporation of nanoHA decreased the swelling of SF/nanoHA network, perhaps due to the lower water uptake ability of nanoHA compared to SF protein. Thein-Han and Misra also described a decrease in the swelling degree by addition of nanoHA aggregates to chitosan scaffolds [55]. Similarly, Peter *et al* studied chitosan-gelatin/nanohydroxyapatite composite scaffolds and observed that the addition of nanoHA decreased the water uptake capacity [56]. Moreover, the swelling degree was higher for frozen hydrogels and this behavior could be explained by the higher pore sizes for these hydrogels as compared to non-frozen hydrogels. This trend is in agreement with previously reported observations. Kim *et al* observed that the swelling ratio of the SF scaffolds decreased gradually with a decrease in pore size [30]. Mandal *et al* also observed that SF/polyacrylamide hydrogels presented a higher swelling ratio compared to pure polyacrylamide based hydrogels due to the larger diameter of the pores of the composite hydrogels [57]. Swelling and porosity aid in the supply of nutrients to the interior of the composite scaffolds and also increase the surface area for the cells to adhere that is essential for tissue engineering scaffolds. But increased swelling affects the mechanical property of the material, thus a controlled swelling is appreciated for any tissue engineering application, indicating that

the SF/nanoHA composite hydrogels are more adequate when compared to the SF hydrogels [56].

SF/nanoHA hydrogels are intended to be implanted at small bone defects in order to accelerate the rate of bone healing and regeneration. For that, the scaffold has to be biocompatible, facilitate cell proliferation and should not elicit a body immune response. To assess biological properties of hydrogels, these were seeded with MG63 osteoblastic cells. Resazurin assay revealed higher cell metabolic activity in the composite materials with nanoHA compared with SF hydrogels and, additionally, cell ingrowth was well evident on the porous composite scaffolds. Since it is well established that HA is bone-bioactive, SF/nanoHA hydrogels would have a high affinity for bone cells. It was reported that the addition of HA to polycaprolactone and poly(L-lactic acid) polymers could improve the cell viability and activity [58]. ALP activity, a common indicator of the expression of osteoblastic phenotype [59], was higher on the composite hydrogels, showing the efficiency of the nanoHA aggregates in enhancing the osteoblastic phenotype expression level. These findings indicate that these composites hydrogels are able to improve the functional activity of the bone-derived cells. Moreover, as the HA is an osteoconductive material, it may increase the rate of bone regeneration [60]. Additionally, the frozen SF/nanoHA composites showed increased metabolic activity compared to the non-frozen composites, a behavior that is most probably related to the larger pore sizes on the frozen scaffolds favouring cell migration. Therefore, results suggest that the composite hydrogels prepared in this work showed favorable cell-compatible characteristics and may be considered as an efficient material for cell ingrowth promotion in bone tissue engineering applications.

5. Conclusions

The aim of this study was to develop a novel composite hydrogel consisting of silk fibroin and nanohydroxyapatite, wherein the nanoHA particles were uniformly dispersed within the SF matrix. The macro/microporous structures with interconnected pores were successfully obtained. The compression modulus of

composite hydrogels increased as the nanoHA concentration increased from 10 to 15 wt%. Considering the results from XRD and FTIR spectroscopy analysis, nanoHA and the silk II conformation of SF existed in the structure of the composite hydrogels. The incorporation of nanoHA in composite hydrogels was associated to a decrease in swelling properties. In addition, the incorporation of nanoHA in the SF matrix resulted in a composite with improved cellular metabolic activity and ALP activity. Based on the promising physicochemical performance of the developed composite hydrogels, further *in vitro* studies (with mesenchymal stem cells) are envisioned in order to fully evaluate the biological performance of the SF/nanoHA composite hydrogels. In conclusion, compared to the SF hydrogels the composite hydrogels with nanoHA were found to be more promising materials for bone tissue engineering purposes.

Acknowledgments

This work was financed by *FEDER funds through the Programa Operacional Factores de Competitividade – COMPETE* and by *Portuguese funds through FCT – Fundação para a Ciência e a Tecnologia* in the framework of the NaNOBiofilm project (PTDC/SAUBMA/111233/2009) and PhD grant (SFRH/BD/90400/2012), whose support is acknowledged. The support of Project 346/13 CAPES (Brazil)-FCT (Portugal) Call 21/2012, and CNPq (Brazil) is acknowledged.

References

[1] Murugan R, Ramakrishna S. Development of nanocomposites for bone grafting. Compos Sci Technol. 2005;65(15-16):2385-2406.

[2] Valente JFA, Valente TAM, Alves P, Ferreira P, Silva A, Correia IJ. Alginate based scaffolds for bone tissue engineering. Mat Sci Eng C-Mater. 2012;32(8):2596-2603.

[3] Langer R, Vacanti JP. Tissue Engineering. Science. 1993;260(5110):920-926.

[4] Gloria A, De Santis R, Ambrosio L. Polymer-based composite scaffolds for tissue engineering. J Appl Biomater Biom. 2010;8(2):57-67.

[5] Mandal BB, Kapoor S, Kundu SC. Silk fibroin/polyacrylamide Semi-interpenetrating network hydrogels for controlled drug release. Biomaterials. 2009;30(14):2826-2836.

[6] Costa-Pinto AR, Reis RL, Neves NM. Scaffolds Based Bone Tissue Engineering: The Role of Chitosan. Tissue Eng Part B-Re. 2011;17(5):331-347.

[7] Altman GH, Diaz F, Jakuba C, Calabro T, Horan RL, Chen JS, et al. Silk-based biomaterials. Biomaterials. 2003;24(3):401-416.

[8] Wang YZ, Kim HJ, Vunjak-Novakovic G, Kaplan DL. Stem cell-based tissue engineering with silk biomaterials. Biomaterials. 2006;27(36):6064-6082.

[9] Vepari C, Kaplan DL. Silk as a biomaterial. Prog Polym Sci. 2007;32(8-9):991-1007.

[10] Bhardwaj N, Chakraborty S, Kundu SC. Freeze-gelled silk fibroin protein scaffolds for potential applications in soft tissue engineering. Int J Biol Macromol. 2011;49(3):260-267.

[11] Motta A, Fambri L, Migliaresi C. Regenerated silk fibroin films: Thermal and dynamic mechanical analysis. Macromol Chem Physic. 2002;203(10-11):1658-1665.

[12] Sashina ES, Bochek AM, Novoselov NP, Kirichenko DA. Structure and solubility of natural silk fibroin. Russ J Appl Chem+. 2006;79(6):869-876.

[13] Vasconcelos A, Freddi G, Cavaco-Paulo A. Biodegradable materials based on silk fibroin and keratin. Biomacromolecules. 2008;9(4):1299-1305.

[14] Horan RL, Antle K, Collette AL, Huang YZ, Huang J, Moreau JE, et al. In vitro degradation of silk fibroin. Biomaterials. 2005;26(17):3385-3393.

[15] Meinel L, Betz O, Fajardo R, Hofmann S, Nazarian A, Cory E, et al. Silk based biomaterials to heal critical sized femur defects. Bone. 2006;39(4):922-931.

[16] Nogueira GM, Aimoli CG, Weska RF, Nascimento LS, Beppu MM. "In vitro" calcification of silk fibroin hydrogel. Bioceramics, Vol 20, Pts 1 and 2. 2008;361-363:503-506.

[17] Nogueira GM, Weska RF, Vieira WC, Polakiewicz B, Rodas ACD, Higa OZ, et al. A New Method to Prepare Porous Silk Fibroin Membranes Suitable for Tissue Scaffolding Applications. J Appl Polym Sci. 2009;114(1):617-623.

[18] Ferraz MP, Monteiro FJ, Manuel CM. Hydroxyapatite nanoparticles: A review of preparation methodologies. Journal of applied biomaterials & biomechanics : JABB. 2004;2(2):74-80.

[19] Teixeira S, Rodriguez MA, Pena P, De Aza AH, De Aza S, Ferraz MP, et al. Physical characterization of hydroxyapatite porous scaffolds for tissue engineering. Mat Sci Eng C-Bio S. 2009;29(5):1510-1514.

[20] Prabakaran K, Rajeswari S. Spectroscopic investigations on the synthesis of nano-hydroxyapatite from calcined eggshell by hydrothermal method using cationic surfactant as template. Spectrochim Acta A. 2009;74(5):1127-1134.

[21] Raksujarit A, Pengpat K, Rujijanagul G, Tunkasiri T. Processing and properties of nanoporous hydroxyapatite ceramics. Mater Design. 2010;31(4):1658-1660.

[22] Kalita SJ, Verma S. Nanocrystalline hydroxyapatite bioceramic using microwave radiation: Synthesis and characterization. Mat Sci Eng C-Mater. 2010;30(2):295-303.

[23] Zhang LJ, Webster TJ. Nanotechnology and nanomaterials: Promises for improved tissue regeneration. Nano today. 2009;4(1):66-80.

[24] Zhang ZZ, Li MY, Chen W, Zhu SZ, Liu NN, Zhu LY. Immobilization of lead and cadmium from aqueous solution and contaminated sediment using nano-hydroxyapatite. Environ Pollut. 2010;158(2):514-519.

[25] Ferraz MP, Mateus AY, Sousa JC, Monteiro FJ. Nanohydroxyapatite microspheres as delivery system for antibiotics: Release kinetics, antimicrobial activity, and interaction with osteoblasts. J Biomed Mater Res A. 2007;81A(4):994-1004.

[26] Oliveira GM, Ferraz MP, Gonzalez PG, Serra J, Leon B, Perez-Amor M, et al. PLD bioactive ceramic films: the influence of CaO-P2O5 glass additions to hydroxyapatite on the proliferation and morphology of osteblastic like-cells. Journal of materials science Materials in medicine. 2008;19(4):1775-1785.

[27] de Moraes MA, Nogueira GM, Weska RF, Beppu MM. Preparation and Characterization of Insoluble Silk Fibroin/Chitosan Blend Films. Polymers-Basel. 2010;2(4):719-727.

[28] Kim UJ, Park JY, Li CM, Jin HJ, Valluzzi R, Kaplan DL. Structure and properties of silk hydrogels. Biomacromolecules. 2004;5(3):786-792.

[29] Liu Y, Cheng YD, Xiong SY, Li PJ, Wei YQ, Li MZ. The Effect of Shearing Force on the Gel Formation and Structural Transitions of Regenerated Silk Fibroin. Text Bioeng Inform S. 2010:309-315.

[30] Kim UJ, Park J, Kim HJ, Wada M, Kaplan DL. Three-dimensional aqueous-derived biomaterial scaffolds from silk fibroin. Biomaterials. 2005;26(15):2775-2785.

[31] Wang L, Li CZ. Preparation and physicochemical properties of a novel hydroxyapatite/chitosan-silk fibroin composite. Carbohyd Polym. 2007;68(4):740-745.

[32] Venkatesan J, Kim SK. Effect of Temperature on Isolation and Characterization of Hydroxyapatite from Tuna (Thunnus obesus) Bone. Materials. 2010;3(10):4761-4772.

[33] Hu X, Shmelev K, Sun L, Gil ES, Park SH, Cebe P, et al. Regulation of silk material structure by temperature-controlled water vapor annealing. Biomacromolecules. 2011;12(5):1686-1696.

[34] Hu X, Kaplan D, Cebe P. Determining Beta-Sheet Crystallinity in Fibrous Proteins by Thermal Analysis and Infrared Spectroscopy. Macromolecules. 2006;39(18):6161-6170.

[35] Lu Q, Hu X, Wang X, Kluge JA, Lu S, Cebe P, et al. Water-insoluble silk films with silk I structure. Acta biomaterialia. 2010;6(4):1380-1387.

[36] Cilurzo F, Gennari CGM, Selmin F, Marotta LA, Minghetti P, Montanari L. An investigation into silk fibroin conformation in composite materials intended for drug delivery. Int J Pharm. 2011;414(1–2):218-224.

[37] Chang MC, Tanaka J. FT-IR study for hydroxyapatite/collagen nanocomposite cross-linked by glutaraldehyde. Biomaterials. 2002;23(24):4811-4818.

[38] Laranjeira MS, Fernandes MH, Monteiro FJ. Innovative macroporous granules of nanostructured-hydroxyapatite agglomerates: Bioactivity and osteoblast-like cell behaviour. J Biomed Mater Res A. 2010;95A(3):891-900.

[39] Singh R, Lee PD, Lindley TC, Dashwood RJ, Ferrie E, Imwinkelried T. Characterization of the structure and permeability of titanium foams for spinal fusion devices. Acta biomaterialia. 2009;5(1):477-487.

[40] Wei J, Jia J, Wu F, Wei S, Zhou H, Zhang H, et al. Hierarchically microporous/macroporous scaffold of magnesium-calcium phosphate for bone tissue regeneration. Biomaterials. 2010;31(6):1260-1269.

[41] Rucker M, Laschke MW, Junker D, Carvalho C, Tavassol F, Mulhaupt R, et al. Vascularization and biocompatibility of scaffolds consisting of different calcium phosphate compounds. J Biomed Mater Res A. 2008;86A(4):1002-1011.

[42] Kong L, Ao Q, Wang A, Gong K, Wang X, Lu G, et al. Preparation and characterization of a multilayer biomimetic scaffold for bone tissue engineering. Journal of biomaterials applications. 2007;22(3):223-239.

[43] Lu JX, Flautre B, Anselme K, Hardouin P, Gallur A, Descamps M, et al. Role of interconnections in porous bioceramics on bone recolonization in vitro and in vivo. Journal of materials science Materials in medicine. 1999;10(2):111-120.

[44] Gauthier O, Bouler JM, Aguado E, Pilet P, Daculsi G. Macroporous biphasic calcium phosphate ceramics: influence of macropore diameter and macroporosity percentage on bone ingrowth. Biomaterials. 1998;19(1-3):133-139.

[45] Sopyan I, Mel M, Ramesh S, Khalid KA. Porous hydroxyapatite for artificial bone applications. Sci Technol Adv Mat. 2007;8(1-2):116-123.

[46] Chang BS, Lee CK, Hong KS, Youn HJ, Ryu HS, Chung SS, et al. Osteoconduction at porous hydroxyapatite with various pore configurations. Biomaterials. 2000;21(12):1291-1298.

[47] Kim UJ, Park J, Li C, Jin HJ, Valluzzi R, Kaplan DL. Structure and properties of silk hydrogels. Biomacromolecules. 2004;5(3):786-792.

[48] Harris LD, Kim BS, Mooney DJ. Open pore biodegradable matrices formed with gas foaming. J Biomed Mater Res. 1998;42(3):396-402.

[49] Nazarov R, Jin HJ, Kaplan DL. Porous 3-D scaffolds from regenerated silk fibroin. Biomacromolecules. 2004;5(3):718-726.

[50] Xiao W, He J, Nichol JW, Wang L, Hutson CB, Wang B, et al. Synthesis and characterization of photocrosslinkable gelatin and silk fibroin interpenetrating polymer network hydrogels. Acta biomaterialia. 2011;7(6):2384-2393.

[51] Elia R, Newhide DR, Pedevillano PD, Reiss GR, Firpo MA, Hsu EW, et al. Silk-hyaluronan-based composite hydrogels: a novel, securable vehicle for drug delivery. Journal of biomaterials applications. 2013;27(6):749-762.

[52] Rhee S-H, Tanaka J. Self-assembly phenomenon of hydroxyapatite nanocrystals on chondroitin sulfate. Journal of Materials Science: Materials in Medicine. 2002;13(6):597-600.

[53] Murugan R, Ramakrishna S. Bioresorbable composite bone paste using polysaccharide based nano hydroxyapatite. Biomaterials. 2004;25(17):3829-3835.

[54] Um IC, Kweon HY, Park YH, Hudson S. Structural characteristics and properties of the regenerated silk fibroin prepared from formic acid. Int J Biol Macromol. 2001;29(2):91-97.

[55] Thein-Han WW, Misra RD. Biomimetic chitosan-nanohydroxyapatite composite scaffolds for bone tissue engineering. Acta biomaterialia. 2009;5(4):1182-1197.

[56] Peter M, Ganesh N, Selvamurugan N, Nair SV, Furuike T, Tamura H, et al. Preparation and characterization of chitosan–gelatin/nanohydroxyapatite composite scaffolds for tissue engineering applications. Carbohyd Polym. 2010;80(3):687-694.

[57] Mandal BB, Kapoor S, Kundu SC. Silk fibroin/polyacrylamide semi-interpenetrating network hydrogels for controlled drug release. Biomaterials. 2009;30(14):2826-2836.

[58] Rizzi SC, Heath DJ, Coombes AGA, Bock N, Textor M, Downes S. Biodegradable polymer/hydroxyapatite composites: Surface analysis and initial attachment of human osteoblasts. J Biomed Mater Res. 2001;55(4):475-486.

[59] Ren L, Tsuru K, Hayakawa S, Osaka A. Novel approach to fabricate porous gelatin-siloxane hybrids for bone tissue engineering. Biomaterials. 2002;23(24):4765-4773.

[60] Lin H-R, Yeh Y-J. Porous alginate/hydroxyapatite composite scaffolds for bone tissue engineering: Preparation, characterization, and in vitro studies. Journal of Biomedical Materials Research Part B: Applied Biomaterials. 2004;71B(1):52-65.

CHAPTER IV

Silk fibroin/nanohydroxyapatite hydrogels for promoted bioactivity and osteoblastic proliferation and differentiation of human bone marrow stromal cells

Marta Ribeiro [1,2,3,*], Maria H. Fernandes [4,5], Marisa M. Beppu [6], Fernando J. Monteiro [1,2,3], Maria P. Ferraz [7]

[1] i3S - Instituto de Investigação e Inovação em Saúde, Universidade do Porto, Porto, 4200-135, Portugal

[2] INEB - Instituto de Engenharia Biomédica, Universidade do Porto, Porto, 4150-180, Portugal.

[3] FEUP - Faculdade de Engenharia da Universidade do Porto, Departamento de Engenharia Metalúrgica e Materiais, Porto, 4200-465, Portugal.

[4] Laboratory for Bone Metabolism and Regeneration, Faculdade de Medicina Dentária, Universidade do Porto, Porto, 4200-393, Portugal.

[5]REQUIMTE/LAQV – U. Porto – Porto/Portugal

[6] School of Chemical Engineering, University of Campinas, Campinas-SP, 13083-852, Brazil.

[7] FP-ENAS/CEBIMED - University Fernando Pessoa Energy, Environment and Health Research Unit/Biomedical Research Center, Porto, 4249-004, Portugal.

Submitted.

Abstract

Silk fibroin (SF) is a natural, biocompatible, and biodegradable polymer having a great potential for the successful regeneration of damaged bone tissue. In the present work, nanohydroxyapatite (nanoHA) was incorporated into SF polymer to form a bioactive composite hydrogel for applications as bone implants. The degradation and bioactive properties of SF/nanoHA composite hydrogels were evaluated. Additionally, biological investigations of human bone marrow stromal cells (hBMSCs) viability, proliferation and differentiation to the osteoblastic phenotype were conducted. The incorporation of nanoHA in SF polymer matrices improved the bioactivity of the hydrogels. The biological results highlighted that the SF/nanoHA composite hydrogels are suitable for hBMSCs attachment and proliferation, while a test for alkaline phosphatase (ALP) and bone morphogenetic protein 2 (BMP-2) expression suggested osteoblast differentiation. Additionally, a cell staining method for ALP allowed to observe cell infiltration with active production of ALP by the infiltrated cells, paving the way to use the proposed composite hydrogel for bone tissue regeneration.

Keywords: silk fibroin; nanohydroxyapatite; bioactivity; osteoblast differentiation

1. Introduction

Scaffolds and cells are essential components in bone regenerative approaches. These scaffolds focus on developing biologically-based substitutes with similar structure and functionality to the extracellular matrix (ECM) in order to assist cell adhesion and proliferation. Biological scaffolds should gradually degrade to support the cell ingrowth and bone formation through the regeneration process, as well as to avoid the risk of complications that may be associated with the long-term presence of a foreign material [1-4]. Hydrogels have attracted extensive interest because of their advantageous properties similar to those of the native ECM, such as biocompatibility and the ability to absorb high amounts of water or biological fluids without dissolving, thus maintaining their three-dimensional (3D) structure and function. Their high permeability allows the exchange of oxygen, nutrients, and soluble metabolites [5-7].

Silk fibroin (SF) is a protein polymer derived from the cocoons of *Bombyx mori* which possesses adequate properties for bone tissue engineering scaffolds, such as biocompatibility, biodegradability, high permeability to oxygen and water vapor, versatile processing, and adjustable mechanical and biochemical properties [8-11].

SF-based composite hydrogels incorporating relevant molecules of the extracellular matrix such as SF/hyaluronic acid [12] and SF/collagen [13] have been reported to present enhanced physicochemical and biological properties for tissue engineering applications. In a different approach, the incorporation of a bioactive ceramic in the hydrogel matrix is expected to improve the osteogenic potential of the resulting composite. The presence of the bioactive ceramic inside a polymeric matrix would mimic the inorganic phase of the extracellular matrix favoring bone cell behavior and the interaction with the surrounding bone tissue [14, 15]. In a previous study, we described the preparation of novel SF-hydrogels incorporating different percentages of nanophased hydroxyapatite (HA) by using a new and innovative method, in which ethanol was used as gelling agent [8]. The SF hydrogel incorporating 15wt% of nanoHA, obtained by a freezing method, yielded a composite with improved mechanical properties together with a higher amount of uniformly dispersed

particles throughout the matrix, in combination with interconnected micro- and macroporosity suitable for new bone formation. Additionally, preliminary biological data performed with MG63 cells showed promising results regarding osteoblastic cell response [8].

Consequently, the main goal of the current work was to exploit the suitability of the SF/15% wt% nanoHA hydrogel for bone regenerative strategies. For that, the SF/nanoHA hydrogel was prepared as described previously [8] and evaluated for enzymatic degradation, bioactivity and ability to promote the proliferation and osteoblastic differentiation of human bone marrow stromal cells.

2. Materials and Methods

2.1. Preparation of silk fibroin solution

Cocoons of *Bombyx mori* silkworm (supplied by Bratac, São Paulo, Brazil) were degummed in 1 g/L Na_2CO_3 solution at 85°C for 1 h 30 min, with Na_2CO_3 being changed every 30 min to remove the sericin of the cocoons and obtain pure SF fibers. Then, SF fibers were dried and dissolved in a ternary solvent of $CaCl_2$:CH_3CH_2OH:H_2O, in a molar ratio of 1:2:8, at 85 °C until total dissolution, to a SF salt solution of 10% (w/v). The SF salt solution was then dialyzed (cellulose membrane, Viscofan 22 EU – 20 USA) against distilled water for 3 days, at 8 °C, with water being changed every 24 hours. The final concentration of the SF aqueous solution was 4% (w/v), which was determined by weighing the remaining solid after drying.

2.2. Preparation of silk fibroin/nanoHA hydrogels

SF/nanoHA hydrogels were prepared according to our previously established method [8]. Briefly, the dry power of nanoHA aggregates (Fluidinova S.A., Maia, Portugal) was first mixed with 70% ethanol and then slowly mixed with the SF aqueous solution at 37ºC. SF and nanoHA were mixed at ratios of SF/nanoHA 100/0 and 85/15 wt%. The hydrogel containing 15% of nanoHA was called SF/nanoHA15. A part of these

hydrogels was frozen to evaluate differences in the properties of frozen and non-frozen hydrogels. These hydrogels were identified with the letter F.

2.3. *In vitro* enzymatic degradation

In vitro enzymatic degradation of the hydrogels was measured versus time, by incubating the gels in protease XIV solution (*Streptomyces griseus*, Sigma) and monitoring the hydrogel mass. Hydrogels sections with 7 mm diameter and 5 mm thickness were carefully transferred to 48-well plates and soaked in phosphate-buffered saline solution (PBS, pH 7.4) overnight to reach swelling equilibrium. The gels were removed from PBS, excess liquid was blotted from the surface with filter paper, and the gel masses were determined. The gels were incubated at 37ºC in 1 mL phosphate-buffered saline solution (PBS, pH 7.4) containing the protease. The enzyme concentrations used in this test were 0.5 and 1.0 mg/mL [16]. The enzyme solution was replaced daily with freshly prepared solution. The control hydrogels were immersed in 1 mL PBS which was also refreshed daily. At designated time points (1, 3, 7 and 10 days), groups of samples were rinsed in distilled water and prepared for mass balance and scanning electron microscopy (SEM).

The percentage of weight loss [W (%)] of hydrogels was determined based on the following equation:

$$W\ (\%) = (W_0 - W_d)/W_0 \times 100$$

where W_0 is the initial weight of the hydrogel sample and W_d is the weight of the sample after degradation at predetermined days.

2.4. Biodegradation and bioactivity assessment in SBF

The *in vitro* degradation and bioactivity of the hydrogels were carried out using standard simulated body fluid (SBF) containing inorganic ion concentrations similar to those of human blood plasma [17]. The SBF solution was prepared by dissolving NaCl (8.035 g), $NaHCO_3$ (0.355 g), KCl (0.225 g), $K_2HPO_4.3H_2O$ (0.231 g), $MgCl_2.6H_2O$ (0.311 g), $CaCl_2$ (0.292 g) and Na_2SO_4 (0.072 g) into 700 mL ultrapure water. The solution

was buffered at physiological pH 7.4 with Tris buffer (6.118 g) and HCl. Then the total volume of solution was filled up to 1000 mL with ultrapure water [17].

Hydrogels sections with 7 mm diameter and 5 mm thickness were carefully transferred to 48-well plates and were soaked in ultrapure water overnight to reach swelling equilibrium. The gels were removed from ultrapure water, excess liquid was blotted from the surface with filter paper, and the gel masses were determined. Then, the samples were immersed separately in 20 mL SBF in closed falcon tubes at 37 °C for 1, 3, 7, 14 and 21 days. After the different incubation time-points, the materials were removed from SBF solution, washed with ultrapure water and prepared for mass balance. Finally the hydrogels were freeze-dried, sectioned and viewed using SEM for apatite layer formation.

2.5. SEM

SEM was used to observe the morphology of samples after enzymatic degradation with protease XIV solution, as well as the apatite layer formation in the hydrogels after immersion in SBF. The analysis was performed on samples sputter coated (SPI-Module) with a thin gold/palladium film and then examined by SEM using a FEI Quanta 400 FEG/ESEM (FEI) scanning electron microscope at an accelerating voltage of 15 kV.

2.6. In vitro biological studies

2.6.1. hBMSCs isolation and culture

Human Bone Marrow Stromal Cells (hBMSCs) were obtained from bone marrow following orthopaedic surgery procedures, with patient's informed consent. The bone fragments (which would be otherwise discharged) were broken in small pieces and washed with alpha minimum essential medium (α-MEM, Sigma-Aldrich) supplemented with 10% (v/v) fetal bovine serum (FBS, Gibco), 100 IU/mL/ 2.5 µg/mL penicillin-streptomycin solution (Gibco) and 2.5 µg/mL amphotericin B (Gibco). The cell suspension was seeded in Petri dishes for 10 days. Afterwards, at 70 – 80%

confluence, the cell monolayer was washed with PBS twice and cells were detached with trypsin solution (0.04%, Gibco) and subcultured. All assays were conducted with cells in passage 4.

Prior to cell seeding, the hydrogel sections with 7 mm diameter and 5 mm thickness were sterilized in ethanol solution at 70% (v/v) and subsequently washed twice with phosphate-buffered saline (PBS). For cell seeding, a suspension of 10^5 cells/scaffold was added on the top of each hydrogel. For the osteogenic medium, the above described medium was supplemented with 10 mM β-glycerophosphate (Sigma) and 10^{-8} M dexamethasone (Sigma). The seeded scaffolds were incubated in a humidified atmosphere of 95% air and 5% CO_2 at 37 °C. All samples were cultured for 1, 7, 14 and 21 days. The hBMSCs-seeded hydrogels were assessed for cell viability, proliferation, alkaline phosphatase (ALP) activity, total protein content, and F-actin cytoskeleton, ALP and BMP-2 immunostaining. The SF hydrogels were used as controls of the SF/nanoHA hydrogels.

2.6.2. Metabolic activity

At each time point, the metabolic activity was evaluated by the resazurin assay. The same sample was followed throughout the culture time, i.e. it was assessed at all-time points. In the resazurin assay, a non-fluorescent blue component is reduced by the living cells to a pink fluorescent component. Fresh medium with 10% (v/v) of resazurin was added to the cells, which were incubated at 37 °C in a humidified atmosphere of 95% air and 5% CO_2 for 3 h. Then, 100 µL were transferred to a 96-well plate and the fluorescence intensity was measured in a microplate reader (Synergy HT, BioTek) at 535 nm excitation wavelength and 590 nm emission wavelength. The data reported were the average of measurements from three samples.

2.6.3. DNA content

Cell proliferation was assessed by the DNA extraction assay, at days 1, 7, 14 and 21. DNA content was measured using the PicoGreen DNA quantification assay (Quant-iT™ Picogreen dsDNA assay, Molecular Probes, Invitrogen), according to the

manufacturer's instructions. After washing the hydrogels with PBS, they were immersed in 0.5 mL of ultrapure water and placed at 37 °C /5% CO_2 for 1 h, and then placed in a freezer at -80 °C. Subsequently, the hydrogels were thawed at room temperature to lyse the cell membranes. The fluorescence intensity was measured in a microplate reader (Synergy HT, BioTek) at 480 and 520 nm, excitation and emission, respectively.

2.6.4. Alkaline phosphatase activity and protein content

At each time point, colonized hydrogels were washed twice with PBS and immersed in 0.5 mL ultrapure water at 37 °C /5% CO_2 for 1 h. They were then placed in a freezer at -80 °C and then thawed at room temperature to lyse the cell membranes. Alkaline phosphatase (ALP) activity was assayed by the hydrolysis of p-nitrophenol phosphate (Sigma), in alkaline buffer solution, 2-amino-2-methyl-1-propanol (Sigma), at pH 10.5. After 1 h of incubation at 37 °C, the reaction was stopped by adding NaOH (5M, Sigma), and the absorbance of the hydrolysis product (p-nitrophenol) was measured at 405 nm, using a plate reader (BioTek). ALP activity was normalized to total protein content and was expressed as nanomoles of p-nitrophenol produced per minute per microgram of total protein (nmol min^{-1}/μg protein). Total protein content was measured by Lowry's method with bovine serum albumin used as a standard.

2.6.5. F-actin cytoskeleton, ALP and BMP-2 immunostaining

For F-actin cytoskeleton and BMP-2 immunostaining, seeded hydrogel samples were fixed in 3.7% formaldehyde (Sigma) for 15 min and washed twice with PBS. Then, cells were permeabilized with 0.1% (v/v) Triton X-100 solution (Sigma) for 30 min. Afterwards, samples were washed twice in PBS and incubated in 1% bovine serum albumin solution in PBS (BSA, Sigma) for 30 min to avoid nonspecific binding. For F-actin cytoskeleton immunostaining, cells were stained with Alexafluor phalloidin 488 (Invitrogen) in 1% BSA solution for 30 min at room temperature. Samples were washed twice with PBS and cell nuclei were stained with a buffer of Propidium iodide and RNase (BD Pharmigen) for 10 min. For BMP-2 immunostaining, cells were incubated with the primary antibody rabbit anti-BMP2 (1:200; Abcam) overnight at 4

°C. Samples were then washed twice in PBS and incubated with the secondary antibody Alexa Fluor 488 goat anti-rabbit igG for 1h (1:1000; Molecular Probes).

ALP staining was performed in live cells by using an Alkaline Phosphatase (AP) Live Stain kit (Molecular Probes, Life Technologies), according to the manufacturer's instructions. Briefly, the culture medium was removed and the seeded hydrogels were washed twice with fresh medium. Then, and appropriate amount of 1X AP Live Stain solution was directly applied to the seeded hydrogels, followed by a 30 min incubation. Finally, the AP Live Stain was removed and the hydrogels were washed twice with fresh medium.

Immunostained hydrogels were observed under a Spectral Confocal Microscope Leica TCS-SP5 AOBS (Leica).

2.7. Statistical analysis

The results were expressed as the average ± standard deviation. The statistical analysis of the results was carried out using the one-way analysis of variance (ANOVA) followed by *post hoc* Tukey HSD multiple comparison test. Levels of $p < 0.05$ were considered to be statistically significant.

3. Results

3.1. Enzymatic degradation

The degradation behavior of the SF and SF/nanoHA hydrogels was assessed by incubating the materials in protease XIV and PBS (as a control) to evaluate quantitative changes. Figures 1A and 1B show the weight loss of the SF and SF/nanoHA hydrogels, respectively, over time during a degradation period of 10 days. All materials presented progressive loss of mass by enzymatic hydrolysis over time. In contrast to SF hydrogels, which were fully degraded within 10 days, the percentage of weight loss of non-frozen and frozen SF/nanoHA hydrogels was 75.8% and 79.7%, respectively, for protease concentration of 0.5 mg/mL. Using the protease concentration of 1.0 mg/mL the degradation was 86.3% and 89.9% for non-frozen

and frozen composite hydrogels, respectively. The differences between non-frozen and frozen hydrogels were not significant ($p>0.05$) at any of the time points for both protease concentrations. The hydrogels incubated in PBS showed no significant degradation within 10 days and the structure integrity was maintained over time (data not shown).

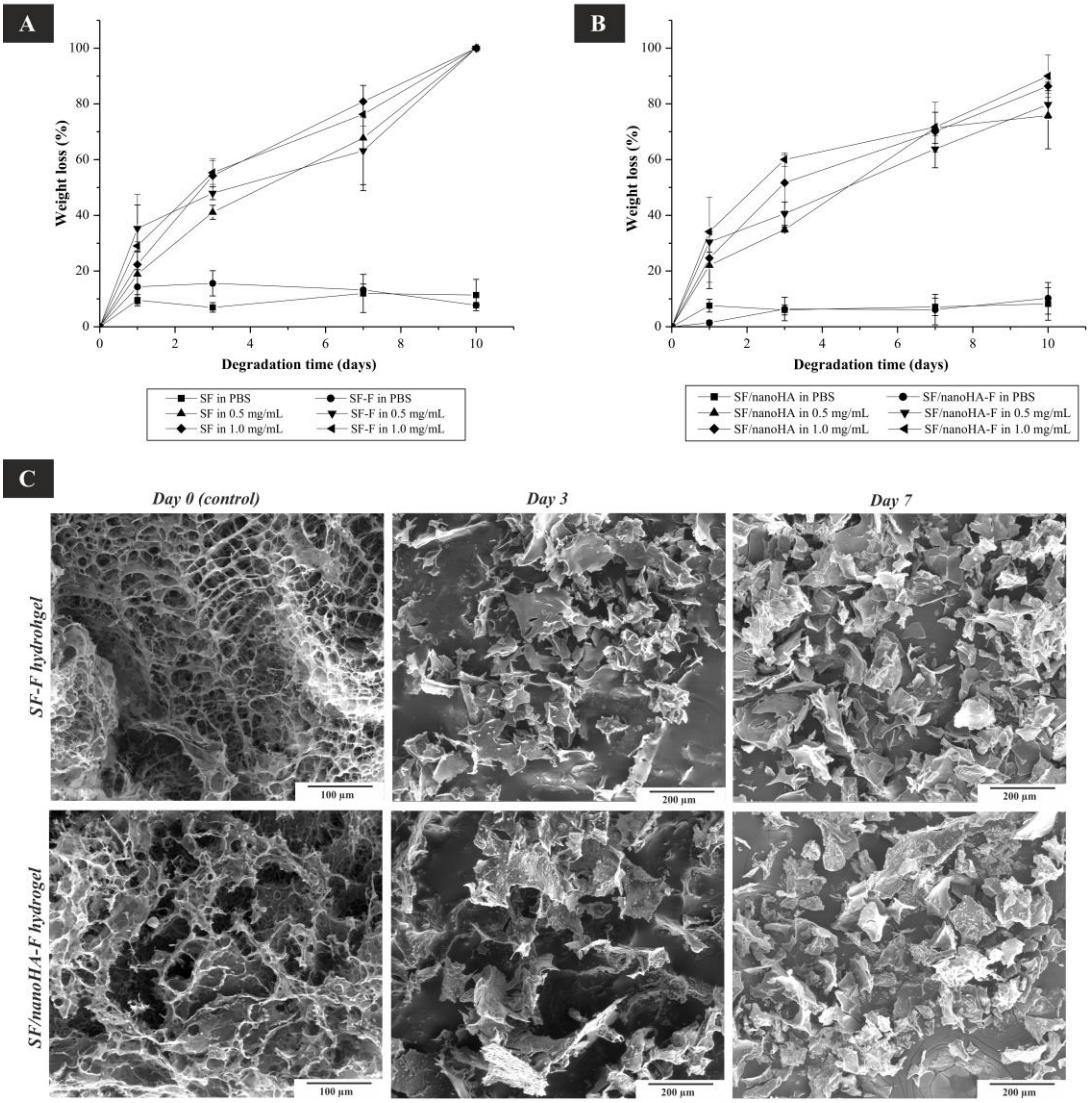

Figure 1 – Weight loss of non-frozen and frozen (A) SF and (B) SF/nanoHA hydrogels over time during a degradation period of 10 days by protease, and (C) SEM images of frozen hydrogels before degradation and after 3 and 7 days of degradation.

Figure 1C shows the morphological changes of hydrogels before degradation and after 3 and 7 days degradation by protease XIV. Similar morphological changes were

observed for non-frozen and frozen hydrogels, and therefore only SEM images of frozen materials are shown. Before incubation, the porous structure of SF and SF/nanoHA hydrogels was intact and with interconnected pores (Figure 1C). After incubation in the enzyme solution, the morphology of both hydrogels exhibited a drastic change, where the hydrogels could not keep its original form and collapsed, completely losing the porous structure.

Although a significant degradation was also observed in the composite hydrogels, an interesting phenomenon concerning to nanoHA distribution could not be neglected. As shown in Figure 2, after the degradation of the porous structure it was clearly visible that the nanoHA aggregates were deposited uniformly in the SF matrix.

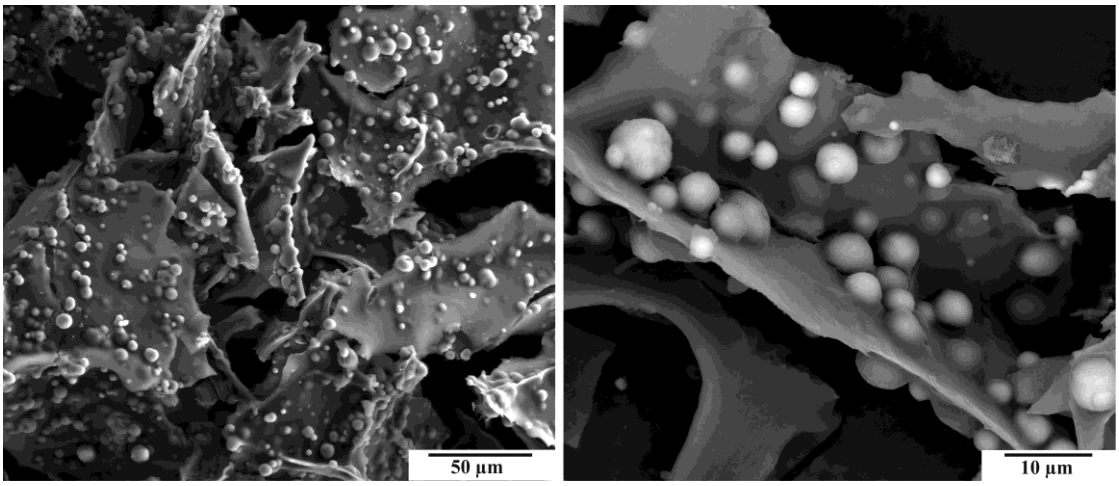

Figure 2 – NanoHA distribution in the SF/nanoHA hydrogels after the enzymatic degradation of the porous structure.

3.2. Apatite forming ability

3.2.1. Morphology and EDS analysis

The bioactive character of the hydrogels was tested *in vitro* by analyzing the ability to form apatite at their surface after being immersed in SBF. The prepared materials were immersed in SBF up to 21 days. Figure 3 shows the SEM images of apatite layer formation on the hydrogels after 7 and 21 days. Similar apatite formation was observed for non-frozen and frozen hydrogels, and therefore only SEM images of

frozen materials are shown. After 7 days in SBF, apatite structures had already been formed. After 21 days in solution, the apatite layer increased in density and was distributed over the entire surface of the two hydrogels. A more marked apatite formation was seen on hydrogels containing nanoHA.

The analysis of the energy dispersive spectroscopy (EDS) spectra of the frozen SF and SF/nanoHA hydrogels revealed the presence of the Ca and P elements, which corresponds to an apatite-like layer (Figure 3). The weight percentages of Ca and P were similar for both hydrogels at day 7. Nevertheless, at day 21, the percentage of these elements only slightly increased for SF hydrogels while presenting a significant increase for SF/nanoHA hydrogels.

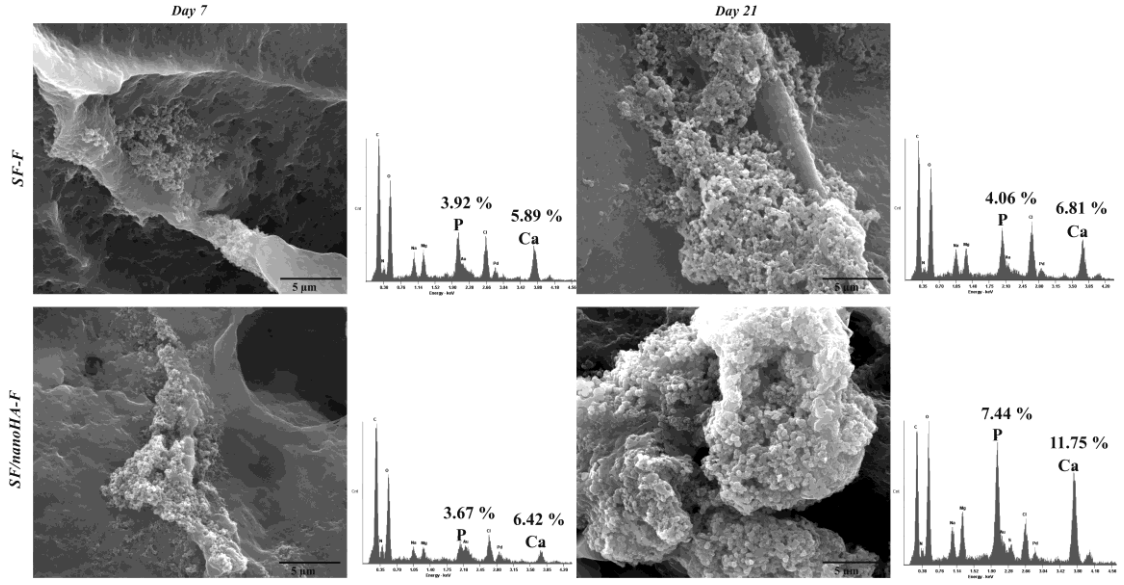

Figure 3 - SEM images and respective EDS spectra of frozen SF and SF/nanoHA hydrogels showing the formation of apatite after 7 and 21 days of immersion in SBF. The weight percentages of Ca and P are shown in the EDS spectra.

3.2.2. Degradation

Figure 4 shows the weight loss of non-frozen and frozen SF and SF/nanoHA hydrogels in SBF at various time intervals. The mass of non-frozen and frozen SF hydrogels did not significantly change over 21 days. The weight loss of non-frozen and frozen composite hydrogels was also not significant until day 14. However, afterwards, the weight loss of these composites continuously decreases so that, at day 21, the

samples gained weight when comparing to the initial value, before immersion in SBF, meaning that a deposit has been formed. This observation is in agreement with the results reported in the previous section, showing significant apatite formation in the composites, at later incubation times, compared to that observed in SF hydrogels.

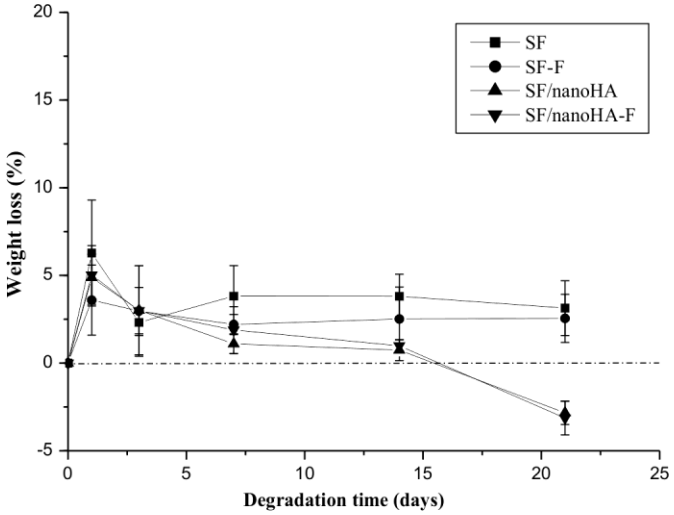

Figure 4 - Weight loss of non-frozen and frozen SF and SF/nanoHA hydrogels in SBF at various time intervals.

3.3. Biological studies

3.3.1. Cell metabolic activity and proliferation

Figure 5 shows the results of the metabolic activity, DNA quantification and confocal microscopy images for the SF and SF/nanoHA hydrogels seeded with hBMSCs, at different time-points.

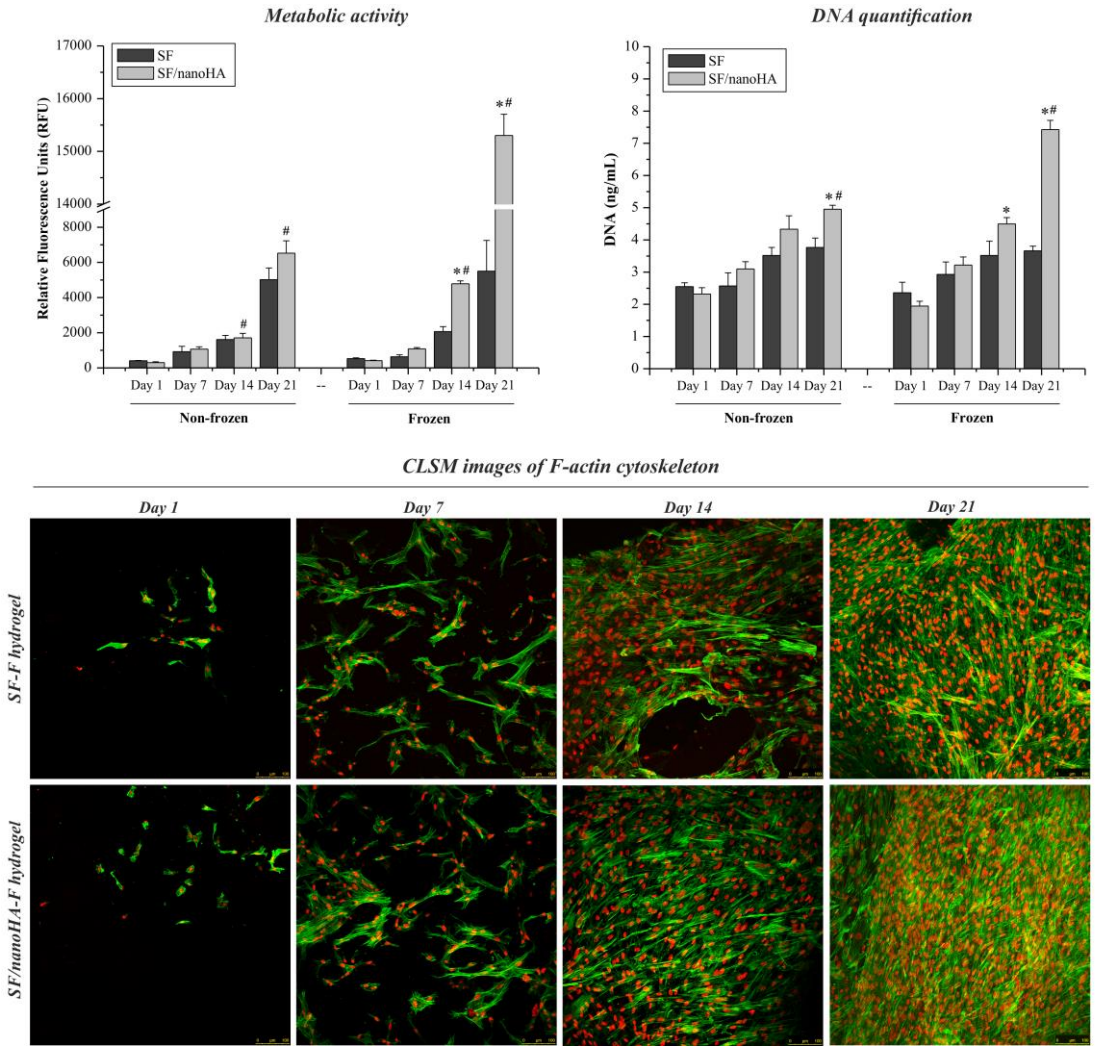

Figure 5 - Cell metabolic activity and DNA content of hBMSCs cultured on non-frozen and frozen SF and SF/nanoHA hydrogels, and CLSM images of hBMSCs on frozen SF and SF/nanoHA hydrogels, for 1, 7, 14 and 21 days of culture. * indicate significant differences ($p<0.05$) between SF and SF/nanoHA hydrogels at the same culture time. # indicate significant differences ($p<0.05$) between non-frozen and frozen SF/nanoHA hydrogels. Data are presented as the average ± SD. hBMSCs cells were stained for F-actin cytoskeleton with Alexafluor phalloidin (green) and nuclei with Propidium iodide (red).

Metabolic activity increased throughout the 21 days culture time for all tested hydrogels. For non-frozen SF and SF/nanoHA hydrogels, no significant differences in metabolic activity were observed, except for a slightly increased value for the composite hydrogel at day 21. On the contrary, for frozen materials, a significant

increase in metabolic activity was observed for SF/nanoHA hydrogels at day 14 (> 100%) and, particularly, at day 21 (~3 fold), comparatively to SF hydrogels. When comparing the materials of these two groups, non-frozen and frozen, no significant differences in metabolic activity were observed for SF hydrogels; however, the frozen SF/nanoHA hydrogels presented significantly increased values at days 14 and 21.

Concerning to DNA content, the same trend of cell response was observed for SF and SF/nanoHA hydrogels, considering non-frozen and frozen samples.

CLSM images of the frozen hydrogels showed that hBMSCs easily attached to the hydrogels and spread over the surface. At day 7, images showed cells with elongated morphology and cell-to-cell contact in both materials. At day 14, the cells were well spread out with notable cell-to-cell contact, forming an organized cell layer. At day 21, both hydrogels were completely covered with a dense cell layer. Images also suggested that the SF/nanoHA hydrogels showed a denser cell layer compared to SF hydrogels.

3.3.2. Alkaline phosphatase (ALP) activity and staining

ALP activity of hBMSCs cultured on non-frozen and frozen SF and SF/nanoHA hydrogels was analyzed at days 7, 14, and 21 (Figure 6A). ALP activity on non-frozen SF/nanoHA and SF hydrogels was similar during the 21 days of culture. In contrast, in the frozen hydrogels, at day 21, ALP activity of SF/nanoHA hydrogels was significantly higher than that for SF hydrogels.

The presence of ALP was also examined in live cells, using an alkaline live stain (Figure 6B). The ALP live stain showed that the cells were alive, functional, and homogeneously distributed throughout the hydrogels. On the SF hydrogel, stained cells were seen dispersed through the sample with irregular morphology and areas of higher intensity staining. Better cell response appears to occur with the SF/nanoHA composites. Cells presented elongated morphologies, with uniform ALP staining, cell-to-cell contact and establishing a continuous cell layer.

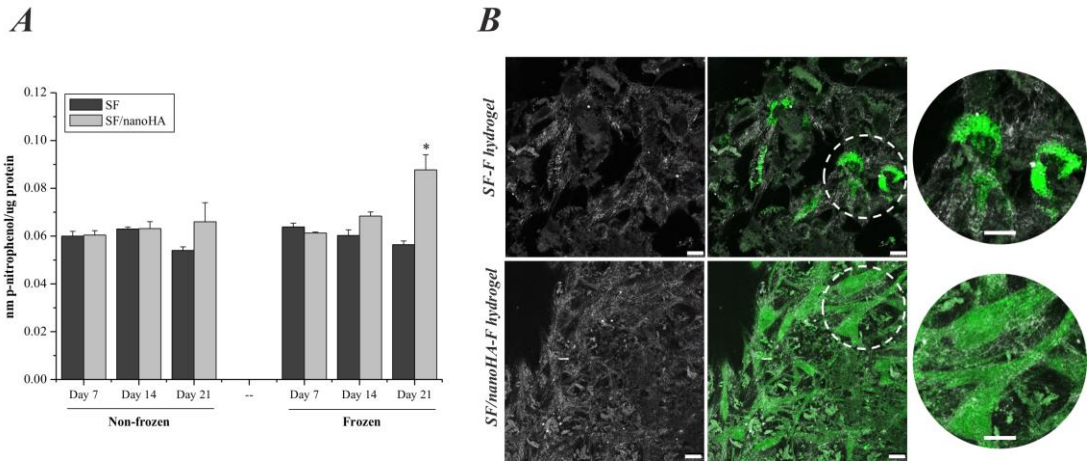

Figure 6 – (A) ALP activity of hBMSCs on non-frozen and frozen SF and SF/nanoHA hydrogels for 7, 14 and 21 days of culture, and (B) fluorescence images showing hBMSCs stained for ALP on frozen SF and SF/nanoHA hydrogels at 21 days. * indicate significant differences ($p<0.05$) in relation to SF hydrogel at the same culture time. Data are presented as the average ± SD. Scale bar: 25 µm.

3.3.3. BMP-2 expression

The BMP-2 protein expression was investigated through immunostaining analysis as shown in Figure 7. A strong staining intensity of BMP-2 expression was observed, at 21 days of culture, on frozen SF/nanoHA hydrogels in comparison to SF materials.

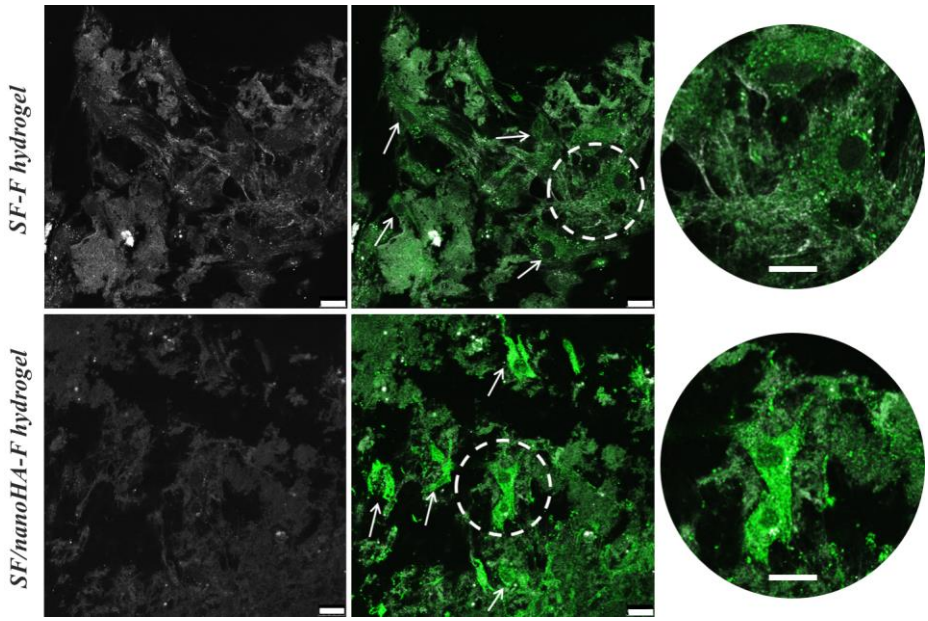

Figure 7 – Fluorescence images showing BMP-2 expression in hBMSCs cultured on frozen SF and SF/nanoHA hydrogels at 21 days. Scale bar: 25 µm.

3.3.4. Cellular ingrowth inwards the porous structure

Figure 8 presents a sequence of CLSM images showing a detail of the cell growth observed in the colonized frozen SF/nanoHA hydrogel inside a pore, at 21 days of culture. Clear evidence of cell infiltration through the pores was observed. Additionally, cells stained intensively for ALP through the porous structure, evidencing their functional activity both at the surface and within the pores walls.

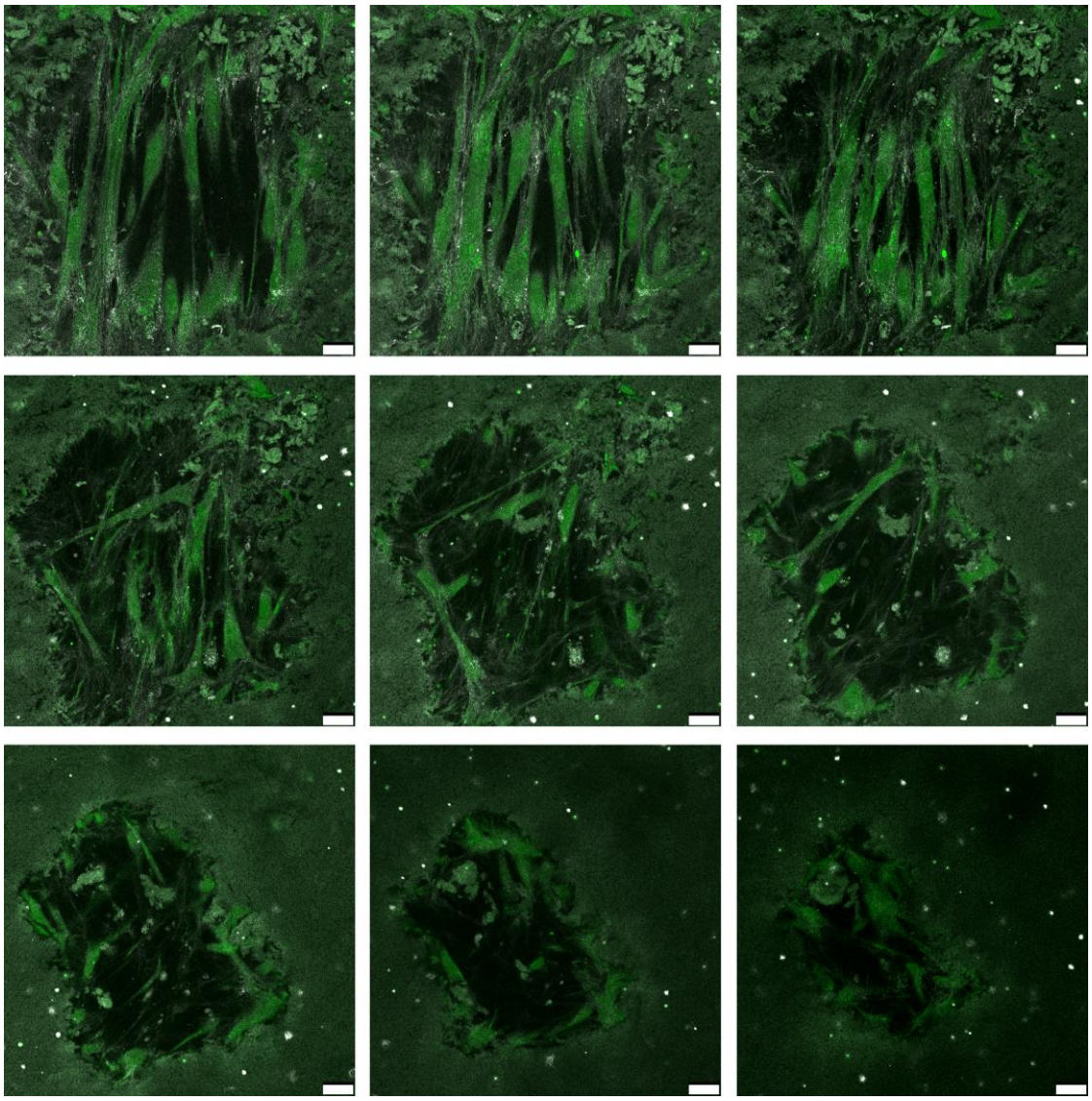

Figure 8 – Representative sequence of CLSM images showing the infiltration of hBMSCs on frozen SF/nanoHA composite hydrogel inside a pore, at 21 days of culture. Cells were stained with an ALP live stain (green). Scale bar: 25 µm.

4. Discussion

The incorporation of bioactive ceramics in biodegradable polymer matrices to produce three-dimensional (3D) scaffold materials is an additional design feature needed for bone tissue engineering applications. In a previous work, a SF hydrogel incorporating 15% (wt%) of nanoHA with larger pore sizes, due to a freezing method, was developed. The micro- and macroporosity obtained combined with interconnective porous structure and an uniform dispersion of nanoHA particles throughout the fibroin matrix, makes this composite hydrogel a very promising alternative to be applied in bone regeneration. Therefore, the main goal of this work was to exploit the *in vitro* biological response of this SF/nano hydrogel using human bone marrow stromal cells.

An appropriate degradation rate of the hydrogels is essential for bone tissue regeneration. It is desired that the scaffold degradation rate *in vivo* might match the rate of *de novo* tissue formation so that the porous structure is replaced by new tissue [18]. *In vitro* enzymatic hydrolysis provides a general idea of the biodegradability of a material. Generally, the enzymatic degradation of biomaterials is a two-step process. At first, proteolytic enzymes are adsorbed to the SF biomaterials, which demands that the enzymes must find binding domains on the material's surface. Afterwards, SF biomaterials are enzymatically digested leading to the corresponding amino acids, which are easily disposed *in vivo*, an advantage of SF used in the biomedical applications [19, 20]. In the present work, while the SF hydrogels incubated with the protease were fully degraded within 10 days, the materials incubated in phosphate buffer showed no significant degradation, confirming that the mass loss was due solely to enzymatic hydrolysis. This marked degradation shows the potential of SF as a biodegradable material. Additionally, with the incorporation of nanoHA aggregates into the hydrogels the degradation rate was similar to that found in control SF materials. Furthermore, a uniform dispersion of nanoHA particles throughout the fibroin matrix was observed after the enzymatic degradation, which is crucial for a good performance of the composite hydrogel in bone tissue engineering. The degradation rate and the morphological structure

changes were similar for the non-frozen and frozen hydrogels, suggesting that pore size did not correlate to degradation rate. This is in agreement with previous results reported by Kim U. *et al* in SF scaffolds with different pore sizes exposed to a protease solution [21].

To be effectively used for bone tissue regeneration, it is beneficial that a material might promote bone-like apatite formation when in contact with physiological fluid. SF and SF/nanoHA hydrogels were evaluated for their bioactivity using SBF. The morphological analysis combined with the EDS analysis confirmed the presence of a CaP layer on the surface of non-frozen and frozen SF and SF/nanoHA hydrogels. Nevertheless, the composite hydrogel containing nanoHA had greater ability to induce the apatite layer formation *in vitro*. The nanoHA aggregates in the composite could act as nucleation sites and consequently the apatite could be formed more effectively on the composite hydrogels than on the SF hydrogels. This is in line with previous studies performed in chitosan-gelatin scaffolds incorporating nanophase hydroxyapatite [22], also in a poly(L-lactic acid) (PLLA) matrix with the addition of HA particles [23]. Additionally, in the later study, the implantation of the apatite-coated poly(L-lactic acid)/hydroxyapatite (PLLA/HA) composite scaffold in the subchondral bone of healthy sheep femoral condyle yielded better integration in comparison to non-coated PLLA scaffolds [23]. Back to the present work, immersion of SF hydrogels in SBF did not result in significant weight loss during the 21 days. However, in the SF/nanoHA hydrogels, the weight increased from day 14 until day 21, which could be attributed to deposition of apatite particles (Ca^{2+} and PO_4^{3-} ions) on the surface of the composite hydrogels. The present results showed an improvement of bioactivity on the composite hydrogels indicating that these materials have great potential for bone tissue engineering.

Hydrogels for bone regeneration must be cytocompatible and actively encourage ingrowth of cells. As evaluated by the resazurin assay and DNA quantification, the increase of metabolic activity and proliferation, respectively, of hBMSCs on hydrogels over time indicated the cytocompatible of these materials. These results correlated well with confocal images that showed extensive cell spreading and proliferation within the hydrogels. For later culture times, the hBMSCs cultured in the hydrogels

with nanoHA proliferated significantly, showing an inductive effect of the presence of nanoHA. Previous studies had also proven that the inclusion of nanoHA in scaffolds of pullulan and dextran could enhance the proliferation of hBMSCs in the hydrogels [24]. Moreover, this tendency was particularly confirmed in the case of frozen SF/nanoHA hydrogels, showing that the increase of pore size of frozen materials [8] may play a prominent role in metabolic cell activities and proliferation. Bhardwaj N *et al* also reported that the metabolic activity and proliferation ability of the cells was higher in SF/chitosan scaffolds with larger pores [25].

One of the most attractive characters that hBMSCs show is their multiple differentiation potential. Under appropriate conditions, hBMSCs are able to differentiate towards several cell lineages, including osteoblasts, adipocytes chondrocytes, and myocytes. Differentiation is induced through addition of "cocktails" of morphogens and chemicals inducing the differentiation of a particular cell type. *In vitro,* differentiation is verified by demonstrating the induction of specific gene expression and proteins [26-28]. In osteogenesis, differentiation of hBMSCs into osteoblasts is a key step and ALP is an important early marker for cells undergoing differentiation to form osteoblast [29]. ALP activity, normalized as a function of the protein content, was the highest in the case of frozen SF/nanoHA composite hydrogels at 21 days of culture, showing the efficacy of nanoHA aggregates in enhancing the osteoblastic phenotype expression level. Furthermore, it is worth noting that this difference in ALP expression between frozen SF and SF/nanoHA materials was observed in a quantitative assay and also in a live cell staining. Several other works can be found in the literature indicating the effect of nanoHA in the ALP expression in different composite materials, such as poly(L/DL)-lactide/nanoHA membranes [30], nanoHA/polyamide scaffolds [31], and poly(L-lactic acid)/poly-benzyl-L-glutamate/collagen/nanoHA scaffolds [32].

Immunofluorescent staining of BMP-2 protein showed greater expression in the SF/nanoHA composite hydrogels compared to that of control SF materials. Bone morphogenetic proteins (BMPs) play an important role in osteoblast differentiation and deposition of bone matrix. The high osteoinductive potential of some BMPs is illustrated by their ability to induce bone formation. Among them, BMP-2 protein is

essential to induce the expression of Runt-related transcription factor 2 (Runx-2) and Osterix, the two critical transcription factors in osteoblast differentiation. Runx-2 is the main regulator for the expression of downstream key genes, as collagen type I, alkaline phosphatase, osteopontin, bone sialoprotein and osteocalcin, at an early stage of osteoblastic differentiation. Runx-2 has also a role in the regulation of the Osterix expression, a later key transcription factor for osteoblastic differentiation, which is involved in collagen type I and osteocalcin gene activation, being also a downstream regulator for Runx-2 activity [33-36].

Hydrogels should have the ability to regenerate functional bone tissue at the site of injury through a cell migration process in a carefully orchestrated manner. Initial attachment of cells is especially critical for long-term cells stability and differentiation. The ability of the composite hydrogel to support hBMSCs adhesion and proliferation was also evaluated using a live cell fluorescence staining for ALP. CLSM images showed that hBMSCs were able to infiltrate and migrate within the hydrogel, through the porous structure. Furthermore, one interesting finding in this work was that ALP expression in hBMSCs was observed within the SF/nanoHA hydrogel, indicating not only cell infiltration into the material, but also active production of ALP by the infiltrated cells.

The results of the current work support the potential of this composite hydrogel as a material for stimulating new bone tissue formation.

5. Conclusions

Advances in bone tissue engineering require biofunctional hydrogels that interact with bone forming cells. To achieve this goal, a SF/nanoHA composite hydrogel with improved bioactivity was developed. The SF/nanoHA hydrogels can act as matrix for hBMSCs viability and proliferation, which was significantly improved on frozen composite materials. Confocal images showed that hBMSCs could spread and proliferate on these hydrogels during 21 days of culture. Furthermore, an improvement of the osteogenic response, as seen by ALP and BMP-2 expression, was

observed for composite materials. Also, evident infiltration of functionally active cells through the porous hydrogel structure was noticed. This work therefore enlightens to the development of new bone implantable scaffolds potentially useful in regenerative medicine.

Acknowledgements

This work was financed by FEDER - Fundo Europeu de Desenvolvimento Regional funds through the COMPETE 2020 – Operacional Programme for Competitiveness and Internationalisation (POCI), Portugal 2020, and by Portuguese funds through FCT - Fundação para a Ciência e a Tecnologia/ Ministério da Ciência, Tecnologia e Inovação in the framework of the project "Institute for Research and Innovation in Health Sciences (POCI-01-0145-FEDER-007274)" and PhD grant (SFRH/BD/90400/2012), whose support is acknowledged. Financial support from the European Union (FEDER funds POCI/01/0145/FEDER/007265) and National Funds (FCT/MEC, Fundação para a Ciência e Tecnologia and Ministério da Educação e Ciência) under the Partnership Agreement PT2020 UID/QUI/50006/2013, is also acknowledged. The authors thank FLUIDINOVA S.A. (Maia-Portugal) for the provision of nanoHA.

References

[1] Tortelli F, Cancedda R. Three-dimensional cultures of osteogenic and chondrogenic cells: a tissue engineering approach to mimic bone and cartilage in vitro. European cells & materials 2009;17:1-14.

[2] Hutmacher DW, Schantz JT, Lam CX, Tan KC, Lim TC. State of the art and future directions of scaffold-based bone engineering from a biomaterials perspective. J Tissue Eng Regen Med 2007;1:245-60.

[3] Azevedo HS, Gama FM, Reis RL. In Vitro Assessment of the Enzymatic Degradation of Several Starch Based Biomaterials. Biomacromolecules 2003;4:1703-12.

[4] Annor AH, Tang ME, Pui CL, Ebersole GC, Frisella MM, Matthews BD, et al. Effect of enzymatic degradation on the mechanical properties of biological scaffold materials. Surgical endoscopy 2012;26:2767-78.

[5] Ahearne M, Yang Y, El Haj AJ, Then KY, Liu KK. Characterizing the viscoelastic properties of thin hydrogel-based constructs for tissue engineering applications. Journal of the Royal Society, Interface / the Royal Society 2005;2:455-63.

[6] Peppas NA, Hilt JZ, Khademhosseini A, Langer R. Hydrogels in Biology and Medicine: From Molecular Principles to Bionanotechnology. Advanced Materials 2006;18:1345-60.

[7] Geckil H, Xu F, Zhang X, Moon S, Demirci U. Engineering hydrogels as extracellular matrix mimics. Nanomedicine (London, England) 2010;5:469-84.

[8] Ribeiro M, de Moraes MA, Beppu MM, Garcia MP, Fernandes MH, Monteiro FJ, et al. Development of silk fibroin/nanohydroxyapatite composite hydrogels for bone tissue engineering. European Polymer Journal 2015;67:66-77.

[9] Rockwood DN, Preda RC, Yucel T, Wang X, Lovett ML, Kaplan DL. Materials fabrication from Bombyx mori silk fibroin. Nat Protoc 2011;6:1612-31.

[10] Bhardwaj N, Chakraborty S, Kundu SC. Freeze-gelled silk fibroin protein scaffolds for potential applications in soft tissue engineering. Int J Biol Macromol 2011;49:260-7.

[11] Meinel AJ, Kubow KE, Klotzsch E, Garcia-Fuentes M, Smith ML, Vogel V, et al. Optimization strategies for electrospun silk fibroin tissue engineering scaffolds. Biomaterials 2009;30:3058-67.

[12] Hu X, Lu Q, Sun L, Cebe P, Wang X, Zhang X, et al. Biomaterials from Ultrasonication-Induced Silk Fibroin−Hyaluronic Acid Hydrogels. Biomacromolecules 2010;11:3178-88.

[13] Lv Q, Hu K, Feng Q, Cui F. Fibroin/collagen hybrid hydrogels with crosslinking method: preparation, properties, and cytocompatibility. J Biomed Mater Res A 2008;84:198-207.

[14] Puppi D, Chiellini F, Piras AM, Chiellini E. Polymeric materials for bone and cartilage repair. Progress in Polymer Science 2010;35:403-40.

[15] Poursamar SA, Azami M, Mozafari M. Controllable synthesis and characterization of porous polyvinyl alcohol/hydroxyapatite nanocomposite scaffolds via an in situ colloidal technique. Colloids and surfaces B, Biointerfaces 2011;84:310-6.

[16] Rajkhowa R, Gil ES, Kluge J, Numata K, Wang L, Wang X, et al. Reinforcing silk scaffolds with silk particles. Macromol Biosci 2010;10:599-611.

[17] Kokubo T, Takadama H. How useful is SBF in predicting in vivo bone bioactivity? Biomaterials 2006;27:2907-15.

[18] Nie L, Chen D, Fu J, Yang S, Hou R, Suo J. Macroporous biphasic calcium phosphate scaffolds reinforced by poly-L-lactic acid/hydroxyapatite nanocomposite coatings for bone regeneration. Biochemical Engineering Journal 2015;98:29-37.

[19] Nair LS, Laurencin CT. Biodegradable polymers as biomaterials. Progress in Polymer Science 2007;32:762-98.

[20] Cao Y, Wang B. Biodegradation of Silk Biomaterials. International Journal of Molecular Sciences 2009;10:1514-24.

[21] Kim UJ, Park J, Kim HJ, Wada M, Kaplan DL. Three-dimensional aqueous-derived biomaterial scaffolds from silk fibroin. Biomaterials 2005;26:2775-85.

[22] Peter M, Ganesh N, Selvamurugan N, Nair SV, Furuike T, Tamura H, et al. Preparation and characterization of chitosan–gelatin/nanohydroxyapatite composite scaffolds for tissue engineering applications. Carbohydrate polymers 2010;80:687-94.

[23] Deplaine H, Lebourg M, Ripalda P, Vidaurre A, Sanz-Ramos P, Mora G, et al. Biomimetic hydroxyapatite coating on pore walls improves osteointegration of poly(L-lactic acid) scaffolds. J Biomed Mater Res B Appl Biomater 2013;101:173-86.

[24] Fricain JC, Schlaubitz S, Le Visage C, Arnault I, Derkaoui SM, Siadous R, et al. A nano-hydroxyapatite--pullulan/dextran polysaccharide composite macroporous material for bone tissue engineering. Biomaterials 2013;34:2947-59.

[25] Bhardwaj N, Kundu SC. Chondrogenic differentiation of rat MSCs on porous scaffolds of silk fibroin/chitosan blends. Biomaterials 2012;33:2848-57.

[26] Kassem M, Abdallah BM, Saeed H. Osteoblastic cells: Differentiation and trans-differentiation. Archives of Biochemistry and Biophysics 2008;473:183-7.

[27] Rauh J, Milan F, Gunther KP, Stiehler M. Bioreactor systems for bone tissue engineering. Tissue Eng Part B Rev 2011;17:263-80.

[28] Lu H, Lian L, Shi D, Zhao H, Dai Y. Hepcidin promotes osteogenic differentiation through the bone morphogenetic protein 2/small mothers against decapentaplegic and mitogen-activated protein kinase/P38 signaling pathways in mesenchymal stem cells. Molecular Medicine Reports 2015;11:143-50.

[29] Fielding GA, Roy M, Bandyopadhyay A, Bose S. Antibacterial and biological characteristics of silver containing and strontium doped plasma sprayed hydroxyapatite coatings. Acta Biomater 2012;8:3144-52.

[30] Rajzer I, Menaszek E, Kwiatkowski R, Chrzanowski W. Bioactive nanocomposite PLDL/nano-hydroxyapatite electrospun membranes for bone tissue engineering. Journal of materials science Materials in medicine 2014;25:1239-47.

[31] Wang H, Li Y, Zuo Y, Li J, Ma S, Cheng L. Biocompatibility and osteogenesis of biomimetic nano-hydroxyapatite/polyamide composite scaffolds for bone tissue engineering. Biomaterials 2007;28:3338-48.

[32] Ravichandran R, Venugopal JR, Sundarrajan S, Mukherjee S, Ramakrishna S. Precipitation of nanohydroxyapatite on PLLA/PBLG/Collagen nanofibrous structures for the differentiation of adipose derived stem cells to osteogenic lineage. Biomaterials 2012;33:846-55.

[33] Kang Q, Sun MH, Cheng H, Peng Y, Montag AG, Deyrup AT, et al. Characterization of the distinct orthotopic bone-forming activity of 14 BMPs using recombinant adenovirus-mediated gene delivery. Gene Ther 2004;11:1312-20.

[34] Datta HK, Ng WF, Walker JA, Tuck SP, Varanasi SS. The cell biology of bone metabolism. Journal of clinical pathology 2008;61:577-87.

[35] Raida M, Heymann AC, Gunther C, Niederwieser D. Role of bone morphogenetic protein 2 in the crosstalk between endothelial progenitor cells and mesenchymal stem cells. International journal of molecular medicine 2006;18:735-9.

[36] Fernandes MH, Gomes PS. Bone Cells Dynamics during Peri-Implantitis: a Theoretical Analysis. J Oral Maxillofac Res 2016;7:e6.

CHAPTER V

Antibacterial silk fibroin/nanohydroxyapatite hydrogels with silver and gold nanoparticles for bone regeneration

Marta Ribeiro [a, b, c, *], Maria P. Ferraz [b, d], Fernando J. Monteiro [a, b, c], Maria H. Fernandes [e], Marisa M. Beppu [f], Daniele Mantione [g], Haritz Sardon [g, *]

[a] i3S - Instituto de Investigação e Inovação em Saúde, Universidade do Porto, Porto, 4200-135, Portugal

[b] INEB - Instituto de Engenharia Biomédica, Universidade do Porto, Porto, 4150-180, Portugal.

[c] FEUP - Faculdade de Engenharia da Universidade do Porto, Departamento de Engenharia Metalúrgica e Materiais, Porto, 4200-465, Portugal.

[d] FP-ENAS/CEBIMED - University Fernando Pessoa Energy, Environment and Health Research Unit/Biomedical Research Center, Porto, 4249-004, Portugal.

[e] Laboratory for Bone Metabolism and Regeneration, Faculdade de Medicina Dentária, Universidade do Porto, Porto, 4200-393, Portugal

[f] School of Chemical Engineering, University of Campinas, Campinas-SP, 13083-852, Brazil.

[g] POLYMAT University of the Basque Country UPV/EHU, Joxe Mari Korta Center, 20018 Donostia-San Sebastian, Spain.

Nanomedicine: Nanotechnology, Biology, and Medicine, 2016; 13:231-239.

Abstract

The rapid emergence of antibiotic resistance is becoming an imminent problem in bone tissue engineering, and therefore biomaterials must be modified to promote the tissue integration before bacterial adhesion. In this work, silk fibroin/nanohydroxyapatite hydrogel was modified with *in situ* synthesized silver and gold nanoparticles (AgNPs and AuNPs), taking advantage of the tyrosine amino acid. The presence of AgNPs and AuNPs in the hydrogels was characterized by UV spectrophotometer, transmission electron microscopy and thermogravimetric analysis. *In vitro* antimicrobial studies revealed that hydrogels with AgNPs and AuNPs exhibited significant inhibition ability against both Gram-positive and Gram-negative bacteria. Cytocompatibility studies carried out using osteoblastic cells revealed that up to 0.5 wt% of AgNPs, and for all concentrations of AuNPs, the hydrogels can be effectively used as antimicrobial materials, without compromising cell behavior. On the basis of the aforementioned observations, these hydrogels are very attractive for bone tissue engineering.

Keywords: Silk fibroin; nanohydroxyapatite; silver nanoparticles; gold nanoparticles; antimicrobial activity

1. Background

The ideal approach for bone tissue engineering is that the tissue integration occurs prior to bacterial adhesion, thereby preventing material colonization for certain bacterial species. Adhesion of bacteria to human tissue and implanted biomaterials is the first critical step in the pathogenesis of infection, whereby the bacteria can divide and colonize the surface. After adhering to the surface, some bacterial strains, particularly *Staphylococcus epidermidis*, secrete a layer of slime, which serve to anchor the bacterial cells. Bacterial biofilms are particularly problematic because sessile bacteria can often withstand host immune response and antibiotic therapies. Additionally, these sessile biofilms can give rise to nonsessile individuals, planktonic bacteria that can rapidly multiply and disperse. [1-4] A very large proportion of biomaterial-associated infections in orthopedics are caused by *S. aureus* and *S. epidermidis*, the main responsible agents for the two major types of infection affecting bone, septic arthritis and osteomyelitis, with consequent devastating effects on bone and surrounding soft tissues. Treatment for *S. aureus* infections is often complex, namely due to the emergence of methicillin-resistant *S. aureus* (MRSA) strains and resistance to other classes of antibiotics. [1, 5]

The increase in antibiotic-resistant bacterial strains has prompted a renewed interest in the development of new antimicrobial approaches. [6-8] Metallic elements have garnered prominent consideration as they present antimicrobial properties. Moreover, these metallic elements in the form of nanoparticles are excellent candidates for antimicrobial applications due to their large surface area to volume ratio, providing better contact with microorganisms, and these nanoparticles are also an encouraging approach concerning their chemical stability, long life, and heat resistance. [9, 10] In recent years, silver nanoparticles (AgNPs) have attracted much attention for a range of biomedical applications owing to their potent antimicrobial activity against a large number of bacteria, including antibiotic-resistant strains. [11-13] The antibacterial activity of AgNPs has been related to inhibition of enzymatic activities, prevention of DNA replication and disruption of bacterial cell membranes. [9, 14] Gold nanoparticles (AuNPs) are also getting huge attention since their antimicrobial activity has been recently

reported. [15, 16] The exact mechanism of bacterial growth inhibition have not been elucidated yet, however some reports present the bacterial wall damage as the cause of the bacterial cell death. [17]

Silk fibroin (SF) is a natural, biocompatible, biodegradable and low-cost polymer obtained from the cocoons of *Bombyx mori* with 5263 amino acids residues composed of glycine, alanine, serine, tyrosine, valine, and only 4.7% of the other 15 amino acid types. [18, 19] The tyrosine residues in SF has strong electron donating properties making this polymer an appealing template for Ag and Au nanoparticles biosynthesis as both reducing and stabilizing agents. [20]

In a previous work, the incorporation of nanosized HA particles (nanoHA) into porous SF hydrogels showed promising physicochemical performance with improved osteoblastic induction characteristics. [21] Thus, the results of this previous work supported the potential application of this composite as a bone graft substitute for clinical situations when local bone formation is needed. Therefore, providing antimicrobial properties to this composite with nanoHA could greatly improve the current bone tissue engineering strategies. In this context, our work was designated to produce a hydrogel containing SF and nanoHA for bone tissue engineering with antimicrobial properties by forming silver or gold nanoparticles *in situ*, an approach that has been poorly explored.

2. Methods

2.1. Preparation of silk fibroin solution

Cocoons of *Bombyx mori* silkworm (supplied by Bratac, São Paulo, Brazil) were degummed in 1 g/L of Na_2CO_3 solution at 85 °C for 1 h 30 min, with Na_2CO_3 changes every 30 min, to remove the sericin of the cocoons and obtain pure SF fibers. Then, SF fibers were dried and dissolved in a ternary solvent of $CaCl_2$:CH_3CH_2OH:H_2O, at 85 °C until total dissolution, to a SF salt solution of 10% (w/v). The SF salt solution was then dialyzed (cellulose membrane, Viscofan 22 EU – 20) against distilled water for 3 days, with water changes every 24 hours.

2.2. *In situ* synthesis of AgNPs and AuNPs in the SF/nanoHA hydrogels

The synthesis of silver nanoparticles was realized by simply mixing different concentrations of silver nitrate ($AgNO_3$, Sigma) with SF solution, in order to prepare four types of hydrogels with AgNPs concentrations of 0, 0.1, 0.5 and 1%. Afterwards the SF/nanoHA hydrogels were prepared according to our previously established method. [21] Briefly, the dry power of nanoHA aggregates (Fluidinova S.A., Maia, Portugal) was first mixed with 70% ethanol and then slowly mixed with the SF aqueous solution at 37 °C. After forming the hydrogels at 37 °C the reaction process to produce the AgNPs was carried out by exposure the materials to the light at room temperature.

Gold nanoparticles were also obtained by reducing gold ions in SF solution. Different concentrations of gold (III) chloride trihydrate ($HAuCl_4 \cdot 3H_2O$, Sigma) were first mixed with the solution of nanoHA in ethanol. Then, these solutions were slowly mixed with the SF solution to achieve hydrogels with AuNPs concentrations of 0, 0.1, 0.5 and 1%, and the hydrogels were prepared at 37 °C. After, the AuNPs formation into the hydrogels was carried out at 60 °C.

The obtained hydrogels with AgNPs and AuNPs were then frozen at -20 °C for 24 h. Afterwards the hydrogels were thawed and immersed in distilled water, which was replaced at regular intervals over a period of 24 h, to remove unreacted $AgNO_3$ and $HAuCl_4 \cdot 3H_2O$ from the hydrogel network.

2.3. Formation of AgNPs and AuNPs in the hydrogels

The hydrogels were cut into pieces and 5 mg of each hydrogel were immersed in protease XIV solution (1 mg/mL) (*Streptomyces griseus*, Sigma) at room temperature over a period of a week to obtain the AgNPs and AuNPs release solutions. UV-visible spectral measurements of SF/nanoHA hydrogels with silver and gold nanoparticles were performed using a Shimadzu UV-2550 UV-Vis spectrophotometer at room temperature in the wavelength range from 300 to 800 nm. The morphology and size of AgNPs and AuNPs were evaluated by transmission electron microscopy (TEM) using a TECNAI G2 20 TWIN microscope at 75 kV, and the samples were prepared by placing a drop of colloidal dispersion on a carbon-coated copper grid, followed by solvent

evaporation at room temperature. The average particle sizes of AgNPs and AuNPs were measured using ImageJ software to analyze the TEM images. The presence of elemental silver and gold was determined by using EDX Zeiss Evo equipped on the TEM. Thermogravimetric analysis (TGA) was performed using a TA instruments Q500 device. The samples were heated from room temperature to 800 °C with a heating rate of 10 °C/min under nitrogen atmosphere. Afterwards, nitrogen was replaced by air treatment at 800 °C to calculate the inorganic residue content.

2.4. Mechanical properties of hydrogels

To evaluate the rheological properties, the hydrogels were allowed to swell in distilled water for 48 h to reach equilibrium swelling. Rheological measurements were performed in a Haake RSI rheometer under controlled temperature at 37 °C using parallel plates of 20 mm diameter. Once the range of linear viscoelastic response was determined, rheological properties were studied in oscillatory experiments in the frequency range of 0.01-1 Hz. The storage and loss moduli, G' and G'', respectively, were determined as functions of the frequency.

2.5. Antimicrobial activity of hydrogels with AgNPs and AuNPs

2.5.1. Bacterial strains and culture conditions

S. aureus (ATCC 25923, MSSA), *S. aureus* (ATCC 33591, MRSA), *S. epidermidis* RP62A (ATCC 35984), *E. coli* (ATCC 25922), and *P. aeruginosa* (ATCC 27853) were used in all experiments. The cultures were grown on Tryptic Soy Broth (TSB) broth (Liofilchem) over 24 h at 37 °C. The bacterial suspensions were prepared and adjusted to cell density of approximately 10^8 cells/mL in TSB at an optical density of 640 nm. The bacterial suspension (1 mL) was inoculated onto the hydrogels, previously sterilized in 70% ethanol (v/v), and placed in 48-well plates. After incubation at 37 °C during 24 h, the antibacterial activity was evaluated for sessile and planktonic bacteria. Hydrogels without NPs were used as control.

2.5.2. Planktonic bacteria assessment

After 24 h of incubation, 100 µL of supernatant were transferred to 96-well plates and the bacterial density was measured in a microplate reader (Synergy HT, BioTek) at 640 nm. Results were expressed as percentage of the control.

2.5.3. Metabolic activity of sessile bacteria

The metabolic activity of sessile bacteria was evaluated by resazurin assay. After 24 h of incubation at 37 °C the bacterial suspension was removed and the samples were carefully rinsed twice with 0.9% NaCl solution in order to remove loosely attached bacteria. Hydrogels were transferred to 48-well plates and fresh TSB containing 10% of resazurin was added to each well and subsequently the plates were incubated for 3 h at 37 °C. Afterwards, 100 µl were transferred to a 96-well plate and the fluoresce intensity was measured in a microplate reader (Synergy HT, BioTek) at 530 nm excitation wavelength and 590 nm emission wavelength. Results were expressed as percentage of the control.

2.6. *In vitro* cytocompatibility studies

2.6.1. Cell culture

Hydrogel sections with 7 mm diameter and 5 mm thickness were sterilized in 70% ethanol (v/v). Hydrogels without AgNPs and AuNPs were used as controls. Osteoblast-like cells (MG63 cell line) were seeded on the top of the hydrogels at a density of 1×10^5 cells/scaffold in minimum essential medium (MEM) Eagle, alpha modification (a-MEM) supplemented with 10% fetal bovine serum, 100 IU/mL penicillin, 2.5 µg/mL streptomycin, (Gibco) and 2.5 µg/mL amphotericin B (Gibco). The cultures were incubated at 37 °C in a humidified atmosphere of 95% air and 5% carbon dioxide (CO_2).

2.6.2. Resazurin assay

After 1, 4 and 7 days of incubation, the metabolic activity was evaluated using the resazurin assay. The same sample was followed throughout the culture time, i.e. it was assessed at all time-points. Briefly, after each culture time point, fresh medium with

10% (v/v) of resazurin was added to each well and the plates were incubated for 3 h at 37 °C. Subsequently, 100 µl were transferred to a 96-well plate and the fluorescence intensity was measured in a microplate reader (Synergy HT, BioTek) at 535 nm excitation wavelength and 590 nm emission wavelength. Results were expressed as percentage of the control (materials without nanoparticles).

2.6.3. Confocal laser scanning microscopy

Cells were fixed in 3.7% formaldehyde (Sigma) for 15 min and then washed twice in PBS. Afterwards, the cell-seeded surfaces were incubated for 30 min with 0.1% (v/v) Triton X-100 solution (Sigma) and 30 min with 1% bovine serum albumin solution in PBS (BSA, Sigma). Cell cytoskeleton filamentous actin (F-actin) were stained with alexafluor phalloidin 488 (Invitrogen) in 1% BSA solution for 30 min at room temperature. Samples were washed twice with PBS and cell nuclei were stained with a buffer of Propidium iodide and RNase (BD Pharmigen) for 10 min. Then, the materials were washed twice with PBS and the cell morphology was evaluated with a Spectral Confocal Microscope Leica TCS-SP5 AOBS (Leica).

2.7. Statistical analysis

The results were expressed as the average ± standard deviation. The statistical analysis of the results was done using the one-way analysis of variance (One-way ANOVA) followed by post hoc Tukey HSD multiple comparison test. Levels of $p < 0.01$ were considered to be statistically significant.

3. Results

3.1. *In situ* synthesis of AgNPs and AuNPs in SF/nanoHA hydrogels

Different compositions of Ag and Au nanoparticles were incorporated into the SF/nanoHA hydrogels as shown in Figure 1.

The SF/nanoHA hydrogels containing silver nitrate, after exposed to the light at room temperature, gradually changed to yellow, indicating the formation of AgNPs (Figure

1). Moreover, the shade of yellow was dependent on silver nitrate concentration, being darker with increasing silver concentration.

The formation of AuNPs at room temperature was not possible. The reduction of gold ions only occurred when the temperature was raised to 60ºC. In this case the hydrogels containing gold (III) chloride trihydrate gradually changed to violet, indicating the formation of AuNPs. As in the previous case, the color intensity was dependent on gold concentration, being more intense for higher concentrations.

It is worth noting that no color change was observed in the SF/nanoHA hydrogels without $AgNO_3$ or $HAuCl_4 \cdot 3H_2O$, which were kept under the same conditions as the other respective samples.

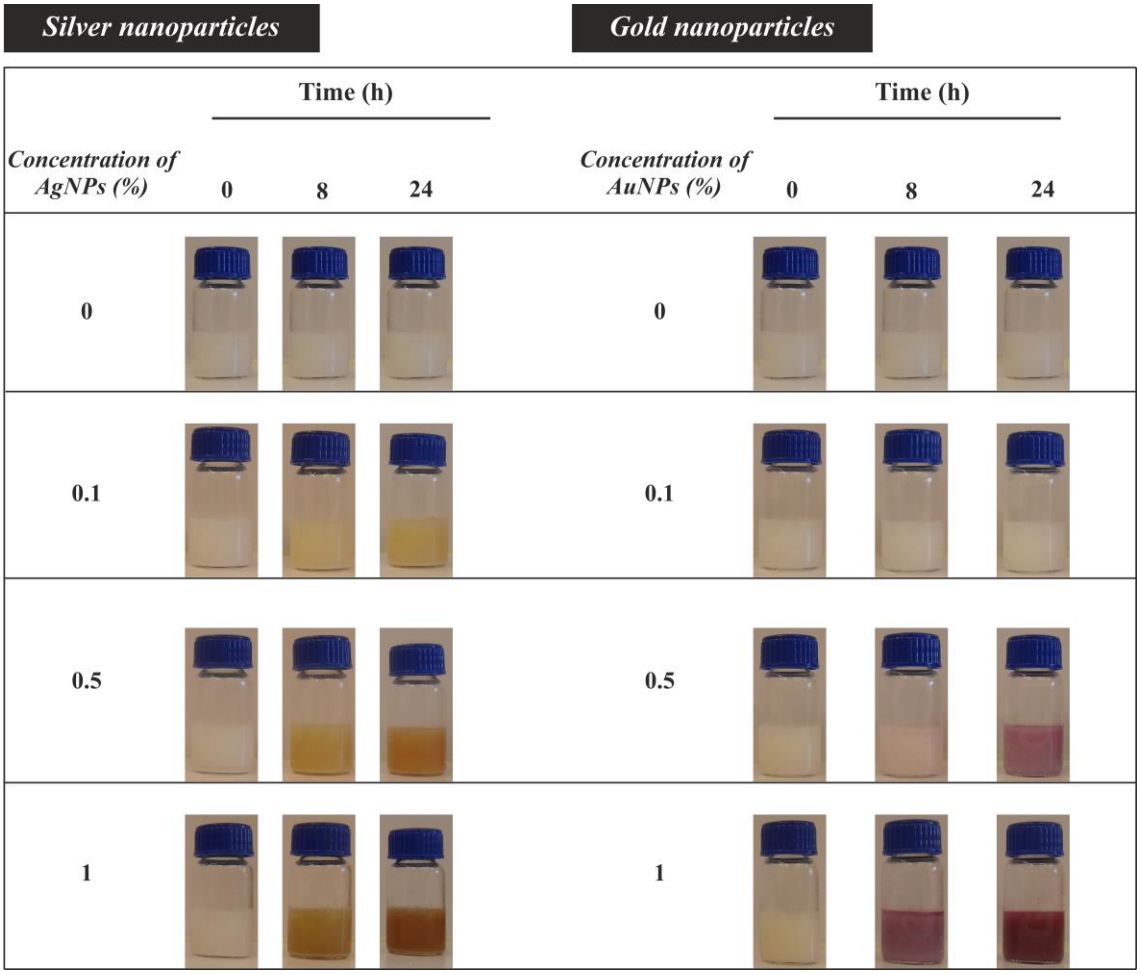

Figure 1 - Photographs illustrating SF/nanoHA hydrogels with different AgNPs and AuNPs concentrations over different periods of time.

3.2. UV–visible spectroscopy

Figure 2 shows the UV-vis spectra recorded from the beginning of the reaction till 30 h later for SF/nanoHA hydrogels with silver and gold nanoparticles. The SF/nanoHA hydrogel was used as control and absorption bands in the range 300-800 nm were not observed. After 8 h a new adsorption bands started to appear at around 400 nm and 525 nm for AgNPs and AuNPs, respectively. These bands increased as the reaction proceeded, reaching a maximum at 24 h. Afterwards, the intensity of the band did not change and the reaction was considered completed.

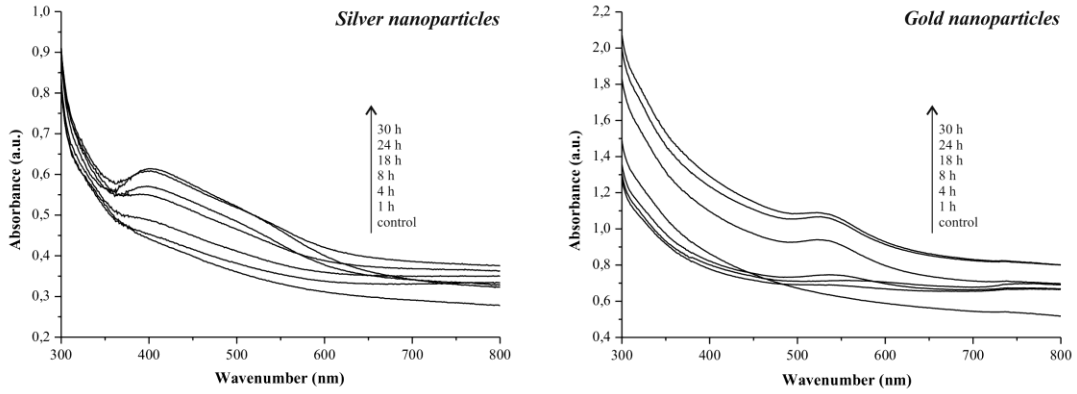

Figure 2 - UV-Vis adsorption spectra of SF/nanoHA hydrogels containing 1% of AgNPs and 1% of AuNPs synthesized *in situ* over different periods of time.

3.3. TEM analysis

The presence of AgNPs and AuNPs was also analyzed by TEM (Figure 3). The TEM images showed that both AgNPs and AuNPs were mainly spherical in shape and uniformly distributed in the hydrogel matrix without aggregation. The resulting average particle size with standard deviations of the silver and gold nanoparticles was determined by measuring 50 nanoparticles. The hydrogels with higher concentration of AgNPs and AuNPs presented larger nanoparticles, with a size distribution ranging from 12.7 to 69.1 nm and 9.3 to 54.7 nm, respectively.

The elemental analysis of the AgNPs and AuNPs was performed using the energy dispersive X-ray analysis (EDX). The EDX spectra showed strong signals corresponding to silver and gold, confirming the presence of these NPs (Figure 3).

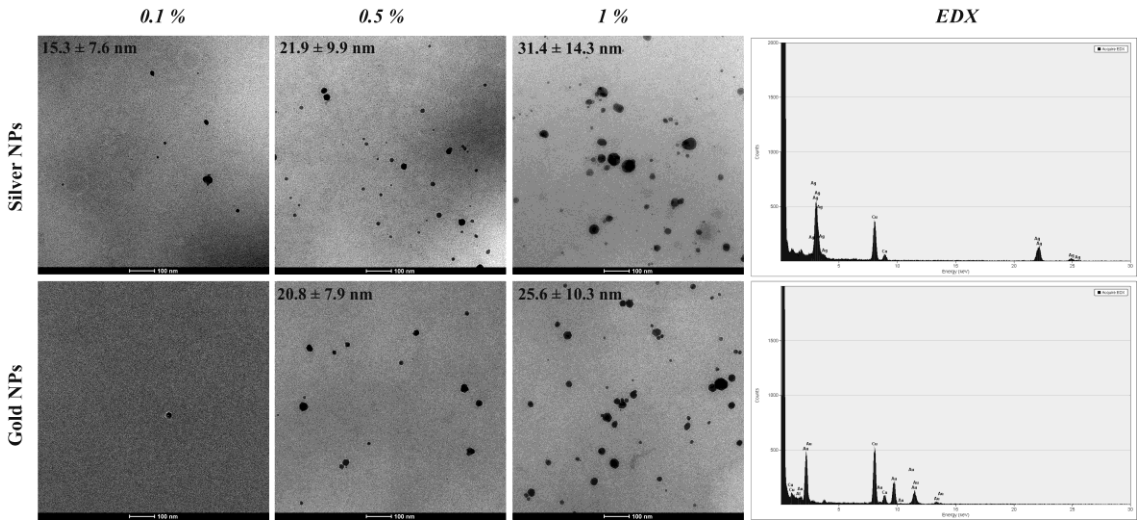

Figure 3 - TEM images with different concentrations of AgNPs and AuNPs and their respective EDX spectra showing the characteristic peaks.

3.4. Rheological measurements

The rheological behavior of the 7 different gels was investigated by measuring the elastic (G') and viscous (G'') moduli as a function of frequency at 37 °C (Figure 4). In all cases, G' was greater than G'' in the entire frequency range. Indeed, the G' values for all hydrogels were above 1000 Pa, while the G'' values were below 500 Pa, over the full frequency range evaluated. It is evident from Figure 4 that the *in situ* reduction of silver nitrate and gold (III) chloride trihydrate within the hydrogel matrices, to form AgNPs and AuNPs respectively, enhanced the hydrogels mechanical stiffness, as illustrated by the increase in G' values as a function of NPs concentration.

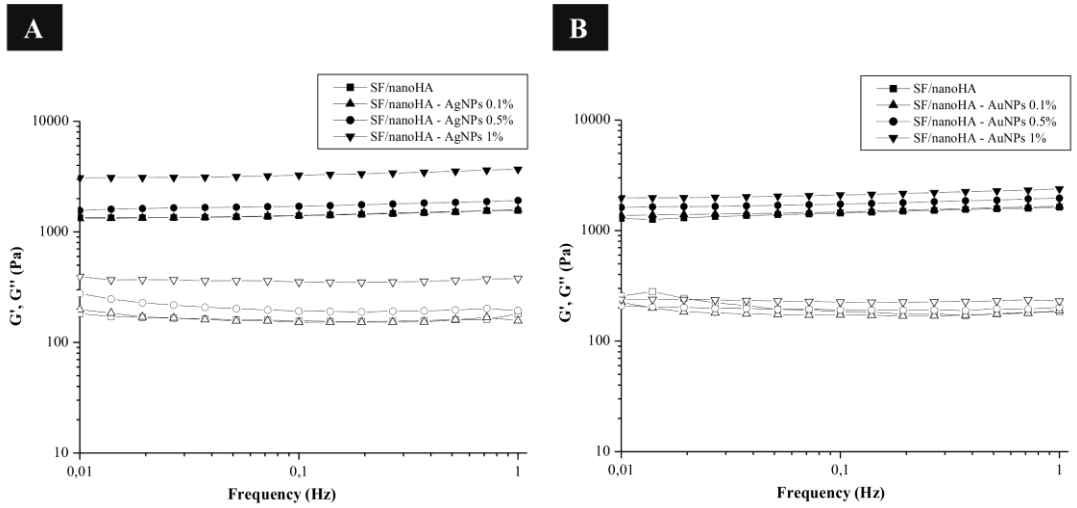

Figure 4 **-** Storage modulus (G' - *solid symbols*) and loss modulus (G'' - *open symbols*) as a function of frequency, for SF/nanoHA hydrogels with different concentrations of AgNPs (A) and AuNPs (B).

3.5. Antimicrobial activity of SF/nanoHA hydrogels with AgNPs and AuNPs

The antimicrobial activity of the synthetized silver and gold nanoparticles against sessile and planktonic bacteria in the medium was investigated against both gram-positive (MSSA, MRSA, *S. epidermidis*) and gram-negative (*E. coli, P. aeruginosa*) bacteria.

The results of metabolically active bacteria attached on hydrogels showed that the hydrogels containing the two highest concentrations of AgNPs exhibited a strong and significant reduction in the sessile bacteria for both gram-positive and gram-negative as shown in Figure 5.

The results concerning to AuNPs were not so linear. Hydrogels with AuNPs didn't show antimicrobial activity toward *S. epidermidis*. Noteworthy, the materials having AuNPs ≥ 0.5% presented antimicrobial activity toward MRSA and *P. aeruginosa*, and hydrogels having ≥ 0.1% showed antimicrobial effect against MSSA and *E. coli*.

Similar trends in antimicrobial activity were also obtained with planktonic bacteria as it can be seen in Figure 5.

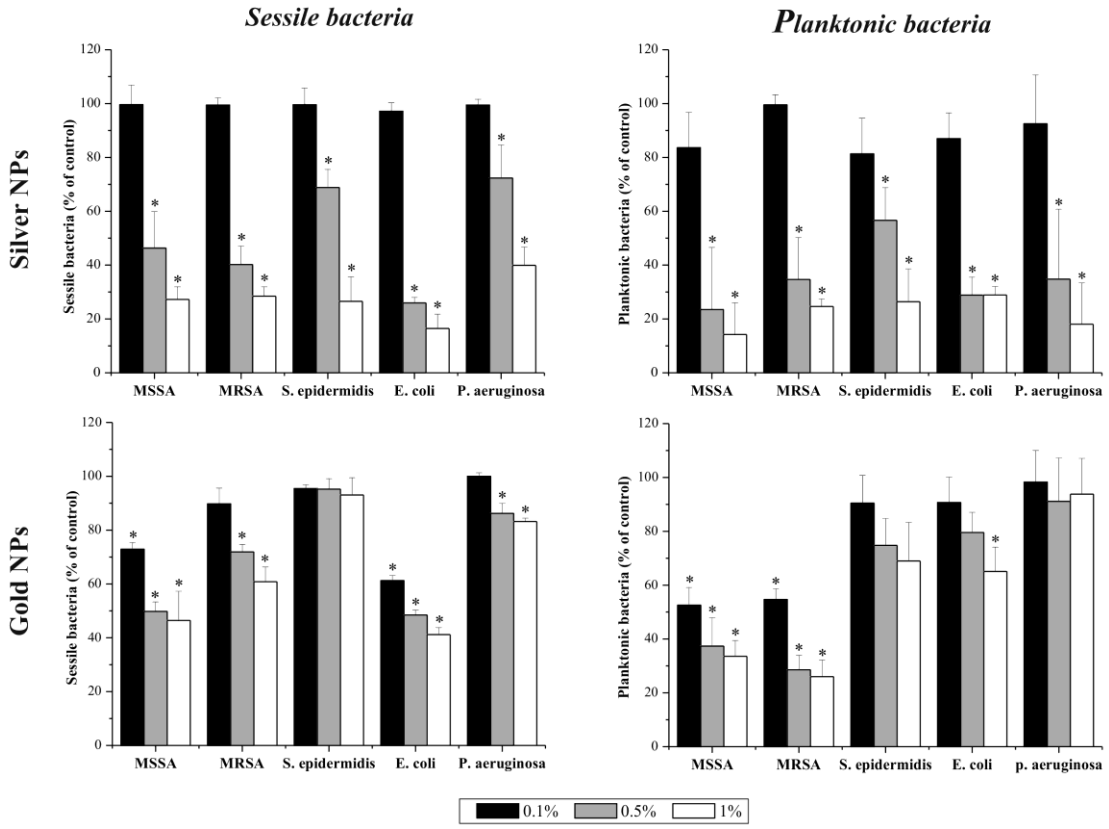

Figure 5 - Sessile and planktonic growth of MSSA, MRSA, *S. epidermidis*, *E. coli* and *P. aeruginosa* on SF/nanoHA hydrogels containing different AgNPs and AuNPs concentrations, as percentage of the control materials without nanoparticles, after 24 h of incubation. *$p < 0.01$, significant reduction compared to hydrogels without NPs.

3.6. Cytocompatibility studies

The *in vitro* cytocompatibility of hydrogels with AgNPs and AuNPs was investigated using resazurin assay on osteoblast cells and the data are presented in Figure 6. The cells were seeded to different concentrations of AgNPs and AuNPs for 1, 4 and 7 days. For the materials with silver nanoparticles a concentration-dependent decrease in cell viability was observed. An initial inhibitory effect followed by cell recovery was observed for the hydrogels with AgNPs at concentrations of 0.1 and 0.5%. However, on the hydrogels with 1% of AgNPs the cellular viability was lower than the control samples, presenting a cell viability of around 30% at day 7. As can be seen in Figure 6, hydrogels with AuNPs shows no toxic effects at all nanoparticles concentration.

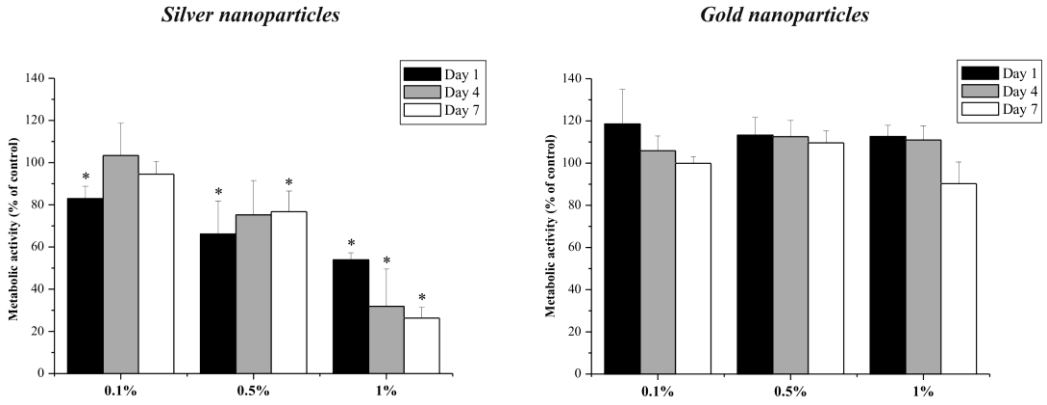

Figure 6 - Influence of different AgNPs and AuNPs concentrations on osteoblast-like cells viability, as a percentage of cells on materials without AgNPs and AuNPs, respectively, after 1, 4 and 7 days of culture. *p < 0.01, significant reduction compared to hydrogels without AgNPs for the same culture time.

To monitor the effects of the nanoparticles on the distribution and morphology of the cells cultured on the materials confocal characterization was carried out (Figure 7). Confocal images showed that the hydrogels with AgNPs, at concentrations up to 0.5%, and the materials with AuNPs, allowed the attachment and spreading of the osteoblast cells, with an elongated morphology and cell-to-cell contacts, similar to the respective controls. On hydrogels with 1% of AgNPs, few cells were visible at day 7.

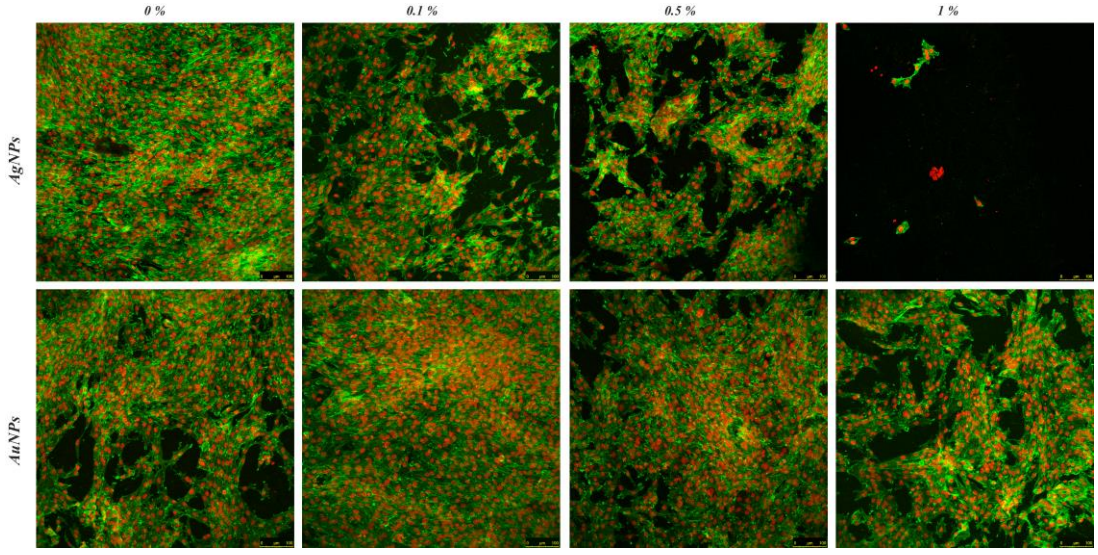

Figure 7 - CLSM images of osteoblastic cells at day 7 on SF/nanoHA hydrogels with different concentrations of AgNPs and AuNPs. MG63 cells were stained for F-actin cytoskeleton with alexafluor phalloidin (green) and nuclei with Propidium iodide (red).

4. Discussion

The best conditions to promote the gelling of SF in the presence of nanoHA were previously studied. [21] Briefly, 4 wt% of SF aqueous solution was mixed with nanoHA previously dissolved in 70% ethanol solution and the hydrogels were prepared at 37ºC for 15 min. In order to prepare well-distributed silver and gold nanoparticles containing SF/nanoHA hydrogels, we relied on the redox ability of one of the amino acids presented in the SF structure, the tyrosine, to prepare AgNPs and AuNPs *in situ*. Chen group demonstrated the capability of SF to reduce Ag^{+} to Ag to prepare silk-silver nanoparticles under the presence of light. [22] Following this approach SF/nanoHA hydrogels with silver and gold nanoparticles were prepared. The gels were placed under light and temperature in the case of silver and gold, respectively, to form the AgNPs or AuNPs containing hydrogels.

The first optical indication of AgNPs and AuNPs formation was given by the color change of the SF/nanoHA hydrogels from colorless to yellow and to violet, respectively. The reduction of silver and gold ions into nanoparticles was then confirmed by UV-Visible spectra as a function of time with absorbance bands around 400 nm and 525 nm reported to be specific for AgNPs [23, 24] and AuNPs [17, 25], respectively. Moreover, the adsorption bands observed around 400 nm and 525 nm suggests the formation of spherical silver [24, 26] and gold [17, 27] nanoparticles, respectively. These results obtained from UV spectra showed good agreement with the data obtained by TEM images that showed the presence of spherical AgNPs and AuNPs with a homogeneous dispersion, confirming a high stabilizing potential of fibroin. Furthermore, both the number and size of these NPs increased when the concentration of silver nitrate and gold (III) chloride trihydrate increased. Previous studies also reported this relationship between the silver and gold contents and the nanoparticles size. [28, 29] Based on these results of photographs, UV-Vis spectroscopy, TEM and TGA it is obvious that fibroin was the main responsible for the formation of Ag and Au nanoparticles.

Rheological measurements showed that for all hydrogels G’ was greater than G’’ in the entire frequency range, neither moduli showing any significant frequency dependence

at low frequencies, which confirmed the gel behaviour. Moreover, as expected well distributed inorganic NPs improved the stiffness of the hydrogels. [30]

New developments for bone tissue engineering should target solutions that cover the most relevant bacterial strains involved in implant-associated infections such as MRSA, that represent the increasing problem of multi-drug resistant infections, and *S. epidermidis* and *P. aeruginosa*, that are well-described strong biofilm producers. [31-33] Hydrogels with AgNPs at concentrations ≥ 0.5% presented a clear dose-dependent antimicrobial activity against all bacteria, including MRSA, *S. epidermidis* and *P. aeruginosa*. A similar effect to the antimicrobial activity of AgNPs in a concentration dependent manner has been stated. [10, 34, 35] There is significant discussion on the mode of antimicrobial activity of AgNPs, and both contact killing and/or ion mediated killing have been proposed. The mechanism of silver ions release was showed by Xiu Z *et al.* where the toxicity of the silver nanoparticles was explained by the presence of released Ag+. [36] However, it has been reported that the antimicrobial activity of AgNPs cannot be attributed solely to the released Ag+ ions but also to the nanoparticle itself. [37, 38] The silver nanoparticles have the ability to attach to the bacterial cell membrane, and also penetrate inside the bacteria causing damage by interacting with phosphorous- and sulfur- containing compounds like DNA. [9] The nanoparticles preferably attack the respiratory chain, cell division finally leading to cell death. [9] An antimicrobial ability of AuNPs was also noticed against MSSA, MRSA, *E. coli* and *P. aeruginosa* but not toward *S. epidermidis*. However, the antimicrobial activity against *P. aeruginosa* was not so active compared to the other bacteria. Also, the hydrogels with 0.5% of AgNPs were not so effective against both *S. epidermidis* and *P. aeruginosa*. This can be related to the ability of these particular strains to colonize the surface, followed by slime production, and to form a biofilm that allows this bacteria to exhibit increased protection. [33, 39] Interestingly, the materials with AuNPs were able to inhibit the bacterial adhesion in lower concentrations than AgNPs. However, the % of inhibition at concentrations of 0.5 and 1% was higher for the hydrogels with AgNPs. Ahmad T. *et al* also showed that AgNPs exhibited higher antimicrobial action as compared to the AuNPs against both *S. aureus* and *E. coli*. [40] This observation may be due to the higher surface activity of the AgNPs as compared to the AuNPs. [40] The

antimicrobial effect of AgNPs and AuNPs was also reflected in the planktonic bacterial cells, similarly to sessile bacteria, which is crucial to prevent post-surgery infection leading to normal healing and osseointegration.

Since antimicrobial materials need to combine antimicrobial activity to fight bacterial infections without compromising cell viability, cytotoxicity assays were carried out with an osteoblast-like cell line. Concerning to materials with AgNPs, increasing the concentration from 0.5% up to 1%, the most cytotoxic effect was observed, where cell viability reduction reached almost a 30%, suggesting that silver nanoparticles beyond 0.5% concentration may be toxic. Sumitha MS *et al*. also showed a toxic effect of AgNPs to cells at higher concentrations. [41] Likewise, Agarwal A *et al*. reported that high loadings of silver nanoparticles were found to be toxic to a murine fibroblast cell line. [42] Reversely, the hydrogels with AuNPs showed no toxic effects even at higher nanoparticles concentration presenting outstanding cell viability. The microscopic observations supported the resazurin results, showing a remarkable reduction of cell number for the materials with 1% of AgNPs. On the contrary, the osteoblastic cells, cultured on hydrogels with AgNPs up to 0.5% and on materials with AuNPs, displayed their typical structure with an organized actin network and elongated morphology.

Overall, the hydrogels containing 0.5% of AgNPs presented strong antimicrobial activity, both anti-sessile and anti-planktonic bacteria properties, reducing the bacteria attachment and further accumulation. These materials simultaneously allowed the adhesion and spreading of osteoblastic cells. The hydrogels with AuNPs also showed antimicrobial activity and no toxicity against osteoblastic cells.

Acknowledgments

This work was financed by FEDER - Fundo Europeu de Desenvolvimento Regional funds through the COMPETE 2020 - Operacional Programme for Competitiveness and Internationalisation (POCI), Portugal 2020, and by Portuguese funds through FCT - Fundação para a Ciência e a Tecnologia/ Ministério da Ciência, Tecnologia e Inovação in the framework of the project "Institute for Research and Innovation in Health

Sciences (POCI-01-0145-FEDER-007274)" and PhD grant (SFRH/BD/90400/2012), whose support is acknowledged. The authors would like to thank the European Commission for their financial support through the project SUSPOL-EJD 642671. Haritz Sardon gratefully acknowledges financial support from MINECO through project FDI 16507.

Supplementary Material

The TGA data are included in the Supplementary Material.

References

1. M. Ribeiro, F. J. Monteiro and M. P. Ferraz, Infection of orthopedic implants with emphasis on bacterial adhesion process and techniques used in studying bacterial-material interactions. *Biomatter*. 2012;2:176-94

2. J. W. Costerton, P. S. Stewart and E. P. Greenberg, Bacterial biofilms: a common cause of persistent infections. *Science*. 1999;284:1318-22

3. K. Lewis, Riddle of biofilm resistance. *Antimicrobial agents and chemotherapy*. 2001;45:999-1007

4. J. P. O'Gara and H. Humphreys, Staphylococcus epidermidis biofilms: importance and implications. *Journal of medical microbiology*. 2001;50:582-7

5. C. R. Arciola, D. Campoccia, P. Speziale, L. Montanaro and J. W. Costerton, Biofilm formation in Staphylococcus implant infections. A review of molecular mechanisms and implications for biofilm-resistant materials. *Biomaterials*. 2012;33:5967-82

6. N. Stobie, B. Duffy, D. E. McCormack, J. Colreavy, M. Hidalgo, P. McHale, et al., Prevention of Staphylococcus epidermidis biofilm formation using a low-temperature processed silver-doped phenyltriethoxysilane sol-gel coating. *Biomaterials*. 2008;29:963-9

7. V. W. Ng, J. M. Chan, H. Sardon, R. J. Ono, J. M. Garcia, Y. Y. Yang, et al., Antimicrobial hydrogels: a new weapon in the arsenal against multidrug-resistant infections. *Advanced drug delivery reviews*. 2014;78:46-62

8. A. Pascual, J. P. Tan, A. Yuen, J. M. Chan, D. J. Coady, D. Mecerreyes, et al., Broad-spectrum antimicrobial polycarbonate hydrogels with fast degradability. *Biomacromolecules*. 2015;16:1169-78

9. M. Rai, A. Yadav and A. Gade, Silver nanoparticles as a new generation of antimicrobials. *Biotechnology Advances*. 2009;27:76-83

10. R. Bryaskova, D. Pencheva, G. M. Kale, U. Lad and T. Kantardjiev, Synthesis, characterisation and antibacterial activity of PVA/TEOS/Ag-Np hybrid thin films. *Journal of Colloid and Interface Science*. 2010;349:77-85

11. A. Panacek, L. Kvitek, R. Prucek, M. Kolar, R. Vecerova, N. Pizurova, et al., Silver colloid nanoparticles: synthesis, characterization, and their antibacterial activity. *The journal of physical chemistry. B*. 2006;110:16248-53

12. B. Boonkaew, P. Suwanpreuksa, L. Cuttle, P. M. Barber and P. Supaphol, Hydrogels containing silver nanoparticles for burn wounds show antimicrobial activity without cytotoxicity. *Journal of Applied Polymer Science*. 2014;131:n/a-n/a

13. J. Wu, Y. Zheng, W. Song, J. Luan, X. Wen, Z. Wu, et al., In situ synthesis of silver-nanoparticles/bacterial cellulose composites for slow-released antimicrobial wound dressing. *Carbohydrate polymers*. 2014;102:762-71

14. S. Prabhu and E. Poulose, Silver nanoparticles: mechanism of antimicrobial action, synthesis, medical applications, and toxicity effects. *Int Nano Lett*. 2012;2:1-10

15. V. D. Badwaik, L. M. Vangala, D. S. Pender, C. B. Willis, Z. P. Aguilar, M. S. Gonzalez, et al., Size-dependent antimicrobial properties of sugar-encapsulated gold nanoparticles synthesized by a green method. *Nanoscale research letters*. 2012;7:623

16. Y. Zhang, H. Peng, W. Huang, Y. Zhou and D. Yan, Facile preparation and characterization of highly antimicrobial colloid Ag or Au nanoparticles. *J Colloid Interface Sci*. 2008;325:371-6

17. A. Regiel-Futyra, M. Kus-Liskiewicz, V. Sebastian, S. Irusta, M. Arruebo, G. Stochel, et al., Development of noncytotoxic chitosan-gold nanocomposites as efficient antibacterial materials. *ACS applied materials & interfaces*. 2015;7:1087-99

18. Y. Yang, Z. Shao, X. Chen and P. Zhou, Optical spectroscopy to investigate the structure of regenerated Bombyx mori silk fibroin in solution. *Biomacromolecules*. 2004;5:773-9

19. M. Ribeiro, M. A. de Moraes, M. M. Beppu, F. J. Monteiro and M. P. Ferraz, The role of dialysis and freezing on structural conformation, thermal properties and morphology of silk fibroin hydrogels. *Biomatter*. 2014;4:e28536

20. Q. Dong, H. Su and D. Zhang, In situ depositing silver nanoclusters on silk fibroin fibers supports by a novel biotemplate redox technique at room temperature. *The journal of physical chemistry. B*. 2005;109:17429-34

21. M. Ribeiro, M. A. de Moraes, M. M. Beppu, M. P. Garcia, M. H. Fernandes, F. J. Monteiro, et al., Development of silk fibroin/nanohydroxyapatite composite hydrogels for bone tissue engineering. *European Polymer Journal*. 2015;67:66-77

22. X. Fei, M. Jia, X. Du, Y. Yang, R. Zhang, Z. Shao, et al., Green synthesis of silk fibroin-silver nanoparticle composites with effective antibacterial and biofilm-disrupting properties. *Biomacromolecules*. 2013;14:4483-8

23. M. S. Sumitha, K. T. Shalumon, V. N. Sreeja, R. Jayakumar, S. V. Nair and D. Menon, Biocompatible and Antibacterial Nanofibrous Poly(ϵ-caprolactone)-Nanosilver Composite Scaffolds for Tissue Engineering Applications. *Journal of Macromolecular Science, Part A*. 2012;49:131-138

24. M. Darroudi, M. B. Ahmad, R. Zamiri, A. H. Abdullah, N. A. Ibrahim, K. Shameli, et al., Preparation and characterization of gelatin mediated silver nanoparticles by laser ablation. *Journal of Alloys and Compounds*. 2011;509:1301-1304

25. G. Di Carlo, A. Curulli, R. G. Toro, C. Bianchini, T. De Caro, G. Padeletti, et al., Green synthesis of gold-chitosan nanocomposites for caffeic acid sensing. *Langmuir : the ACS journal of surfaces and colloids*. 2012;28:5471-9

26. K. Shameli, M. B. Ahmad, S. D. Jazayeri, P. Shabanzadeh, P. Sangpour, H. Jahangirian, et al., Investigation of antibacterial properties silver nanoparticles prepared via green method. *Chemistry Central journal*. 2012;6:73

27. W. Haiss, N. T. Thanh, J. Aveyard and D. G. Fernig, Determination of size and concentration of gold nanoparticles from UV-vis spectra. *Analytical chemistry*. 2007;79:4215-21

28. X. L. Cao, C. Cheng, Y. L. Ma and C. S. Zhao, Preparation of silver nanoparticles with antimicrobial activities and the researches of their biocompatibilities. *Journal of materials science. Materials in medicine*. 2010;21:2861-8

29. B. Tang, L. Sun, J. Kaur, Y. Yu and X. Wang, In-situ synthesis of gold nanoparticles for multifunctionalization of silk fabrics. *Dyes and Pigments*. 2014;103:183-190

30. C.-X. Zhao and W.-D. Zhang, Preparation of waterborne polyurethane nanocomposites: Polymerization from functionalized hydroxyapatite. *European Polymer Journal*. 2008;44:1988-1995

31. M. Otto, MRSA virulence and spread. *Cellular microbiology*. 2012;14:1513-21

32. H. Rohde, S. Frankenberger, U. Zahringer and D. Mack, Structure, function and contribution of polysaccharide intercellular adhesin (PIA) to Staphylococcus epidermidis biofilm formation and pathogenesis of biomaterial-associated infections. *European journal of cell biology*. 2010;89:103-11

33. K. Tote, T. Horemans, D. Vanden Berghe, L. Maes and P. Cos, Inhibitory effect of biocides on the viable masses and matrices of Staphylococcus aureus and Pseudomonas aeruginosa biofilms. *Appl Environ Microbiol*. 2010;76:3135-42

34. G. Yang, J. Xie, Y. Deng, Y. Bian and F. Hong, Hydrothermal synthesis of bacterial cellulose/AgNPs composite: A "green" route for antibacterial application. *Carbohydrate polymers*. 2012;87:2482-2487

35. R. Bryaskova, D. Pencheva, M. Kyulavska, D. Bozukova, A. Debuigne and C. Detrembleur, Antibacterial activity of poly(vinyl alcohol)-b-poly(acrylonitrile) based micelles loaded with silver nanoparticles. *J Colloid Interface Sci*. 2010;344:424-8

36. Z. M. Xiu, Q. B. Zhang, H. L. Puppala, V. L. Colvin and P. J. Alvarez, Negligible particle-specific antibacterial activity of silver nanoparticles. *Nano Lett*. 2012;12:4271-5

37. N. Lubick, Nanosilver toxicity: ions, nanoparticles--or both? *Environ Sci Technol*. 2008;42:8617

38. J. Fabrega, S. R. Fawcett, J. C. Renshaw and J. R. Lead, Silver nanoparticle impact on bacterial growth: effect of pH, concentration, and organic matter. *Environ Sci Technol*. 2009;43:7285-90

39. M. Ribeiro, F. J. Monteiro and M. P. Ferraz, Staphylococcus aureus and Staphylococcus epidermidis adhesion to nanohydroxyapatite in the presence of model proteins. *Biomedical materials*. 2012;7:045010

40. T. Ahmad, I. A. Wani, N. Manzoor, J. Ahmed and A. M. Asiri, Biosynthesis, structural characterization and antimicrobial activity of gold and silver nanoparticles. *Colloids and surfaces. B, Biointerfaces*. 2013;107:227-34

41. M. S. Sumitha, K. T. Shalumon, V. N. Sreeja, R. Jayakumar, S. V. Nair and D. Menon, Biocompatible and Antibacterial Nanofibrous Poly(epsilon-caprolactone)-Nanosilver Composite Scaffolds for Tissue Engineering Applications. *J Macromol Sci A*. 2012;49:131-138

42. A. Agarwal, T. L. Weis, M. J. Schurr, N. G. Faith, C. J. Czuprynski, J. F. McAnulty, et al., Surfaces modified with nanometer-thick silver-impregnated polymeric films that kill bacteria but support growth of mammalian cells. *Biomaterials*. 2010;31:680-90

Supplementary Material

TGA data

The thermogravimetric behavior of the SF/nanoHA hydrogels with AgNPs and AuNPs was analyzed with TGA (Figure S1). All the curves showed two degradation steps, the first started from around 100ºC, indicating the evaporation of adsorbed water, and the second step, which started to decline sharply at around 300ºC, was due to the thermal degradation of silk fibroin protein. [21] Moreover, the TGA data showed that the materials, with and without nanoparticles, presented a similar pattern in their curves, indicating no significant differences in their thermal stability. With the incorporation of AgNPs and AuNPs the residual weight increased slightly compared to hydrogels without NPs, confirming the *in situ* synthesis of these nanoparticles.

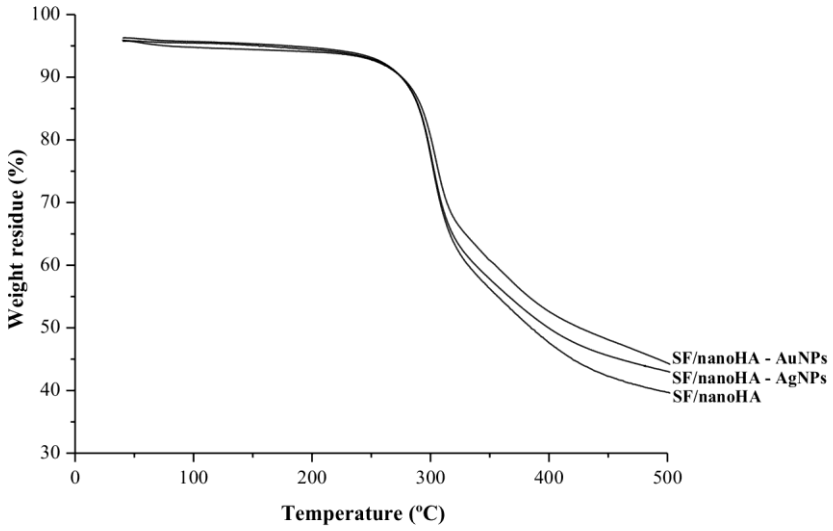

Figure S1 - TGA curves of SF/nanoHA hydrogels without and with AgNPs and AuNPs.

CHAPTER VI

General discussion and future perspectives

There is a substantial unmet demand for materials to repair injured, degenerated or congenitally defected bone tissues. Bone tissue engineering has been proposing solutions to address these clinical problems. Successful strategies in most cases require 3-dimensional scaffolds with controllable structural, morphological and degradation features matched to the targeted clinical application. The use of natural polymers as scaffolds in bone tissue engineering has been gaining widespread attention owing to their significant similarities with the extracellular matrix (ECM), biocompatibility, biodegradability, chemical versatility, low cost and ease of processing [1, 2]. The interplay of factors such as concentration of polymer used in processing, structural stability, pore size, tissue ingrowth, and degradation are keys to the understanding of the scaffold behavior. Among naturally derived polymers, silk fibroin, a natural fibrous protein, meets most of the requirements for a biomaterial, including excellent processability, biocompatibility, controlled degradation rate, high oxygen and water vapor permeability, the presence of easily accessible chemical groups for functional modifications, low cost, and material format versatility [3, 4]. The utility of silk fibroin as a biomaterial has evolved tremendously over the years to include an impressive portfolio of applications (drug delivery vehicles, implants, tissue scaffolds), which are continuously expanding [3, 5]. Due to the above mentioned reasons, recent advances have greatly expanded the processing windows for three-dimensional SF porous hydrogels [6-10]. In the context of creating more effective bioactive hydrogels, applying bioceramics is one of the best-known methods to improve bone repairing [11, 12]. As a biocompatible, bioactive and osteoconductive material, nanoHA is one of the most widely used calcium phosphate ceramics due to its chemical similarities to the inorganic component of natural bone tissue [13].

The main goal of the present work was to evaluate the effect of nanoHA incorporation into SF hydrogels on physiochemical and biological behavior. Therefore, novel SF based hydrogels incorporating different percentages of nanophased hydroxyapatite (nanoHA), by using a new and innovative method, were developed through non-freezing and freezing methodologies. These composite hydrogels involving a biodegradable SF polymer and a bioactive nanoHA ceramic can offer the desired properties for bone tissue ingrowth, such as appropriate porosity, adequate

mechanical properties, bioactivity and osteoconductivity, improving their biological properties.

Three-dimensional and interconnected porous hydrogels of SF incorporated with nanoHA, in combination with large pore sizes for bone tissue engineering, were obtained by the freezing method, exhibiting both microporosity and macroporosity structure. This 3D architectural parameters of the hydrogel (porous structure, pore size, and interconnectivity) are believed to contribute significantly to the development of biological functions in tissue [14], being crucial to provide adequate space for cell attachment and proliferation, cell-matrix interactions, diffusion of nutrients and metabolites, and vascularization to the developing bone tissue. While large pores allow effective nutrient supply, gas diffusion, and metabolic waste removal, small pores are essential for the cell attachment and intracellular signaling. Consequently, the conception of hydrogels containing both micro- and macroporosity may provide the essential physical support for cellular growth [15-17].

The ability of the hydrogels to take up fluids from the surrounding medium also plays an important role in tissue engineering. The water swelling of hydrogels occurred rapidly, and the materials were capable to hold the amount of water uptake in its network structure, showing that the hydrogels possess good hydration ability while maintaining their structural integrity. The incorporation of nanoHA in the polymeric matrix decreased the swelling capability of composite hydrogels, perhaps due to the lower water uptake ability of this ceramic, when compared to SF protein, which is consistent with previous studies [18, 19]. For example, Thein-Han W *et al* also reported a decrease in the swelling degree due to addition of nanoHA aggregates to chitosan scaffolds [19]. Furthermore, the frozen materials presented higher swelling capacity, which can be attributed to the different porosities of the hydrogels. This trend is in agreement with previously reported observations [20]. Swelling and porosity aid in the supply of nutrients to the interior of the 3D materials and also increase the surface area for cell proliferation. Thus, a controlled swelling is appreciated for tissue engineering applications, indicating that the frozen SF/nanoHA composite hydrogels could be more adequate.

Degradability of a bone substitute is another important characteristic for whether the material will be accepted widely for tissue engineering applications. The ideal implant should degrade at a rate compatible with the rate of bone growth, physically creating open space for new bone tissue formation, until full regeneration is achieved. *In vitro* enzymatic hydrolysis provides a general idea of the biodegradability of a material. As a protein, SF is susceptible to biological degradation by proteolytic enzymes, such as protease [21]. The hydrogels incubated in phosphate buffer without the enzyme showed no significant degradation. On the contrary, materials incubated with protease were enzymatically degraded, which confirmed that the mass loss was due solely to enzymatic hydrolysis, showing the potential of SF as a biodegradable material. The final wastes of the enzymatic degradation of SF biomaterials are the corresponding amino acids, which are easily disposed *in vivo*. This is a crucial advantage of SF used in biomedical applications [21]. Furthermore, the degradation rate and the morphological structure changes were similar for the non-frozen and frozen hydrogels suggesting that pore size did not correlate with degradation rate. This has earlier been shown by Kim U. *et al* in SF scaffolds with different pore sizes exposed to a protease solution [22].

Besides the aforementioned needful properties, which were successfully achieved, a strong argument to indicate a better performance with respect to bone regeneration, and that is being useful for predicting the *in vivo* bone bioactivity of a material, is the ability of the hydrogel to promote an apatite layer formation [23]. As for the apatite-forming ability, SF/nanoHA hydrogels performed best with the highest amount of apatite being formed, and hence, increased osteoconductivity and tissue in-growth are expected after implantation. These results are in line with previous studies, showing that composite materials incorporating nanoHA improve apatite formation, which can be attributed to the dissolution of calcium and phosphate ions from nanoHA, and consequently this ceramic acts as nucleation agent at different sites for the growth of apatite crystals [18, 24].

Considering the promising structural and physicochemical properties of frozen SF/nanoHA hydrogels developed in this work, these composites materials may provide a promising engineering solution to control the adhesion, proliferation and osteogenic differentiation of human bone marrow stromal cells (hBMSCs), which are critical cells

responsible for osteogenesis. For this reason, *in vitro* studies with hBMSCs were performed on both non-frozen and frozen SF and SF/nanoHA hydrogels. hBMSCs were able to adhere and proliferate on all materials, however cells in the hydrogels with nanoHA presented higher metabolic activity and proliferation rates, showing an inductive effect of the presence of nanoHA, consistent with previous studies that examined bone-related cell behavior on this ceramic [25-27]. For example, Xia Y *et al* reported that poly-ε-caprolactone (PCL) scaffolds incorporating nanoHA enabled better the attachment and proliferation of human bone marrow stromal cells in comparison with pure PCL scaffolds [27]. In the present work, this tendency was particularly achieved in the frozen composite hydrogels, which could be attributed to the well-constructed porous structure with larger pore sizes on frozen materials. An enhanced cell attachment and proliferation thorough SF/chitosan porous scaffolds with larger pores was also observed in a study conducted by Bhardwaj N *et al* [28]. Furthermore, a more prominent hBMSCs attachment, evidenced from more development of actin filaments, was observed in these frozen composite materials. Additionally, hBMSCs attached on SF/nanoHA hydrogels successfully expressed higher levels of ALP activity, an early osteoblastic differentiation marker widely used to evaluate the *in vitro* osteogenic differentiation [29]. Likewise, an ALP live cell stain assay showed that the cells were alive and functional, with better cell response in the SF/nanoHA hydrogels. The osteogenic induction of the composite materials containing nanoHA was found consistent with previous studies [30, 31]. The osteogenic potential of the SF/nanoHA hydrogels on the hBMSCs differentiation was also evidenced by the increased intensity of BMP-2 expression, which is a protein known to participate in the regulation of cell growth and differentiation, along with the induction of osteogenic progenitor cells in bone defects sites during the healing process [32]. Furthermore, BMP-2 has a critical role in inducing Runx-2 and Osterix expression to promote osteoblast differentiation [33, 34]. One interesting observation, in this work, was that ALP expression in hBMSCs was observed within the SF/nanoHA porous hydrogel, indicating not only cell infiltration into the material, and consequently migration, but also active production of ALP by the infiltrated cells. This cell migration at different levels in the 3D hydrogels constitute a main pillar of scaffold colonization ensuring

bone in-growth and bone tissue regeneration [35]. These biological findings are in line with the apatite-forming ability of the composite hydrogels, which proved that these materials provided a more bioactive substrate for cellular attachment, proliferation and differentiation.

The possibility of promoting bone tissue growth while preventing bacterial adhesion and, consequently, implant-related infections, is undoubtedly highly desirable. Implant-associated infections are the result of microbial adhesion and subsequent biofilm formation at the implantation site protecting bacteria against host defenses and antibiotics. Additionally, an estimated 80% of bacterial infections in humans are caused by biofilms, and consequently the most pressing clinical impediments of the century [36, 37]. The uprising of antibiotic resistance a few years from its implementation has prompted the search for new fighting strategies. Metallic nanoparticles are a promising class of inorganic antimicrobial compounds, as they have broad spectrum of activity, and higher durability and stability promoting a long-term shelf-life, which is a key condition for the use of a biomaterial in clinical settings [38]. Furthermore, this experimental strategy may mitigate concerns about multi-drug resistant microorganisms commonly seen in approaches based on conventional antibiotics. Because of the well-known antimicrobial activity of silver [39] and gold [40] nanoparticles, the present SF/nanoHA hydrogel was modified with small amounts of *in situ* synthetized Ag or Au NPs. The resulting hydrogels endowed significant inhibition ability against major agents of biomaterial-associated infections in orthopedics, without hampering cell behavior. Hydrogels containing 0.5% of AgNPs presented strong antibacterial activity, both anti-sessile and anti-planktonic properties, reducing the bacteria attachment and further accumulation, and simultaneously allowed the adhesion and spreading of osteoblastic cells. The bacterial inhibition of hydrogels with AuNPs was not so high, as observed by others researchers [41], and may be due to the higher surface activity of the AgNPs as compared to the AuNPs [41]. However, the high degree of citocompatibility observed for the hydrogels with AuNPs toward osteoblast cells may be an interesting point to further studies, to evaluate if hydrogels modified with higher concentrations AuNPs could maintain the citocompatibility, and at same time improve the antimicrobial properties. Furthermore, it would be interesting to

assess if that higher concentrations of AuNPs could enhance the osteoblast proliferation and differentiation, since some studies with functionalized AuNPs have been reported to improve the bone tissue regeneration by promoting the proliferation of osteoblasts and osteogenic differentiation acting as osteogenic agents [42, 43].

Gathering all the information of the current study, it is possible to conclude that frozen SF/nanoHA hydrogels presented excellent citocompatibility properties, since they provided an adequate environment for hBMSCs adhesion, proliferation and migration, and osteoblast differentiation. In addition, these composite hydrogels provided a convenient substrate for the inclusion of silver and gold nanoparticles, reducing the bacterial attachment and further accumulation, which could improve clinical outcomes related to biomaterial implant-associated infections.

The results achieved in the present work suggested that SF/nanoHA hydrogels offer great potential to be considered as bone fillers for tissue engineering applications. To move a step forward in the characterization of this scaffold material, *in vivo* studies should be performed in order to validate the *in vitro* results, aiming at evaluating whether the newly developed composite hydrogels fulfil the requirements of biocompatibility and osteogenic potential. Secondly, the antimicrobial efficacy should be assessed using an animal model of bone infection.

References

[1] Armentano I, Dottori M, Fortunati E, Mattioli S, Kenny JM. Biodegradable polymer matrix nanocomposites for tissue engineering: A review. Polymer Degradation and Stability 2010;95:2126-46.

[2] Puppi D, Chiellini F, Piras AM, Chiellini E. Polymeric materials for bone and cartilage repair. Progress in Polymer Science 2010;35:403-40.

[3] Kundu B, Kurland NE, Bano S, Patra C, Engel FB, Yadavalli VK, et al. Silk proteins for biomedical applications: Bioengineering perspectives. Progress in Polymer Science 2014;39:251-67.

[4] Rockwood DN, Preda RC, Yucel T, Wang X, Lovett ML, Kaplan DL. Materials fabrication from Bombyx mori silk fibroin. Nat Protocols 2011;6:1612-31.

[5] Altman GH, Diaz F, Jakuba C, Calabro T, Horan RL, Chen J, et al. Silk-based biomaterials. Biomaterials 2003;24:401-16.

[6] Kim U-J, Park J, Li C, Jin H-J, Valluzzi R, Kaplan DL. Structure and Properties of Silk Hydrogels. Biomacromolecules 2004;5:786-92.

[7] Motta A, Migliaresi C, Faccioni F, Torricelli P, Fini M, Giardino R. Fibroin hydrogels for biomedical applications: preparation, characterization and in vitro cell culture studies. J Biomater Sci Polym Ed 2004;15:851-64.

[8] Fini M, Motta A, Torricelli P, Giavaresi G, Nicoli Aldini N, Tschon M, et al. The healing of confined critical size cancellous defects in the presence of silk fibroin hydrogel. Biomaterials 2005;26:3527-36.

[9] Yucel T, Cebe P, Kaplan DL. Vortex-Induced Injectable Silk Fibroin Hydrogels. Biophysical Journal 2009;97:2044-50.

[10] Nogueira GM, de Moraes MA, Rodas ACD, Higa OZ, Beppu MM. Hydrogels from silk fibroin metastable solution: Formation and characterization from a biomaterial perspective. Materials Science and Engineering: C 2011;31:997-1001.

[11] Gaharwar AK, Dammu SA, Canter JM, Wu C-J, Schmidt G. Highly Extensible, Tough, and Elastomeric Nanocomposite Hydrogels from Poly(ethylene glycol) and Hydroxyapatite Nanoparticles. Biomacromolecules 2011;12:1641-50.

[12] Fu S, Ni P, Wang B, Chu B, Zheng L, Luo F, et al. Injectable and thermo-sensitive PEG-PCL-PEG copolymer/collagen/n-HA hydrogel composite for guided bone regeneration. Biomaterials 2012;33:4801-9.

[13] Zhou H, Lee J. Nanoscale hydroxyapatite particles for bone tissue engineering. Acta Biomaterialia 2011;7:2769-81.

[14] Liu X, Smith LA, Hu J, Ma PX. Biomimetic nanofibrous gelatin/apatite composite scaffolds for bone tissue engineering. Biomaterials 2009;30:2252-8.

[15] Autissier A, Le Visage C, Pouzet C, Chaubet F, Letourneur D. Fabrication of porous polysaccharide-based scaffolds using a combined freeze-drying/cross-linking process. Acta Biomater 2010;6:3640-8.

[16] Wei J, Jia J, Wu F, Wei S, Zhou H, Zhang H, et al. Hierarchically microporous/macroporous scaffold of magnesium-calcium phosphate for bone tissue regeneration. Biomaterials 2010;31:1260-9.

[17] Dehghani F, Annabi N. Engineering porous scaffolds using gas-based techniques. Current Opinion in Biotechnology 2011;22:661-6.

[18] Peter M, Ganesh N, Selvamurugan N, Nair SV, Furuike T, Tamura H, et al. Preparation and characterization of chitosan–gelatin/nanohydroxyapatite composite scaffolds for tissue engineering applications. Carbohydrate polymers 2010;80:687-94.

[19] Thein-Han WW, Misra RDK. Biomimetic chitosan–nanohydroxyapatite composite scaffolds for bone tissue engineering. Acta Biomaterialia 2009;5:1182-97.

[20] Mandal BB, Kapoor S, Kundu SC. Silk fibroin/polyacrylamide semi-interpenetrating network hydrogels for controlled drug release. Biomaterials 2009;30:2826-36.

[21] Cao Y, Wang B. Biodegradation of Silk Biomaterials. International Journal of Molecular Sciences 2009;10:1514-24.

[22] Kim U-J, Park J, Joo Kim H, Wada M, Kaplan DL. Three-dimensional aqueous-derived biomaterial scaffolds from silk fibroin. Biomaterials 2005;26:2775-85.

[23] Kokubo T, Takadama H. How useful is SBF in predicting in vivo bone bioactivity? Biomaterials 2006;27:2907-15.

[24] Kumar PT, Srinivasan S, Lakshmanan VK, Tamura H, Nair SV, Jayakumar R. Synthesis, characterization and cytocompatibility studies of alpha-chitin hydrogel/nano hydroxyapatite composite scaffolds. Int J Biol Macromol 2011;49:20-31.

[25] Shi Z, Huang X, Cai Y, Tang R, Yang D. Size effect of hydroxyapatite nanoparticles on proliferation and apoptosis of osteoblast-like cells. Acta Biomaterialia 2009;5:338-45.

[26] Zandi M, Mirzadeh H, Mayer C, Urch H, Eslaminejad MB, Bagheri F, et al. Biocompatibility evaluation of nano-rod hydroxyapatite/gelatin coated with nano-HAp as a novel scaffold using mesenchymal stem cells. J Biomed Mater Res A 2010;92:1244-55.

[27] Xia Y, Zhou P, Cheng X, Xie Y, Liang C, Li C, et al. Selective laser sintering fabrication of nano-hydroxyapatite/poly-ε-caprolactone scaffolds for bone tissue engineering applications. International Journal of Nanomedicine 2013;8:4197-213.

[28] Bhardwaj N, Kundu SC. Chondrogenic differentiation of rat MSCs on porous scaffolds of silk fibroin/chitosan blends. Biomaterials 2012;33:2848-57.

[29] Hesse E, Hefferan TE, Tarara JE, Haasper C, Meller R, Krettek C, et al. Collagen type I hydrogel allows migration, proliferation, and osteogenic differentiation of rat bone marrow stromal cells. J Biomed Mater Res A 2010;94:442-9.

[30] Wang H, Li Y, Zuo Y, Li J, Ma S, Cheng L. Biocompatibility and osteogenesis of biomimetic nano-hydroxyapatite/polyamide composite scaffolds for bone tissue engineering. Biomaterials 2007;28:3338-48.

[31] Kang R, Luo Y, Zou L, Xie L, Lysdahl H, Jiang X, et al. Osteogenesis of human induced pluripotent stem cells derived mesenchymal stem cells on hydroxyapatite contained nanofibers. RSC Advances 2014;4:5734-9.

[32] Kim K, Dean D, Lu A, Mikos AG, Fisher JP. Early osteogenic signal expression of rat bone marrow stromal cells is influenced by both hydroxyapatite nanoparticle content and initial cell seeding density in biodegradable nanocomposite scaffolds. Acta Biomater 2011;7:1249-64.

[33] Datta HK, Ng WF, Walker JA, Tuck SP, Varanasi SS. The cell biology of bone metabolism. Journal of clinical pathology 2008;61:577-87.

[34] Fernandes MH, Gomes PS. Bone Cells Dynamics during Peri-Implantitis: a Theoretical Analysis. J Oral Maxillofac Res 2016;7:e6.

[35] Cicuéndez M, Izquierdo-Barba I, Sánchez-Salcedo S, Vila M, Vallet-Regí M. Biological performance of hydroxyapatite–biopolymer foams: In vitro cell response. Acta Biomaterialia 2012;8:802-10.

[36] Bryers JD. Medical biofilms. Biotechnol Bioeng 2008;100:1-18.

[37] Blackledge MS, Worthington RJ, Melander C. Biologically-Inspired Strategies for Combating Bacterial Biofilms. Current opinion in pharmacology 2013;13:699-706.

[38] Bryaskova R, Pencheva D, Kale GM, Lad U, Kantardjiev T. Synthesis, characterisation and antibacterial activity of PVA/TEOS/Ag-Np hybrid thin films. Journal of Colloid and Interface Science 2010;349:77-85.

[39] Blecher K, Nasir A, Friedman A. The growing role of nanotechnology in combating infectious disease. Virulence 2011;2:395-401.

[40] Li X, Robinson SM, Gupta A, Saha K, Jiang Z, Moyano DF, et al. Functional Gold Nanoparticles as Potent Antimicrobial Agents against Multi-Drug-Resistant Bacteria. ACS Nano 2014;8:10682-6.

[41] Ahmad T, Wani IA, Manzoor N, Ahmed J, Asiri AM. Biosynthesis, structural characterization and antimicrobial activity of gold and silver nanoparticles. Colloids and Surfaces B: Biointerfaces 2013;107:227-34.

[42] Heo DN, Ko W-K, Bae MS, Lee JB, Lee D-W, Byun W, et al. Enhanced bone regeneration with a gold nanoparticle-hydrogel complex. Journal of Materials Chemistry B 2014;2:1584-93.

[43] Yi C, Liu D, Fong CC, Zhang J, Yang M. Gold nanoparticles promote osteogenic differentiation of mesenchymal stem cells through p38 MAPK pathway. ACS Nano 2010;4:6439-48.

CHAPTER VII

Conclusions

Engineering composite hydrogels based on biodegradable polymers incorporating a bioactive ceramic represent a potentially interesting platform for the design of medical implants for successful bone regeneration. In this context, this work allowed to develop and optimize a composite hydrogel consisting of silk fibroin and nanoHA particles with enhanced physicochemical properties, which were ultimately favorable in the biological performance. The composite materials provided a more bioactive substrate for attachment, proliferation and osteogenic differentiation of human bone marrow stromal cells. Additionally, antimicrobial properties were provided to the composite material by *in situ* synthetizing of silver and gold nanoparticles. The bacterial inhibition of hydrogels with AuNPs was not so high when compared to materials with AgNPs. The SF/nanoHA hydrogels incorporating 0.5% of AgNPs were found to be a promising material as they presented strong antibacterial activity, reducing the bacterial attachment and further accumulation, while being cytocompatible with osteoblastic cells. This is particularly opportune considering the emergence of new resistant bacterial strains to the most potent antibiotics opening new avenues to prevent implant-related infections.